

# The Decay of Short Period Comets

Mark Andrew Hughes

Department of Physics and Astronomy, University of Sheffield

August 1999

*A thesis submitted to the University of Sheffield*

*in partial fulfilment of the requirements*

*of the degree of Doctor of Philosophy*

**For my parents**

## Declaration

I declare that no part of this thesis has been accepted, or is currently being submitted, for any degree or diploma or certificate or any other qualification in this University or elsewhere.

This thesis is the result of my own work unless otherwise stated.

# The Decay of Short Period Comets

Mark Andrew Hughes

Department of Physics and Astronomy, University of Sheffield

August 1999

## Abstract

This thesis considers both the mass of dust released by short period comets and the size distribution of a decaying cometary population.

The secular variation in the  $H_{10}$  absolute magnitude of comets 2P/Encke, 4P/Faye, 6P/d'Arrest, 7P/Pons-Winnecke and 10P/Tempel 2 is investigated and it is concluded that there is more information in the  $H_{10}$  data than can be found from a linear regression analysis.

A computer program is presented that takes the absolute magnitude of a comet,  $H_{10}$ , the orbital eccentricity and the perihelion distance, and calculates the mass of dust released by the comet per apparition. This model is applied to the  $H_{10}$  data set for the above comets, and it is concluded that 4P/Faye has been a prolific contributor of dust to the inner Solar System, releasing an average of  $(21.6 \pm 0.5) \times 10^{11}$  g per apparition during the last 19 recorded apparitions. This is mainly attributed to an unusual period of activity pre-1910.

A simple model of cometary decay, whereby individual comets lose a constant depth from the cometary nucleus at each apparition is presented. This is used to model the decay of a model population of short period comets. The population is examined at regular time intervals and the mass distribution index is calculated. This index indicates how mass is distributed within the cometary population, and is found to decrease, non-linearly, as comets in the population decay.

The total mass of dust released by a model population of comets, each having only one perihelion passage, is also calculated. The list of cometary orbits for this population is kept fixed and the cometary  $H_{10}$  values are randomly mixed up and reassigned back to the list of orbits. In this way new populations of short period comets are created. It is concluded that the current population of short period comets releases an unusually small total mass of dust, and that this is due to the average value of  $H_{10}$  decreasing as a function of perihelion distance.

# Contents

<b>1</b>	<b>Introduction</b>	<b>1</b>
1.1	Short Period Comets and Dust . . . . .	1
1.2	Summary of this Thesis . . . . .	2
<b>2</b>	<b>Dust from Short Period Comets</b>	<b>4</b>
2.1	Introduction . . . . .	4
2.2	The Short Period Orbit . . . . .	4
2.2.1	The Typical Short Period Comet . . . . .	5
2.3	The Cometary Nucleus . . . . .	7
2.3.1	The Whipple Model . . . . .	7
2.3.2	The Current Model . . . . .	10
2.4	Dust Released from Short Period Comets . . . . .	12
2.4.1	Dust Ejection . . . . .	12
2.4.2	Meteor Streams . . . . .	14
2.5	The Lifetime of a Comet . . . . .	15
2.5.1	Cometary Outbursts . . . . .	15
2.5.2	Dormancy . . . . .	16
2.6	Summary . . . . .	18

<b>3</b>	<b>Absolute Magnitude Data</b>	<b>19</b>
3.1	Cometary Brightness . . . . .	20
3.1.1	The Light Curve . . . . .	22
3.1.2	The $H_{10}$ Absolute Magnitude . . . . .	23
3.2	Uncertainty in the Absolute Magnitudes . . . . .	25
3.2.1	Different Instruments and Different Observers . . . . .	25
3.2.2	The Holetschek Effect . . . . .	26
3.3	The Kresák and Kresáková $H_{10}$ Catalogues . . . . .	27
3.3.1	The Catalogues . . . . .	28
3.3.2	Maximum Absolute Brightness . . . . .	29
3.3.3	The Corrected Apparent Magnitude . . . . .	29
3.3.4	$H_{10}$ Weighting . . . . .	30
3.4	Summary . . . . .	31
<b>4</b>	<b>Secular Variation in Cometary Activity</b>	<b>33</b>
4.1	Introduction . . . . .	33
4.2	A Shrinking Nucleus or a Change in the Size of the Active Areas . .	34
4.3	$H_{10}$ Absolute Magnitudes . . . . .	37
4.3.1	Secular Variation in $H_{10}$ Calculated from a Linear Regression	38
4.4	Uncertainties in the $H_{10}$ Data . . . . .	40
4.4.1	(1) The Kresák and Kresáková $H_{10}$ weights . . . . .	40
4.4.2	(2) Light Curve Asymmetry . . . . .	42
4.4.3	(3) $\pm 0.5$ Magnitude Error Bars . . . . .	43
4.4.4	(4) The Holetschek Effect . . . . .	43
4.4.5	(5) Missed Apparitions . . . . .	43

4.5	The $M_{ap}$ Computer Program . . . . .	45
4.5.1	Overview and Assumptions . . . . .	45
4.5.2	The Calculation of $M_{ap}$ . . . . .	47
4.6	The Orbital Parameters . . . . .	50
4.7	2P/Encke . . . . .	54
4.7.1	Introduction . . . . .	54
4.7.2	Pre-1786 Perihelion Passages . . . . .	56
4.7.3	Light Curve Asymmetry . . . . .	59
4.7.4	Missing Apparitions, Holetschek Effect and the $H_{10}$ Weights	60
4.7.5	The Mass of Dust Released per Apparition, $M_{ap}$ . . . . .	61
4.8	6P/d'Arrest . . . . .	64
4.8.1	Introduction . . . . .	64
4.8.2	$H_{10}$ Absolute Magnitudes . . . . .	67
4.8.3	The Mass of Dust Released per Apparition, $M_{ap}$ . . . . .	70
4.8.4	Discussion . . . . .	71
4.9	10P/Tempel 2 . . . . .	72
4.9.1	Introduction . . . . .	72
4.9.2	$H_{10}$ Absolute Magnitudes, Light Curve Asymmetry, the Ho- letschek Effect and $H_{10}$ Weights . . . . .	72
4.9.3	Active Areas . . . . .	75
4.10	7P/Pons-Winnecke . . . . .	78
4.10.1	Introduction . . . . .	78
4.10.2	$H_{10}$ Absolute Magnitudes, Light Curve Asymmetry and Miss- ing Apparitions . . . . .	78

4.10.3	The Mass of Dust Released per Apparition, $M_{ap}$ . . . . .	82
4.10.4	Active Areas . . . . .	83
4.11	4P/Faye . . . . .	85
4.11.1	Introduction . . . . .	85
4.11.2	$H_{10}$ Absolute Magnitudes, Light Curve Asymmetry and Miss- ing Apparitions . . . . .	85
4.11.3	The Mass of Dust Released per Apparition, $M_{ap}$ . . . . .	89
4.11.4	Active Areas . . . . .	89
4.12	Summary . . . . .	92
<b>5</b>	<b>A Decaying Short Period Comet Population</b>	<b>94</b>
5.1	Introduction . . . . .	94
5.2	The Size Distribution of Cometary Nuclei . . . . .	95
5.2.1	The Size Range of Short Period Comets . . . . .	95
5.2.2	Measuring the Size of a Bare Nucleus . . . . .	96
5.2.3	Measuring the Size of an Active Nucleus . . . . .	97
5.2.4	Producing the Size Distribution . . . . .	100
5.2.5	Describing the Distribution by a Power Law . . . . .	101
5.2.6	The Cumulative Number, $N(\bar{H}_{10})$ . . . . .	102
5.2.7	The Cumulative Number, $N(M)$ . . . . .	103
5.2.8	The Definition of the Mass Distribution Index . . . . .	104
5.2.9	Relating the Mass of the Nucleus to the Effective Radius . .	105
5.3	Are the Faintest Comets Missing? . . . . .	106
5.3.1	Investigating the curved region, $\bar{H}_{10} > 8$ . . . . .	107
5.4	A Decaying Cometary Population . . . . .	111

5.4.1	The 'Apparition Zero' Model Population of Comets . . . . .	113
5.4.2	The Layer Loss Rate . . . . .	113
5.4.3	The Large Comet Region . . . . .	115
5.4.4	How Does $s$ Vary as the Population Decays? . . . . .	119
5.4.5	The Limitation of Using the Mass Distribution Index . . . . .	122
5.4.6	Different Populations? . . . . .	123
5.5	Summary . . . . .	124
<b>6</b>	<b>Is the Known Population Unusual?</b>	<b>127</b>
6.1	Introduction . . . . .	127
6.2	The Assumptions . . . . .	128
6.3	The Model . . . . .	131
6.3.1	The Perihelion Distance and Eccentricity . . . . .	132
6.3.2	The Mean Absolute Magnitude, $\bar{H}_{10}$ . . . . .	132
6.3.3	Creating New Populations . . . . .	133
6.3.4	The Mass of Dust Released by the Known Population of Short Period Comets . . . . .	135
6.3.5	Short Period Comets with Perihelia greater than 2.8 AU . .	135
6.4	The New Populations . . . . .	139
6.4.1	The Population of 89 comets . . . . .	140
6.4.2	The Population of 84 Comets ( $q < 2.8$ AU) . . . . .	142
6.5	Why is $M_{pop}$ so Small for the Current Population? . . . . .	143
6.5.1	$\bar{H}_{10}$ as a Function of Perihelion Distance . . . . .	145
6.5.2	'Correcting' for Cometary Decay . . . . .	148
6.5.3	The Expected Decay Rate . . . . .	149

6.6	The New (Corrected) Populations . . . . .	156
6.6.1	The 89 Comet Population . . . . .	156
6.6.2	The 84 Comet Population ( $q < 2.8$ AU) . . . . .	158
6.7	Discussion . . . . .	161
6.8	Summary . . . . .	164
<b>7</b>	<b>Discussion and Possible Future Work</b>	<b>166</b>
7.1	Discussion . . . . .	166

# List of Figures

- 2.1 The distribution of orbital periods for short and intermediate period  
comets . . . . . 6
- 2.2 Aphelion and perihelion distributions for short and intermediate pe-  
riod comets . . . . . 8
- 2.3 Orbital inclination and eccentricity distributions for short and inter-  
mediate period comets . . . . . 9
- 2.4 The cometary nucleus . . . . . 13
- 3.1 The geometry of the Sun-comet-Earth system . . . . . 21
- 3.2 The light curve of the 1986 apparition of 1P/Halley . . . . . 24
- 3.3 The geometry used to calculate the  $j$  angle for the Holetschek effect 27
- 4.1 Linear regressions used to infer secular fading rates . . . . . 39
- 4.2 The  $H_{10}$  weights for 2P/Encke, 4P/Faye, 6P/d'Arrest, 7P/Pons-  
Winnecke and 10P/Tempel 2 . . . . . 41
- 4.3 The model cometary apparition . . . . . 46
- 4.4 The temporal variation in perihelion distance, orbital period and  
eccentricity . . . . . 53
- 4.5 The temporal variation in aphelion distance for 2P/Encke . . . . . 55

4.6  $H_{10}$  against year,  $M_{ap}$  against year,  $j$  angle against year and  $H_{10}$  against  $j$  angle for 2P/Encke . . . . . 57

4.7 A correction to account for the pre/post perihelion asymmetry in the light curve . . . . . 62

4.8  $H_{10}$  against year,  $\log M_{ap}$  against year,  $j$  angle against year and  $H_{10}$  against  $j$  angle for 6P/d'Arrest . . . . . 65

4.9  $H_{10}$  against year,  $M_{ap}$  against year,  $j$  angle against year and  $H_{10}$  against  $j$  angle for 10P/Tempel 2 . . . . . 73

4.10 The percentage of the 10P/Tempel 2 nucleus surface that was active 77

4.11  $H_{10}$  against year,  $M_{ap}$  against year,  $j$  angle against year and  $H_{10}$  against  $j$  angle for 7P/Pons-Winnecke . . . . . 79

4.12 The percentage of the nucleus surface of 7P/Pons-Winnecke that was active . . . . . 84

4.13  $H_{10}$  against year,  $M_{ap}$  against year,  $j$  angle against year and  $H_{10}$  against  $j$  angle for 4P/Faye . . . . . 86

4.14 The percentage of the nucleus surface of 4P/Faye that was active . 90

5.1 The weighted mean absolute magnitude,  $H_{10}$ , for the 90 short period comets in the Kresák and Kresáková catalogues that have had more than one apparition recorded . . . . . 98

5.2 The short period comet nucleus size distribution . . . . . 100

5.3  $\bar{H}_{10}$  for 89 short period comets plotted in cumulative form . . . . . 106

5.4 The logarithm of the cumulative number of comets with perihelion distances,  $q \leq 1.5$  AU and  $q \leq 1.0$  AU . . . . . 109

5.5	The 'Apparition Zero' distribution for the model population of short period comets . . . . .	112
5.6	The 'Apparition Zero' model population in cumulative form . . . . .	114
5.7	The decaying 'Apparition Zero' population . . . . .	116
5.8	The new decaying 'Apparition Zero' population, (number of small comets is constant) . . . . .	117
5.9	Another new decaying 'Apparition Zero' population, (number of small comets increases with decreasing radius) . . . . .	118
5.10	A cumulative plot for the +800 Ap distribution shown in figure (5.7)	121
5.11	The value of the mass distribution index as the population decays .	121
5.12	A new distribution created by adding apparitions -1200 to 1200 in steps of 200 apparitions from figure (5.7) . . . . .	123
5.13	The expected relationship between the equivalent nucleus radius and the cumulative number of comets . . . . .	125
6.1	The distributions of $M_{pop}$ and the percentage of $M_{pop}$ released by the top 10 dust releasing comets for the 89 and 84 comet populations	141
6.2	$\bar{H}_{10}$ as a function of perihelion distance . . . . .	145
6.3	Fits to the $\bar{H}_{10}$ against $q$ plots . . . . .	150
6.4	The expected shape of the $\bar{H}_{10}$ against $q$ plots . . . . .	151
6.5	The number of perihelion passages that a comet would take reach the lines described in table (6.3) . . . . .	152
6.6	The 89 comet population corrected distributions . . . . .	157
6.7	The 84 comet population corrected distributions . . . . .	159

# List of Tables

2.1	A comparison of the aphelion distance, $Q$ , the perihelion distance, $q$ , the orbital inclination, $i$ and the orbital eccentricity, $e$ , for short and intermediate period comets . . . . .	5
3.1	Short period comets that have been missed at recent returns but are included in the Kresák and Kresáková catalogues . . . . .	28
4.1	The number of apparitions of 2P/Encke, 4P/Faye, 6P/d'Arrest, 7P/Pons-Winnecke and 10P/Tempel 2 that have been missed since their discovery apparitions . . . . .	37
4.2	The secular fading rates, found from linear regressions, of 2P/Encke, 4P/Faye, 6P/d'Arrest, 7P/Pons-Winnecke and 10P/Tempel 2 . . . .	38
4.3	Estimates of the years in which apparitions were missed for 2P/Encke, 4P/Faye, 6P/d'Arrest, 7P/Pons-Winnecke and 10P/Tempel 2 since their discovery apparitions . . . . .	44
4.4	Close approaches between 7P/Pons-Winnecke and the Earth . . . . .	82
4.5	The total mass of dust released by 2P/Encke, 4P/Faye, 6P/d'Arrest, 7P/Pons-Winnecke and 10P/Tempel 2 during all the recorded apparitions . . . . .	92

4.6	The variation in the percentage of the cometary nucleus surface that was active for 4P/Faye, 7P/Pons-Winnecke and 10P/Tempel 2 . . .	92
5.1	The number of comets remaining in the $R > 0.2$ km region of the model population after cometary decay . . . . .	122
6.1	The top ten dust contributing comets, the ten comets with the lowest $H_{10}$ values and the smallest ten perihelia . . . . .	136
6.2	Short period comets with perihelia greater than 2.8 AU . . . . .	137
6.3	Linear regressions applied to the $\bar{H}_{10}$ against $q$ plots . . . . .	149
6.4	The main characteristics of the distributions shown in figure (6.1), figure (6.6) and figure (6.7) . . . . .	160

# Chapter 1

## Introduction

### 1.1 Short Period Comets and Dust

This thesis discusses the mass of dust released by comets with orbital periods less than 15 years. These *short period* comets provide the best chance for an analysis of the progressive decay of cometary nuclei since, unlike comets of longer periods, several cometary apparitions can be investigated over the course of a human lifetime.

An investigation into the long term decay of comets requires the use of historical data. In this thesis the cometary absolute magnitude<sup>1</sup>,  $H_{10}$ , is used to calculate the mass of dust released by a comet at each apparition (see chapter (4) and chapter (6)), and the mean absolute magnitude,  $\bar{H}_{10}$  is used to calculate the radii of cometary nuclei (see chapter (5)).

The catalogues of  $H_{10}$  data, chosen for use throughout this thesis, were produced by Kresák and Kresáková (1989, 1994) (see chapter (3)). These catalogues span

---

<sup>1</sup>The apparent magnitude the comet would have if it was at a heliocentric distance of 1 AU, a geocentric distance of 1 AU and if the phase angle was zero; see figure (3.1).

approximately 200 years of cometary observations (dating back to the year 1770 for the observation of D/1770 L1 Lexell), and so this defines the time span over which cometary decay is considered in this thesis.

## 1.2 Summary of this Thesis

- **Chapter (2): *Dust from Short Period Comets.***

The typical short period comet is described, both in terms of its orbital parameters and the current interpretation of the cometary nucleus. The association between the dust released from short period comets and meteor streams is briefly reviewed. Also discussed are effects which will either prolong or reduce the average lifetime of a comet, such as cometary dormancy and outbursts.

- **Chapter (3): *Absolute Magnitude Data.***

The definition of the cometary absolute magnitude,  $H_{10}$ , is reviewed. The reasons for selecting the Kresák and Kresáková catalogues as the source of  $H_{10}$  data are given and the uncertainties in the determination of the absolute magnitude are discussed.

- **Chapter (4): *Secular Variation in Cometary Activity.***

The decay of comets 2P/Encke, 4P/Faye, 6P/d'Arrest, 7P/Pons-Winnecke and 10P/Tempel 2 are investigated over several cometary apparitions. A computer program is presented that takes the perihelion distance, eccentricity and absolute magnitude,  $H_{10}$ , and calculates the mass of dust released by a comet during one apparition,  $M_{ap}$ . For comets 4P/Faye, 7P/Pons-Winnecke and 10P/Tempel 2 the fraction of the nucleus surface,  $f$ , that is actively releasing gas and dust is calculated and this is used to explain the change in  $H_{10}$  from apparition to apparition for these

comets.

• **Chapter (5): *A Decaying Short Period Comet Population.***

The mean absolute magnitude,  $\bar{H}_{10}$ , is used to calculate the size range of nucleus radii for short period comets. This size range is combined with the mass distribution of the largest of the known short period comets, and a new model population of comets is created. The comets in this population are then allowed to decay. The size distribution of the largest comets is then calculated at different times in the lifetime of the model population.

• **Chapter (6): *Is the Known Population Unusual?***

The computer program used to calculate the mass of dust released per apparition,  $M_{ap}$ , by a comet (see chapter (4)) is taken a step further and used to calculate the mass of dust released by a population of comets,  $M_{pop}$ . By assuming that the initial orbit of a short period comet is independent of the mass of the cometary nucleus, new populations of comets are created randomly. The value of  $M_{pop}$  for these new populations is calculated and compared with the value for the known population of short period comets.

• **Chapter (7): *Discussion and Possible Future Work.***

The conclusions of the thesis are presented and suggestions of possible future work, based on the results in this thesis, are made

# Chapter 2

## Dust from Short Period Comets

### 2.1 Introduction

In this chapter the short period orbit is defined and the current concept of the cometary nucleus is reviewed.

The role of cometary outbursts and periods of dormancy, *i.e.* perihelion passages when the comet is inactive, are discussed in terms of the lifetime of a short period comet.

### 2.2 The Short Period Orbit

In this thesis the term ‘short period comet’ is used to refer to those comets that have orbital periods of  $P \leq 15$  years (Hughes 1988a). Orbital periods of  $15 \leq P \leq 200$  years are referred to as ‘intermediate’ and those of  $P > 200$  years are called ‘long’ period orbits.

Figure (2.1) shows the distribution of orbital periods for 185 comets with  $P < 200$  years (Marsden & Williams 1996). The data set includes comets that have had

	Short Period Comets ( $P < 15$ years)	Intermediate Period Comets ( $15 \text{ years} < P < 200$ years)
$Q$ (AU)	$6 \pm 1$	$29 \pm 14$
$q$ (AU)	$1.9 \pm 0.9$	85% of comets have $q \leq 2.0$ AU
$i$	$13 \pm 10$	$57 \pm 56$
$e$	$0.5 \pm 0.2$	77% of comets have $e \geq 0.85$

Table 2.1: A comparison of the aphelion distance,  $Q$ , the perihelion distance,  $q$ , the orbital inclination,  $i$  and the orbital eccentricity,  $e$ , for short and intermediate period comets. Where possible the mean and standard deviation of the sample have been calculated. The sample size is 106 comets for the short period class and 13 comets for the intermediate class. The mean perihelion distance, aphelion distance and orbital eccentricity for short period comets imply that the mean orbital period for these comets is  $\sim 8$  years. As the sample of intermediate period comets is so small, the mean perihelion and orbital eccentricity did not seem to represent the data well and therefore only an indication of the clustering of the data is given.

only one perihelion passage and comets that are now classified as defunct<sup>1</sup>. From the list of 185 comets of orbital periods  $P \leq 200$  years, 153 (82.7%) have orbital periods of  $P \leq 15$  years. Short period comets were probably captured by Jupiter and figure (2.1) shows that the orbital period of Jupiter, 11.9 years (Karttunen et al. 1987), falls within the  $P \leq 15$  years definition of the short period class of comets.

## 2.2.1 The Typical Short Period Comet

Frequency distributions for the perihelion distance,  $q$  and the aphelion distance,  $Q$ , for short and intermediate comets are shown in figure (2.2). Figure (2.3) shows the corresponding distributions for the eccentricity,  $e$ , and inclination,  $i$ . The data for these distributions come from the Epoch 1996 Nov. 13.0 TT entry in the *Catalogue of Cometary Orbits 1996* (Marsden & Williams 1996). These elements are therefore a snapshot of the current population and will vary due to gravitational

<sup>1</sup>A defunct comet is one which is known to no longer exist, e.g. 3D/Biela

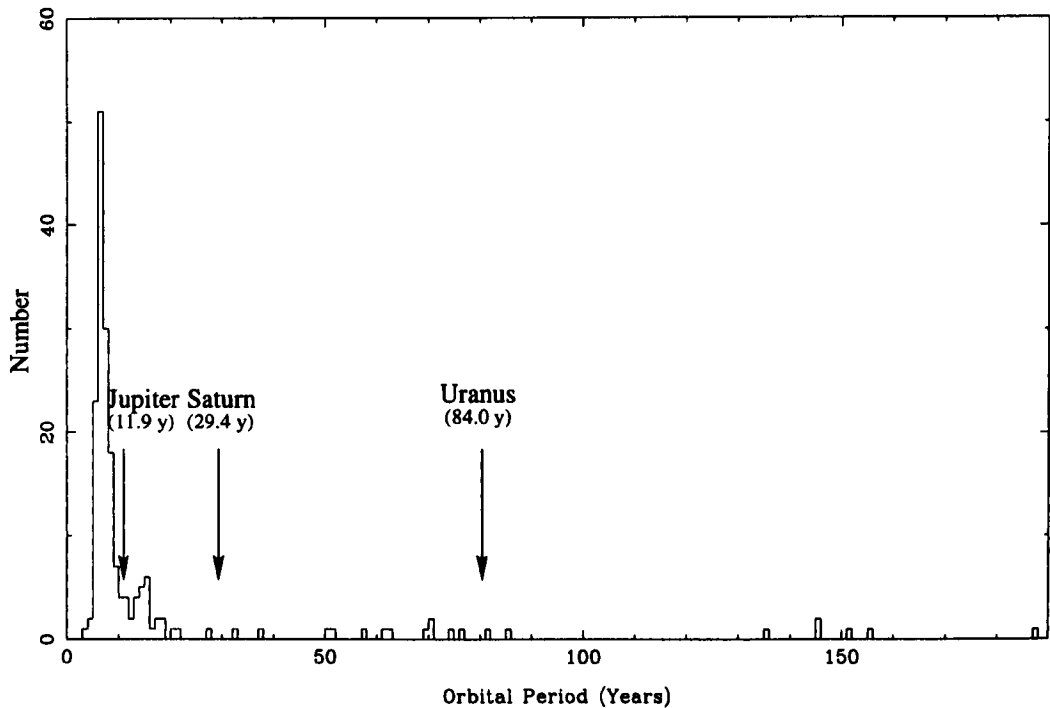


Figure 2.1: The distribution of orbital periods for 185 short and intermediate period comets with orbital periods of  $P \leq 200$  years. Included are comets of only one apparition and those now classified as defunct (Marsden & Williams 1996). The arrows indicate the orbital periods of Jupiter, Saturn and Uranus (Karttunen et al. 1987). The clustering of comets with orbital period  $\leq 15$  years is due the capture of these comets by Jupiter. For this reason, comets are grouped into, (a) **Short period comets** ( $P \leq 15$  years) and (b) **Intermediate period comets** ( $15 \text{ years} < P \leq 200$  years).

perturbations by the planets and non-gravitational forces (see section (2.4.1)).

The data set for these distributions does not include comets that are now classified as defunct or comets that have only made one apparition. Consequently, the number of short period comets in each distribution is 106 and the number of intermediate period comets is only 13.

Figure (2.2) and figure (2.3) show that the typical short period comet has an aphelion distance close to the orbit of Jupiter at 5.2 AU, reaches perihelion within 5 AU of the Sun, has an inclination less than  $32^\circ$  and a eccentricity of  $0.5 \pm 0.2$ . Table (2.1) lists the mean aphelion distances, perihelion distances, inclinations and eccentricities.

Although the number of intermediate comets is only 13 it is clear that the range of orbital elements are different to those for the short period comet population. Intermediate period comets, in this data set, can have higher inclinations, (up to  $162^\circ$  for this sample) and higher eccentricities, (77% of the comets shown in figure (2.3) have  $e \geq 0.85$ ).

## 2.3 The Cometary Nucleus

### 2.3.1 The Whipple Model

The current model of the cometary nucleus is based on the icy conglomerate model first proposed by Whipple (1950). In this model, the nucleus of a comet is a solid body of ‘dirty’ ice. The ice is formed from  $H_2O$ ,  $NH_3$ ,  $CH_4$ ,  $CO_2$  and  $CO$ . Within the ice resides “meteoric material”, *i.e.* material with a composition indicated from the spectra of meteors, which Whipple states as being: Fe, Ca, Mn, Cr, Si, Ni, Al

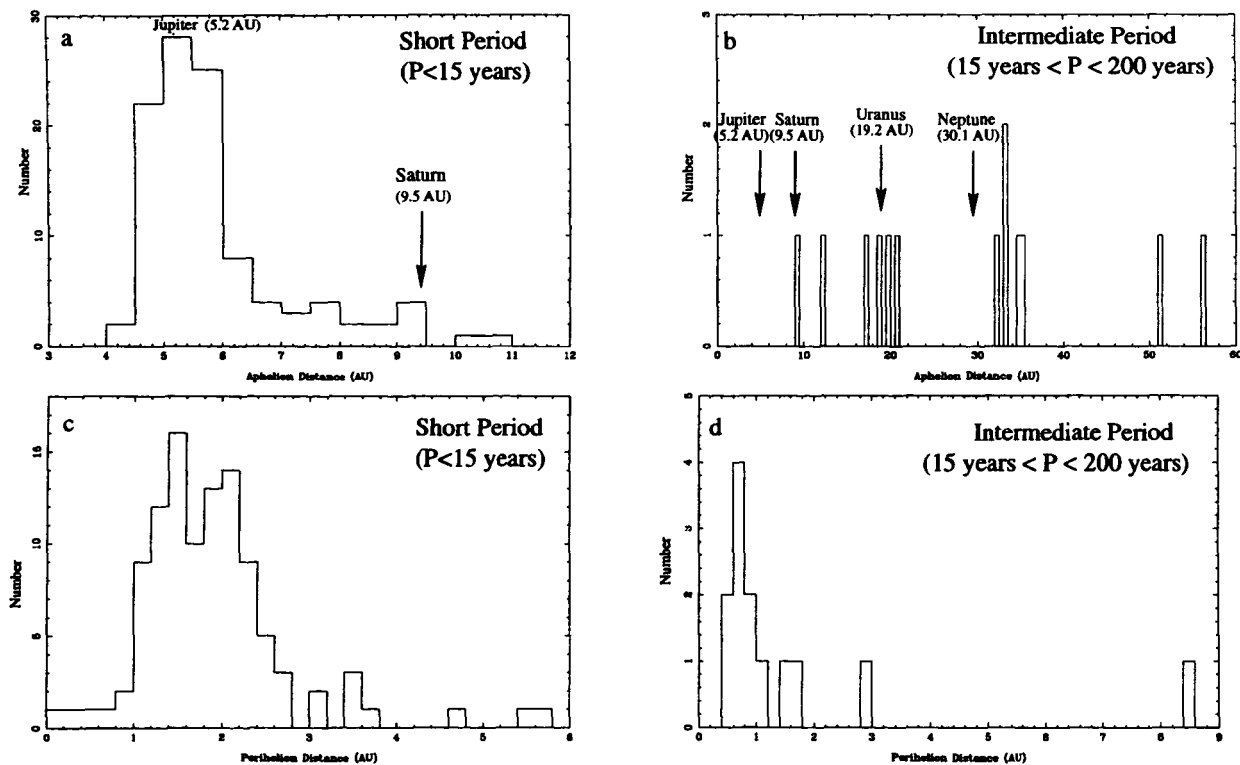


Figure 2.2: Plot (a) and plot (b) show the **aphelia** of 106 short period comets and 13 intermediate period comets respectively. Both plots have a bin size of  $\Delta Q = 0.5$  AU. Plot (c) and plot (d) show the **perihelia** of 106 short period comets and 13 intermediate period comets respectively. Both plots have a bin size of  $\Delta q = 0.2$  AU.

The close relationship between short period comets and Jupiter can be seen in the distribution of aphelia in plot (a). Short period comets were captured onto their present orbits by Jupiter and so the distribution peaks at the semi-major axis of Jupiter (5.2 AU). The intermediate period comets have aphelia up to 56 AU. Short period comets usually have perihelia within the orbit of Jupiter. From the sample of 106 comets, 104 have perihelion distances  $q \leq 5$  AU. The intermediate period comets have perihelia up to 8.5 AU. Planetary elements were taken from Karttunen et al. (1987).

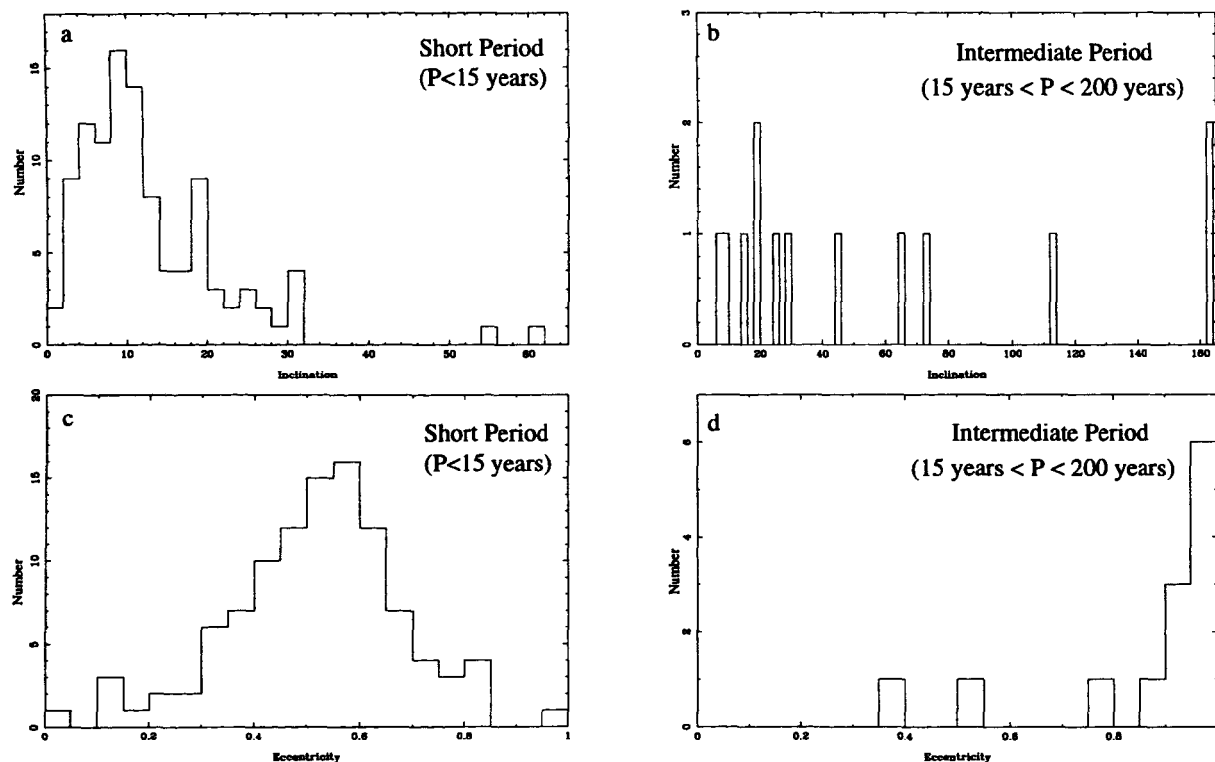


Figure 2.3: Plot (a) and plot (b) show the orbital **inclination** of 106 short period comets and 13 intermediate period comets respectively. The bin size for both plots is  $\Delta i = 2^\circ$ . Plot (c) and plot (d) show the **orbital eccentricity** of 106 short period comets and 13 intermediate period comets respectively. The bin size for both plots is  $\Delta e = 0.05$ . Short period comets have inclinations confined to a smaller range than those for the intermediate period class. Of the 106 short period comets, 104 have inclinations  $i \leq 32^\circ$ . Although there are only 13 comets in the intermediate period sample, the range of inclinations extends up to  $162^\circ$ . Short period comets also have eccentricities confined to a smaller range than those of the intermediate period class. Of the 106 short period comet 75 (71%) have an eccentricity  $e \leq 0.6$ . From the sample of 13 intermediate period comets 10 (77%) have an eccentricity  $e \geq 0.85$ . Planetary elements were taken from Karttunen et al. (1987).

and Na.

As the comet approaches the inner Solar-System the comet is warmed by Solar radiation until the temperature is sufficient for sublimation of the ice to occur. This should occur at a heliocentric distance of 2.8 AU<sup>2</sup>.

As the ice sublimates, the meteoric material contained within the ice is released. Whipple then states that “meteoric material below some limiting size will blow away because of the low gravitational attraction of the nucleus and will begin the formation of a meteor stream”. In the Whipple model any meteoric particles larger than this limiting size remain on the surface of the cometary nucleus and act as an insulating layer, protecting the underlying ice from further sublimation.

### 2.3.2 The Current Model

Greenberg (1998) constrained the chemical composition of the nucleus by combining a) the core-mantle model of interstellar dust<sup>3</sup>, b) the abundance of Solar System dust, c) observations of the composition of dust from 1P/Halley, as observed by *Giotto/VEGA* and d) data on molecules found in cometary comae.

He concluded that up to  $\sim 30\%$  of the mass of a cometary nucleus is  $H_2O$ , 26% is in the form of silicates (combinations of Si, Mg and Fe) and the rest of the comet consists of “complex organic refractory material”, PAH particles, CO,  $CO_2$ ,  $CH_3OH$  and “other simple molecules all contained within a  $H_2O$  mixture”.

In this thesis the word ‘dust’ will be used to refer to the refractory component of the cometary nucleus. Greenberg calculated that the dust to  $H_2O$  mass ratio<sup>4</sup> is

---

<sup>2</sup>At 2.8 AU a black body would have a temperature of about 236 K. For comparison, an inactive object with an albedo of 0.05 (see section (2.3.2)) would have a temperature of 233 K.

<sup>3</sup>A model where ice forms a mantle on the surface of the dust particle.

<sup>4</sup>In this thesis the dust to  $H_2O$  snow mass ratio of 1:2.2, calculated by Hughes (1996a) is

$\approx 2 : 1$ .

Essentially, the current concept of the cometary nucleus is very similar to the Whipple model. The main difference is that the density of cometary nuclei in the current models are lower, *i.e.* the nucleus is more like a snow-ball rather than an ice-ball. Based on a cometary nucleus of the above chemical composition, Greenberg constrained the upper limit of the mean density of a “fully packed” cometary nucleus to be  $\approx 1.65 \text{ gcm}^{-3}$ . Rickman et al. (1987) suggested that, in general, short period comets have densities below  $0.5 \text{ gcm}^{-3}$ . Such estimates of the density are important for cometary physics as, to date, the mass of cometary nuclei have not been directly measured. Once a density has been assumed the mass of the comet can be calculated. For example, Hughes (1985) assumed a density of  $0.5 \text{ gcm}^{-3}$  for the nucleus of 1P/Halley, and by assuming a diameter of 9.4 km, calculated a mass  $2.2 \times 10^{17} \text{ g}$ .

The study of comet 1P/Halley, during its 1986 apparition, by the space probes *Giotto* and *VEGA* has provided the only detailed view, to date, of a cometary nucleus. Because of this, 1P/Halley is often used as a standard short period comet even though it is in the intermediate period class. Although a sample size of one is clearly unsatisfactory, 1P/Halley will remain the standard comet until space probes investigate other cometary nuclei.

Figure (2.4) shows a diagram of a cometary nucleus. *Giotto* measured the size of the nucleus of 1P/Halley and found that the nucleus was non-spherical and had semi-major axes of 8 km, 4.1 km and 4.2 km (Keller et al. 1987). Comets are dark objects and have a mean albedo of  $0.05 \pm 0.04$  (Hartmann et al. 1987).

---

used. Although this differs from the Greenberg value, the main conclusions in this thesis are not significantly altered by changing this ratio.

The surface of the nucleus is likely to be covered in a layer of dust particles that were too massive to be propelled to the escape velocity by the subliming gas. The escape velocity for 1P/Halley is  $2 \text{ ms}^{-1}$  and the largest masses capable of leaving the surface may be  $\sim 1 \text{ kg}$  (Green et al. 1987).

Activity on the 1P/Halley nucleus was confined to 3 distinct regions which constituted only 10% of the nucleus surface (Keller et al. 1987). It is expected that over the lifetime of a comet, individual active areas will have a finite lifetime and that new active areas will form on different regions of the nucleus. If active areas remained in the same place then the cometary nucleus would have an irregular shape instead of the potato shape shown in figure (2.4).

Hughes (1988b) examined the absolute magnitude of 1P/Halley over the last 2000 years and by assuming negligible change in the dimensions of the nucleus, concluded that the mean percentage of the nucleus surface that is active is 3.4%. In chapter (4) the percentage of the nucleus surface that is active is calculated for 2P/Encke, 4P/Faye, 7P/Pons-Winnecke and 10P/Tempel 2. The variation in these active areas is used to explain the change in the absolute magnitude,  $H_{10}$ , of these comets over several apparitions.

## 2.4 Dust Released from Short Period Comets

### 2.4.1 Dust Ejection

As dust is released from the snow it is pushed away from the cometary nucleus by the subliming gas molecules. After a few kilometres the dust reaches its terminal ejection velocity, after which the orbit of the dust particle is determined by solar

radiation pressure and solar gravity (Richter et al. 1991). The ejection of dust and gas from the nucleus produces a recoil effect, or non-gravitational force which will alter the orbit of the comet.

The velocity at which dust is released from the nucleus will be determined by the mass of the dust particles as well as the velocity of the sublimating

the altitude of the particles with

the nucleus is the coma

A nucleus of size

it is formed from the dust and larger particles) of the nucleus.

Several images have been associated with short period comets. For exam-

Comets are dark objects with a mean albedo of  $0.05 \pm 0.04$  (Hartmann et al. 1987). The surface of the nucleus is probably covered in dust particles too massive to be propelled by the sublimating gas up to the escape velocity ( $2 \text{ ms}^{-1}$  for 1P/Halley). In the case of 1P/Halley only 10% of the surface of the nucleus was active and occurred in 3 discrete regions called 'active areas'.

dust that must have been released by the cometary nucleus to form the stream. For example, Seki (1987) found the masses of the Quadrantid, Perseid and Geminid streams to be  $6 \times 10^{14} \text{ g}$ ,  $2 \times 10^{15} \text{ g}$  and  $9 \times 10^{14} \text{ g}$  respectively, while Hughes (1989)

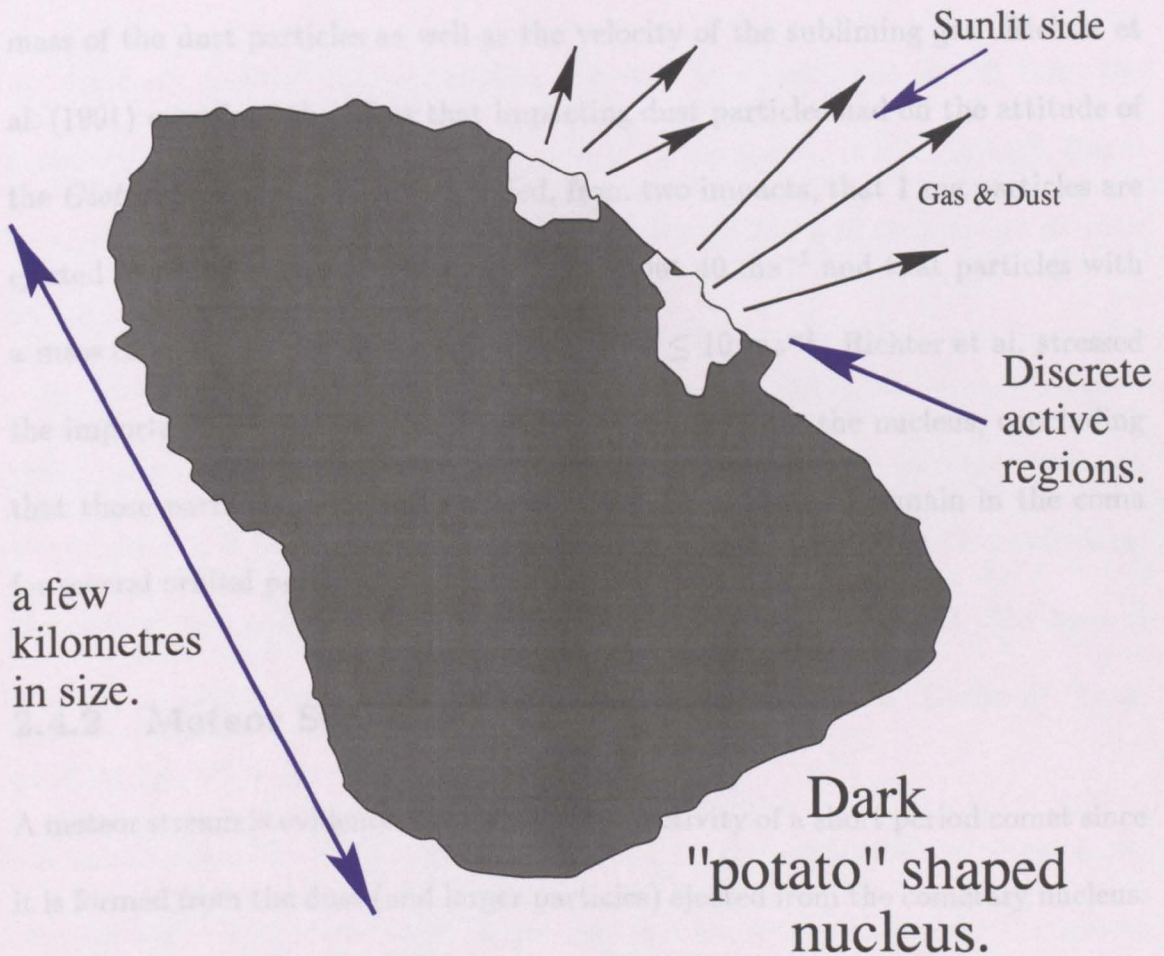


Figure 2.4: The *Giotto* space probe confirmed the idea of a single cometary nucleus. 1P/Halley appeared to be approximately potato shaped with semi-major axes of 8 km, 4.1 km and 4.2 km (Keller et al. 1987).

radiation pressure and solar gravity (Richter et al. 1991). The ejection of dust and gas from the nucleus produces a rocket effect, or *non-gravitational force* which will alter the orbit of the comet.

The velocity at which dust is released from the nucleus will be determined by the mass of the dust particles as well as the velocity of the subliming gas. Richter et al. (1991) examined the affect that impacting dust particles had on the attitude of the *Giotto* space craft. They concluded, from two impacts, that 1 mg particles are ejected from the nucleus with velocities of about  $40 \text{ ms}^{-1}$  and that particles with a mass of about 10 mg have ejection velocities  $\leq 10 \text{ ms}^{-1}$ . Richter et al. stressed the importance of these low dust ejection velocities from the nucleus, concluding that those particles with ejection velocities  $\leq 10 \text{ ms}^{-1}$  could remain in the coma for several orbital periods.

## 2.4.2 Meteor Streams

A meteor stream is evidence for the long term activity of a short period comet since it is formed from the dust (and larger particles) ejected from the cometary nucleus. Several meteor streams have been associated with short period comets. For example, the  $\eta$  Aquarids and the Orionids are associated with 1P/Halley and the Taurids and daytime  $\beta$  Taurids are associated with 2P/Encke (Brandt & Chapman 1981).

The association of meteor streams with comets has allowed some authors (e.g. Hughes & McBride (1989), Kresáková (1987), Štohl (1987)) to calculate the mass of dust that must have been released by the cometary nucleus to form the stream. For example, Štohl (1987) found the masses of the Quadrantid, Perseid and Geminid streams to be  $6 \times 10^{13} \text{ g}$ ,  $2 \times 10^{15} \text{ g}$  and  $9 \times 10^{14} \text{ g}$  respectively, while Hughes (1989)

found the same streams to have masses of  $1.3 \times 10^{15}$  g,  $3.1 \times 10^{17}$  g and  $1.6 \times 10^{16}$  g respectively. Clearly, there is a significant uncertainty when deducing such values.

## 2.5 The Lifetime of a Comet

As cometary mass is not replenished, the rate at which mass is lost from the cometary nucleus will determine the ‘lifetime’ of the comet. It is important, therefore, to be able to calculate the mass of dust that is released by a comet at each apparition.

As more dust is released, the total surface area of the dust in the coma, which will reflect solar radiation, should also increase. Thus, the more active a comet becomes, the brighter it should appear. In chapter (4) a model is presented that calculates the mass of dust released by a comet based on its absolute magnitude. The mass of dust that is released at each apparition,  $M_{ap}$ , is calculated for 2P/Encke, 4P/Faye, 6P/d’Arrest, 7P/Pons-Winnecke and 10P/Tempel 2.

A model where the cometary nucleus decays, by the sublimation of water snow, over successive apparitions until all the mass is exhausted is simplistic. Two effects which can frustrate any calculation of the lifetime of a comet are cometary outbursts and cometary dormancy. While both of these effects are beyond the scope of the models presented in this thesis, they are briefly mentioned here.

### 2.5.1 Cometary Outbursts

“Sudden and unexpected flare-ups in the brightness of a comet, normally of the order of 2-3 magnitudes, sometimes reaching 5 magnitudes, are called outbursts” (Hughes 1990). Hughes suggested that outbursts can be caused by effects internal

to the comet, such as pressure release from gas pockets or external effects, such as impacts with interplanetary boulders. In extreme cases the cometary nucleus may actually split into several components, e.g. 3D/Biela was a single object during its 1832 apparition, but by the time of its 1846 perihelion passage had split into two distinct components, and only made one more observed perihelion passage in 1852 (Marsden & Williams 1996).

Hughes (1990) suggested that outbursts are not unusual. He concluded that whether an outburst is detected or not will depend on the percentage of the nucleus surface that is active just before the outburst occurs. Hughes took the example of an outburst that increases the percentage of the active surface of the nucleus by 2%. For a comet that initially has 0.5% of its surface active this change would produce a change in the magnitude of 1.8 and would probably be noticed. For a nucleus that initially had 20% of its surface active a 2% increase would only reduce the magnitude by 0.1 and would probably go unnoticed.

Hughes (1991) examined the 1991 outburst of 1P/Halley and concluded that to produce the observed 300 fold increase in brightness the comet must have ejected  $1.4 \times 10^{13}$  g of dust. This was equivalent to 5% of the total mass of dust released by 1P/Halley,  $2.8 \times 10^{14}$  g, during its 1910 apparition (Hughes 1985).

### 2.5.2 Dormancy

During its 1986 apparition, the activity of 1P/Halley was confined to 3 regions which made up only 10% of the surface of the cometary nucleus. It is reasonable to question whether this value could ever fall as low 0%, i.e. could the comet 'switch off' and become dormant?

Kresák (1987) suggested that the active lifetimes of short-period comets are disrupted by periods of dormancy, during which the comet is completely inactive. Kresák examined pre-discovery perihelion passages of comets that should have been observed (*i.e.* they should have been bright and “favourably placed”) but were missed. He found suitable missing apparitions for 7 comets and proposed these as evidence of cometary dormancy.

Cometary dormancy has caused the mis-identification of comets as asteroids. To account for the various states of cometary activity, Hartmann et al. (1987) defined 8 terms to distinguish between different small bodies in the Solar System,

1. **“Comet (or comet nucleus):** A body containing volatiles and capable of developing a coma in its present state.
2. **Pristine comet:** A comet nucleus with its original inventory of volatiles.
3. **Active comet:** A comet nucleus losing volatiles in a detectable coma.
4. **Inactive comet:** A comet nucleus that is active during part of its orbit, but at the moment is in a part of its orbit where volatile loss is negligible, and there is no detectable coma.
5. **Dormant comet:** A comet nucleus which, although once active, has essentially no volatile loss, and hence no detectable coma in any part of its present orbit.
6. **Extinct comet:** A comet that has lost its ices, and is thus incapable of producing a coma.

7. **Asteroid:** An interplanetary body that formed without appreciable ice content, and thus never had or can have cometary activity.
8. **Minor planet:** Any interplanetary body of unknown ice content, [and is] not known to display cometary activity.”

As an example of the difficulty in distinguishing between different objects, Sekanina (1982) suggested that C/1980 E1 Bowell, which has been observed to have a coma at heliocentric distances beyond 12 AU, is an “active-looking dormant object”. He estimated that more than  $10^{13}$  g of dust is in the coma and tail but that this dust has either never been in contact with the nucleus or has not been in contact for a long time, *i.e.* there is no subliming gas to propel the dust.

## 2.6 Summary

Comets are kilometeric sized dirty snowballs. They are dark objects probably because of a dust layer which insulates the underlying snow. Activity occurs in discrete regions on the surface of the cometary nucleus. As solar radiation warms these regions the snow sublimates and releases the dust particles that were contained within it. This dust forms the coma and tail of the comet and will contribute to the formation of a meteor stream.

Short period comets,  $P \leq 15$  years, provide the best chance of observing the long term decay of the nucleus as many apparitions can be observed over a few human lifetimes. These comets are, therefore, the subject of this thesis.

# Chapter 3

## Absolute Magnitude Data

Vsekhsvyatskii (1964) in his *Physical Characteristics of Comets* stated that there are three objectives of cometary photometry:

- i “To establish the laws of brightness variation and study them for what they may reveal of the nature of cometary light production.
- ii To investigate the secular variations in brightness of periodic comets and hence the course of their disintegration.
- iii To correlate brightness fluctuations with the changes in solar activity, the comets serving as monitors.”

It is objective (ii) that is the focus of this thesis. Specifically, the relationship between the brightness of a comet and the mass of dust released per apparition from the cometary nucleus is calculated.

In order to compare different cometary apparitions a standard value of the brightness, the absolute magnitude needs to be calculated. In cometary physics, the absolute magnitude is defined as the apparent magnitude the comet would have, at

zero phase angle, if it was both 1 AU from the Sun and 1 AU from the Earth.

A study of the secular variation in cometary brightness inevitably involves the use of historical data that spans not only many decades but also many different observers and observing techniques. Thus, an absolute magnitude catalogue was required that takes account of the uncertainties in calculating individual absolute magnitudes. The catalogues that were chosen, for use throughout this thesis, were produced by Kresák and Kresáková (1989, 1994). Reasons for selecting these catalogues are given in section (3.3).

### 3.1 Cometary Brightness

Cometary brightness is principally dependent on the comet's heliocentric distance, geocentric distance and the surface area that is available for reflecting solar radiation. The geometry of the Sun-comet-Earth system (S-c-E) is shown in figure (3.1). Following Brandt and Chapman (1981), the brightness of a comet,  $B$ , is defined as,

$$B = B_o f(\Delta) F(r) p(\cos \Theta) \quad (3.1)$$

Here,  $f(\Delta)$  is a function that describes how the cometary brightness varies with geocentric distance,  $\Delta$  (AU).  $F(r)$  is a function that describes how the cometary brightness varies with heliocentric distance,  $r$  (AU).  $p(\cos \Theta)$  is a function that describes how the cometary brightness varies with the phase angle,  $\Theta$ . Usually, the

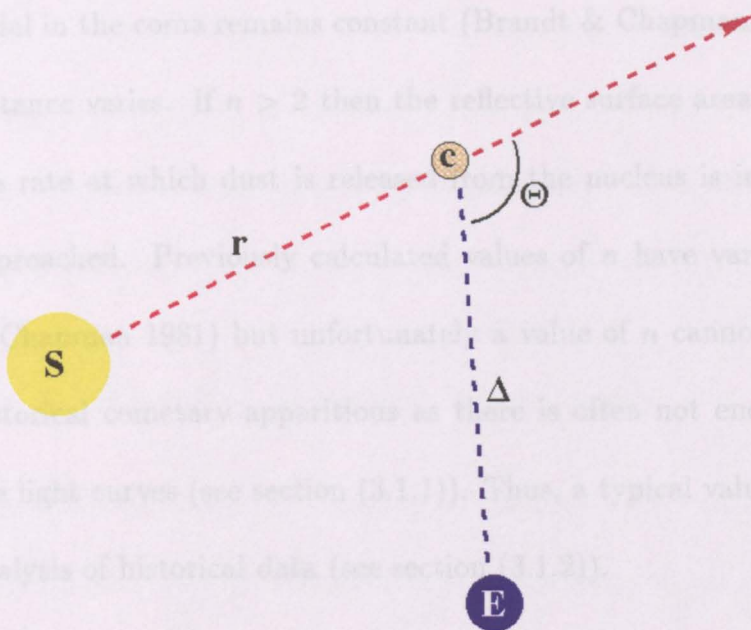


Figure 3.1: The geometry of the Sun-comet-Earth system (S-c-E). The heliocentric distance of the comet is  $r(\text{AU})$ . The geocentric distance of the comet is  $\Delta(\text{AU})$ . The angle  $\Theta$  is used to represent the phase angle of the observations. The phase angle effect is usually presumed to be negligible.

phase angle effect is assumed to be negligible for comets and this function is set to a value of unity.  $B_o$  is the brightness the comet would have at  $\Delta = 1 \text{ AU}$  and  $r = 1 \text{ AU}$ .

The functions that describe the relationship between the geocentric and heliocentric distance and the cometary brightness are normally presumed to be power laws. An inverse square relationship is normally assumed for the function  $f(\Delta)$  and a more general power law is used to describe  $F(r)$ .

Thus, equation (3.1) reduces to,

$$B = \frac{B_o}{\Delta^2 r^n}, \tag{3.2}$$

To find the absolute magnitude of a comet a light curve can be constructed such as

A value of 2 for the exponent  $n$  would indicate that the amount of reflective material in the coma remains constant (Brandt & Chapman 1981) as the heliocentric distance varies. If  $n > 2$  then the reflective surface area is increasing in size, *i.e.* the rate at which dust is released from the nucleus is increasing as perihelion is approached. Previously calculated values of  $n$  have varied from 2 to 6 (Brandt & Chapman 1981) but unfortunately a value of  $n$  cannot be calculated for many historical cometary apparitions as there is often not enough data to reconstruct the light curves (see section (3.1.1)). Thus, a typical value of  $n$  is required for the analysis of historical data (see section (3.1.2)).

### 3.1.1 The Light Curve

The brightness of a comet,  $B$ , can be converted into the apparent magnitude,  $m$ , by,

$$m - H_o = -2.5 \log \frac{B}{B_o}, \quad (3.3)$$

where the brightness  $B_o$  and the absolute magnitude,  $H_o$ , occur at  $\Delta = 1$  AU and  $r = 1$  AU.

Combining equation (3.2) and equation (3.3) produces,

$$m = H_o + 5 \log \Delta + 2.5n \log r \quad (3.4)$$

To find the absolute magnitude of a comet a light curve can be constructed such as

the one shown in figure (3.2) for 1P/Halley. The heliocentric magnitude is defined as  $m - 5 \log \Delta$  so that the effect of the comet's geocentric distance is removed. The gradients of the pre-perihelion and post-perihelion sections of the light curve will produce pre-perihelion and post-perihelion values of  $n$ . The pre-perihelion and post-perihelion values of  $H_0$  are found at  $\log r = 0$  (i.e.  $r = 1$  AU).

### 3.1.2 The $H_{10}$ Absolute Magnitude

As mentioned above, constructing a light curve, such as the one in figure (3.2), with a sufficient number of points to deduce the value of  $n$  is not always practical. This is especially true for historical data where there are often not enough observations to construct a light curve and determine the value of  $n$ . For this reason it is often necessary to find a typical value of  $n$  that can be used to represent the light curves for all historical apparitions of comets. Vsekhsyatskii (1964) examined 82 “independent observations of newly-observed comets” and concluded that comets were well represented by a mean value of  $n = 4$ .

This reduces equation (3.4) to,

$$m = H_{10} + 5 \log \Delta + 10 \log r, \quad (3.5)$$

Forcing  $n$  to a value of 4 when, as can be seen in figure (3.2), some variation from this value is expected, is clearly not satisfactory. Unfortunately, it is an assumption that has to be made because of the lack of observations necessary to recreate the light curves for many historical apparitions of short period comets.

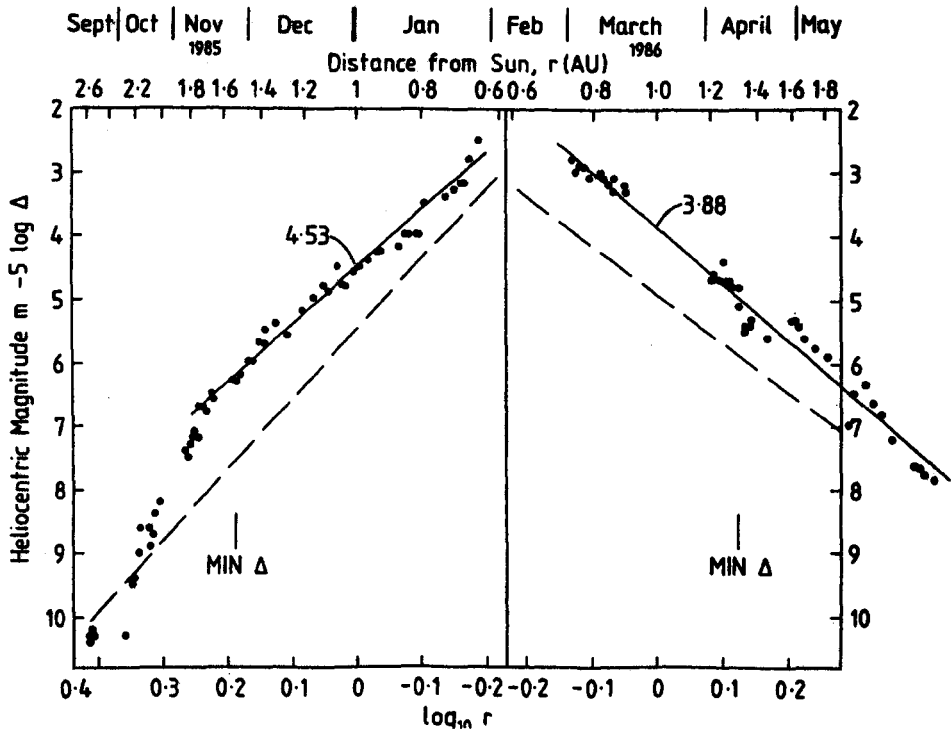


Figure 3.2: A cometary light curve taken from Hughes (1988b). The apparent magnitude is reduced to  $m - 5 \log \Delta$  (i.e. the heliocentric magnitude) and plotted against the logarithm of the heliocentric distance  $\log r(\text{AU})$  for the 1986 apparition of comet 1P/Halley. Hughes applied linear regressions to the pre-perihelion and post-perihelion data separately. Notice the pre/post perihelion asymmetry in the curve.

Allowing the gradient to be determined by the data, Hughes found that for the pre-perihelion data,  $H_o = 4.53 \pm 0.04$  and  $n = 3.37 \pm 0.14$ . For the post-perihelion data,  $H_o = 3.88 \pm 0.04$  and  $n = 3.42 \pm 0.13$ .

For historical apparitions the entire light curve normally cannot be re-constructed and a value of  $n$  must be assumed. A value of  $n = 4$  is used in the Kresák and Kresáková catalogues (1989, 1994).

## 3.2 Uncertainty in the Absolute Magnitudes

There are many uncertainties in the determination of the absolute magnitude of a comet and especially for historical data. The data set used in this thesis (see section (3.3.1)) covers a period of approximately 200 years and this is approximately the period of time during which serious observations of cometary brightness have been conducted.

In chapter (4) the secular variation in cometary absolute magnitude,  $H_{10}$ , is examined. These changes in the value of  $H_{10}$  over several apparitions are expected to be due to a combination of observational uncertainty and real changes. Thus, a catalogue of  $H_{10}$  data that accounted for as many observational uncertainties as possible was required.

### 3.2.1 Different Instruments and Different Observers

Comets appear as diffuse objects in the sky and, consequently, the uncertainty in the apparent magnitude can increase with magnification, *i.e.* at large magnifications the diffuse outer regions of the coma can be missed (Kresak & Kresakova 1987). This lead Kresák and Kresáková to state that “instrumental effects on the comet magnitude are always positive, tend to increase with the comet’s diffuseness...and can amount to more than 5 magnitudes”. Kresák (1974) concluded that “nearly 80% of the apparent secular change in absolute magnitudes is due to direct instrumental effects”.

Magnitude data for short period comets date back to the year 1678 for 6P/d’Arrest and the year 1786 for 2P/Encke<sup>1</sup>. Since the data covers a period of time that is

---

<sup>1</sup>Although 1678 is currently the date of the earliest recorded apparition of a short period

longer than a human lifetime, an investigation into the progressive variation in cometary magnitudes will need to use magnitudes produced by different observers. An inconsistency between magnitudes estimated at different times using different instruments is to be expected, and Kresák (1974) concluded that “the principle source of systematic deviations in the photometric data on comets is the use of largely different instruments and techniques”.

### 3.2.2 The Holetschek Effect

The geometry of the Sun-comet-Earth system can make a comet difficult to observe from the Earth, and this is sometimes referred to as the ‘Holetschek effect’. The geometry is defined by comparing the heliocentric longitude of the perihelion of the comet,  $\lambda_c$ , and the heliocentric longitude of the Earth at the time of the comet’s perihelion,  $\lambda_\oplus$  (see Hughes (1983a) for derivations of these parameters).

Figure (3.3) shows the geometry of the situation. The perihelion of the comet,  $q$ , is dropped onto the plane of the Earth’s orbit. The first point of Aries is indicated by the symbol  $\gamma$ . The angle  $\gamma SA$  is the heliocentric longitude of the comet,  $\lambda_c$ . At the time of cometary perihelion the Earth is in position  $B$  and has a heliocentric longitude of  $\gamma SB$ . The angle  $j = | \lambda_\oplus - \lambda_c |$  is defined as a measure of the quality of the observing geometry. It is expected that viewing conditions are good if  $j$  is small, while as  $j$  approaches  $180^\circ$  the viewing conditions should be poorer.

The Holetschek effect is considered in chapter (4) as a source of uncertainty in the

---

( $P < 15$  years) comet, it was only identified with 6P/d’Arrest more recently by Carusi et al. (1991). A few single apparitions of short period comets have occurred since 1678, such as D/1766 G1 Helfenzrieder ( $P = 4.35$  years) and D/1783 W1 Pigott ( $P = 5.89$  years) but these are now classified as defunct comets (Marsden & Williams 1996). There is then a large gap in the records of *identified non-defunct* short period comets until the first recorded apparition of 2P/Encke in 1786.

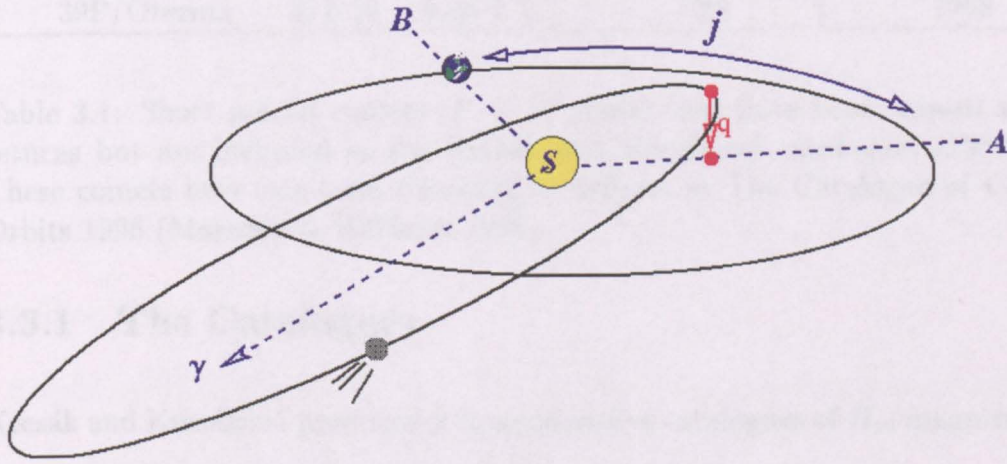


Figure 3.3: The Holetschek Effect. The perihelion point of the comet is dropped onto the plane of the Earth's orbit (shown in red). The angle between this new point and the position of the Earth at the time of the cometary perihelion is the  $j$  angle. It is expected that 'bad' observing geometry occurs as  $j$  tends to  $180^\circ$ . The first point of Aries is indicated by the symbol  $\gamma$ , and defines a fixed point so that  $j = |\gamma SB - \gamma SA|$ .

absolute magnitudes,  $H_{10}$ , calculated for the apparitions of short period comets.

### 3.3 The Kresák and Kresáková $H_{10}$ Catalogues

Several catalogues of  $H_{10}$  magnitudes have been compiled by different authors.

Vsekhsvyatskii (1964) produced a comprehensive catalogue that has served as the basis for many subsequent catalogues, such as the one produced by Hughes (1987).

The main problem with these catalogues is that there is no estimate of the uncertainty on each quoted value of  $H_{10}$ . This was the principle reason for selecting the

Kresák and Kresáková catalogues (1989, 1994) as the source of  $H_{10}$  data for this

thesis.

Comet	q (AU)	e	$\bar{H}_{10}$	Orbital Period (years)	Last recorded perihelion passage
18P/Perrine-Mrkos	1.29	0.64	10.0	6.72	1909
34P/Gale	1.21	0.76	9.5	11.0	1938
39P/Oterma	5.50	0.24	4.1	7.88	1958

Table 3.1: Short period comets ( $P < 15$  years) that have been missed at recent returns but are included in the Kresák and Kresáková catalogues (1989, 1994). These comets have not been classified as defunct in The Catalogue of Cometary Orbits 1996 (Marsden & Williams 1996).

### 3.3.1 The Catalogues

Kresák and Kresáková produced 2 comprehensive catalogues of  $H_{10}$  magnitude data principally based on the Vsekhsvyatskii  $H_{10}$  data set. The first catalogue (Kresák & Kresáková 1989) lists 575 apparitions of 144,  $P < 200$  years, comets observed from 1770<sup>2</sup> to 1987. For 90 of these comets more than one apparition was recorded and a weighted mean absolute magnitude,  $\bar{H}_{10}$ , calculated.

The update to this catalogue (Kresák & Kresáková 1994) lists the  $H_{10}$  magnitudes for 86 cometary apparitions from 1988 until 1993. This increases the number of comets with more than one apparition to 106. Of these, the number of comets with more than one apparition recorded in the catalogues *and* an orbital period less than 15 years is only 90. From these 90 short period comets, table (3.1) lists 3 which have been missed at recent returns (Marsden & Williams 1996) but are recorded in the Kresák and Kresáková catalogues. These have not yet been classified as defunct and so are not removed from the list of absolute magnitudes used in this thesis.

---

<sup>2</sup>D/1770 L1 Lexell had an orbital period calculated at 5.6 years but only one apparition has been recorded since this time and it is thus classified as a defunct comet (Marsden & Williams 1996).

### 3.3.2 Maximum Absolute Brightness

Kresák and Kresáková (1987) did not calculate their values of  $H_{10}$  from a light curve such as that in figure (3.2). Instead, they considered only the time of maximum absolute brightness of the comet and found the apparent magnitude,  $m$ , at that time. This apparent magnitude was then corrected for observational uncertainty (see section (3.3.3)), and the corrected absolute magnitude,  $m_c$ , was used to calculate  $H_{10}$ .

Kresák and Kresáková considered the technique of using only one apparent magnitude to calculate  $H_{10}$  to have two advantages:

1. The maximum absolute brightness should be less susceptible to instrumental uncertainties than other parts of the light curve.
2. The maximum absolute brightness should occur close to the peak of the mass loss rate which is important for a study of the comet's decay.

### 3.3.3 The Corrected Apparent Magnitude

The corrected apparent magnitude, *at the time of maximum absolute brightness*,  $m_c$ , is related to  $H_{10}$  by,

$$m_c = H_{10} - 5 \log \Delta_{m_c} + 10 \log r_{m_c}, \quad (3.6)$$

where  $r_{m_c}$  is the heliocentric distance of the comet and  $\Delta_{m_c}$  is the geocentric distance of the comet at the time of maximum cometary brightness.

Kresák and Kresáková assumed that brighter comets are easier to observe and so applied a larger correction to the fainter comets. Their correction was based on an empirical technique developed in an earlier paper (Kresak & Kresakova 1987), and the relationship between  $m$  and the corrected apparent magnitude,  $m_c$ , that they used was,

$$m_c = m, \quad (3.7)$$

for comets observed with an apparent magnitude,  $m \leq 9$ .

$$m_c = 0.5m + 4.5, \quad (3.8)$$

for  $9 \leq m \leq 14$  and

$$m_c = 0.3m + 7.3, \quad (3.9)$$

for  $m \geq 14$ .

Thus, fainter comets are harder to observe and so have a larger correction factor.

### 3.3.4 $H_{10}$ Weighting

For each value of  $H_{10}$  that Kresák and Kresáková calculated they also produced a corresponding  $H_{10}$  weight. This weight,  $W$ , was defined by,

$$W = 1 - |\log r| - 0.1(m - m_c), \quad (3.10)$$

where  $r(\text{AU})$  is the heliocentric distance at which the apparent magnitude,  $m$ , is reached.  $m_c$  is the corrected apparent magnitude discussed in section (3.3.3).

This means that large corrections applied to the minimum apparent magnitude produce small weights. Correspondingly, those comets that reach maximum absolute brightness at a heliocentric distance close to the orbit of the Earth (*i.e.*  $r = 1 \text{ AU}$ ) will also have a larger weighting. Thus, these weights account for an uncertainty in the ability of the observer to determine the magnitude of a comet and one aspect of the cometary observing geometry.

The  $H_{10}$  weights for 5 short period comets are shown in section (4.4.1) and are used in chapter (4) to see if they can account for the variation in  $H_{10}$ , from apparition to apparition, for these comets.

### 3.4 Summary

Absolute magnitude data that spans a period of 200 years will be subject to many uncertainties. Unfortunately, the use of these historical data is essential if any conclusions are to be made about the long term activity of short period comets.

As the light curves for many cometary apparitions cannot be recreated a typical value for the exponent,  $n$ , was required to be used in equation (3.4). Vsekhsyatskii (1964) used a mean value of  $n = 4$ , and this produces the absolute magnitude  $H_{10}$ . As his catalogues form the basis of many subsequent catalogues (*e.g.* Hughes

(1987)), this is a commonly used form of the absolute magnitude.

Since historical  $H_{10}$  data can be subject to considerable error it was essential that the  $H_{10}$  catalogue used in this thesis accounted for as many of the uncertainties as possible. The Kresák and Kresáková catalogues account for two uncertainties, both the ability of the observer to estimate the brightness of the comet (see the  $m_c$  correction), and the heliocentric distance of the comet at the time of maximum brightness, such that comets that reach maximum brightness close to 1 AU from the Sun have larger  $H_{10}$  weights. For this reason these catalogues were chosen as the source of the  $H_{10}$  data used throughout this thesis.

The  $H_{10}$  data is used for several different purposes in this thesis. In chapter (4) the secular variation in  $H_{10}$  for 5 comets is examined. In chapter (5) and in chapter (6) the weighted mean absolute magnitude,  $\bar{H}_{10}$ , for each comet is used to calculate the size of each cometary nucleus and the fraction of the cometary nucleus surface that is active.

# Chapter 4

## Secular Variation in Cometary

## Activity

### 4.1 Introduction

The manner in which short period comets decay is of fundamental importance for determining how long short period comets will remain active and the rate of their decay.

The variation in the absolute magnitude,  $H_{10}$ , over several apparitions is examined for 2P/Encke, 4P/Faye, 6P/d'Arrest, 7P/Pons-Winnecke and 10P/Tempel 2. Changes in the value of  $H_{10}$  may be due to changes in the size of the cometary nucleus, changes in the size of the active areas on the surface of the nucleus, observational uncertainty or a combination of these factors.

For three of the above comets, estimates of the size of the cometary nucleus were obtained from other authors, and used to calculate the variation in the fraction of the surface area of the nucleus that is active from apparition to apparition. In this

chapter, the variation in the size of active areas on the nucleus is presented as an explanation for much of the temporal variation in  $H_{10}$ . A model is presented that relates  $H_{10}$  to the mass of dust that a comet releases at each apparition,  $M_{ap}$ .

## 4.2 A Shrinking Nucleus or a Change in the Size of the Active Areas

The Kresák and Kresáková catalogues (1989, 1994) cover a period of approximately 200 years of cometary absolute magnitudes. While this period is long when compared to a human lifetime, meaning that observations of a single comet will be made by many different people, it may not be a long enough period for the cometary nucleus to have noticeably decayed (see section (5.4.2) for a discussion about the depth of material lost from the cometary nucleus at each apparition).

Hughes (1989a) calculated the equivalent radius,  $R$ , of short period cometary nuclei by using the mean absolute magnitude of comet 1P/Halley over the last 2000 years ( $5.5 \pm 0.7$ ), and by assuming that the mean density of the nucleus is  $0.2 \text{ gcm}^{-3}$ . He found that,

$$\log R(\text{km}) = 1.114 - 0.5 \log f - 0.2H_{10}, \quad (4.1)$$

where  $H_{10}$  is the absolute magnitude of the comet and  $f$  is the fraction of the nucleus surface that is active.

Hughes then set  $f$  to 0.034, the average fraction of the nuclear surface that has been active during the last 2000 years (Hughes 1988b). This reduced equation (4.1)

to,

$$\log R(km) = 1.848 - 0.2H_{10} \quad (4.2)$$

Equation (4.2) can then be converted into a form which relates the mass of the cometary nucleus,  $M$ , to the absolute magnitude,  $H_{10}$ ,

$$\log M(g) = A - BH_{10}, \quad (4.3)$$

where  $A$  and  $B$  are constants.

Hughes and Daniels (1983) found that previous authors had suggested values of  $A$  ranging from 19.39 to 21 and values of  $B$  from 0.4 to 0.6. Assuming a mean density of  $0.5 \text{ gcm}^{-3}$  for the cometary nucleus, equation (4.2) implies that  $A = 20.87$  and  $B = 0.6$ .

Differentiating equation (4.3) produces,

$$\Delta H_{10} \approx - \left( \frac{\log e}{B} \right) \frac{\Delta M}{M} \quad (4.4)$$

In equation (4.4)  $\frac{\log e}{B} = 0.7$ , however, Hughes and Daniels considered the values of  $A$  and  $B$  used by different authors and concluded that,

$$\Delta H_{10} \cong -0.9 \frac{\Delta M}{M}, \quad (4.5)$$

was a good approximation for the short period comet population.

Equation (4.5) means that the expected rate of change in the absolute magnitude should be very small compared with the rate at which mass is released from the cometary nucleus. To see a change in absolute magnitude of 0.5 a comet would have to release 56% of its total mass. A change of 1 magnitude would require the comet to lose more than its total mass. Thus, Hughes limits the usefulness of equation (4.5) to  $\Delta M \ll M$ .

This indicates that variations in the absolute magnitude from apparition to apparition for a short period comet are unlikely to be due to a substantial change in the mass (or size) of the cometary nucleus. Hughes (1983) considered a mean value of  $\Delta H_{10} = 0.002$  to be reasonable for short period comets which is equivalent to a 0.18% mass loss per perihelion passage.

The alternative to a quickly decaying nucleus is that any variations in  $H_{10}$  are either due to observational uncertainty or a varying degree of activity on the cometary nucleus. The aim of this chapter is to see if the changes in the fraction  $f$  in equation (4.1) can account for secular changes in the absolute magnitudes of short period comets.

Comet	P (years)	Observational Interval	$N_{ap}$	$N_m$	%
2P/Encke	3.28	1786-1990	55	8	12.7
6P/d'Arrest	6.51	1851-1989	15	7	31.8
4P/Faye	7.34	1843-1991	19	2	9.5
7P/Pons-Winnecke	6.37	1819-1989	20	4	16.7
10P/Tempel 2	5.48	1873-1988	18	5	21.7

Table 4.1: Over the last 200 years of observation many apparitions of short period comets have been missed. The orbital period,  $P$ , is the most recent value given in Marsden (1996). ‘Observational Interval’ is the time period over which the magnitudes have been recorded in the Kresák and Kresáková catalogues (1989, 1994).  $N_{ap}$  is the number of apparitions observed during this time.  $N_m$  is the number of apparitions missed and this is expressed as a percentage of the total number of apparitions in the final column.

### 4.3 $H_{10}$ Absolute Magnitudes

Kresák and Kresáková (1989, 1994) produced two catalogues of  $H_{10}$  absolute magnitude data for the short period comet population. The typical orbital period for a short period comet is approximately 8 years. This means that, over the last 200 years of scientific study, a maximum of 25 cometary apparitions could have been recorded for a ‘typical’ short period comet. Unfortunately, for most short period comets, there is not even a record of 25 apparitions. Of the 90 *non-defunct* comets in the Kresák and Kresáková catalogues, that have had more than 1 recorded apparition, only 16 have 10 or more apparitions recorded. 2P/Encke is exceptional because of its 3.3 year orbital period and has 55 recorded apparitions.

From the list of 90 comets, 5 were chosen that had more than 10 recorded apparitions. These were: 2P/Encke, 4P/Faye, 6P/d'Arrest, 7P/Pons-Winnecke and 10P/Tempel 2. Table (4.1) lists the latest orbital periods from the *Catalogue of Cometary Orbits* (Marsden & Williams 1996) and the number of recorded and missed apparitions from the Kresák and Kresáková catalogues.

Comet	Linear Regression	$\sigma_g$	$\sigma_i$	$N_{ap}$	$r^2$
2P/Encke	$H_{10} = 0.098t - 9.4$	0.002	4.0	55	0.29
4P/Faye	$H_{10} = 0.018t - 27.3$	0.004	7.5	19	0.55
6P/d'Arrest	$H_{10} = -0.003t + 13.7$	0.006	10.6	15	0.02
7P/Pons-Winnecke	$H_{10} = 0.009t - 8.1$	0.006	11.9	20	0.10
10P/Tempel 2	$H_{10} = -0.007t + 21.1$	0.005	10.3	18	0.10

Table 4.2: The equations of the linear regressions shown in figure (4.1). The uncertainty in the gradients,  $\sigma_g$  and the intercepts,  $\sigma_i$ , are large. The coefficient of determination,  $r^2$ , indicates that these data are not well described by a straight line.

### 4.3.1 Secular Variation in $H_{10}$ Calculated from a Linear Regression

The traditional approach to treating the long term variation in absolute magnitude data is to plot  $H_{10}$  against time and use a linear regression analysis to find the best fit to the data (Hughes 1983b; Svoreň 1991). The linear regressions are then used to infer the fading rate of the comet.

Linear regressions were applied to the  $H_{10}$  data for 2P/Encke, 4P/Faye, 6P/d'Arrest, 7P/Pons-Winnecke and 10P/Tempel 2, and the fits are shown in figure (4.1). Table (4.2) lists the equations of the lines shown in figure (4.1). The fits are not impressive. This can be seen by the large standard deviations in the gradients and the intercepts. Also listed in table (4.2) are the coefficient of determination,  $r^2$ , for each linear regression. This indicates how well the data is described by a straight line. A value of 1 would indicate that all observed points lie on a straight line (Chatfield 1970). The largest value of  $r^2$  is only 0.55 for 4P/Faye.

One aim of this chapter is to see if there is more information in the  $H_{10}$  absolute magnitude data than can be provided by these linear regressions.

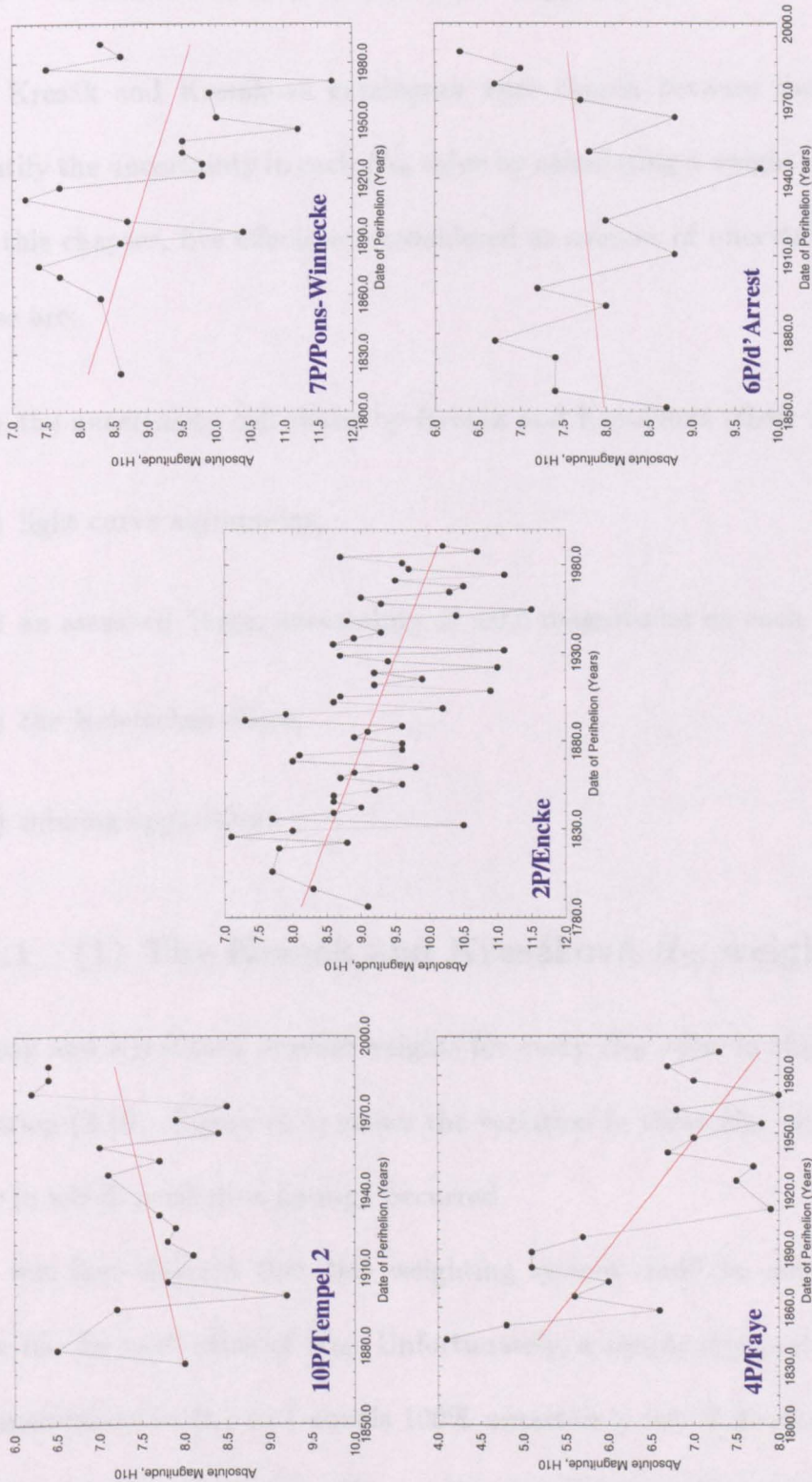


Figure 4.1: The variation in  $H_{10}$  absolute magnitude with the year in which perihelion passage occurred. Linear regressions indicate that while 2P/Encke, 7P/Pons-Winnecke and 4P/Faye are fading, 10P/Tempel 2 and 6P/d'Arrest are *increasing* in brightness. This cannot be reconciled with a variation in the size of the cometary nucleus as it implies that these nuclei are increasing in size. The equations of the lines are shown in table (4.2).

## 4.4 Uncertainties in the $H_{10}$ Data

The Kresák and Kresáková catalogues were chosen because they attempted to quantify the uncertainty in each  $H_{10}$  value by calculating a weight (see chapter (3)).

In this chapter, five effects are considered as sources of uncertainty in the data.

These are:

- (1) the uncertainty calculated by Kresák and Kresáková (their  $H_{10}$  weights),
- (2) light curve asymmetry,
- (3) an assumed, large, uncertainty of  $\pm 0.5$  magnitudes on each value of  $H_{10}$ ,
- (4) the Holetschek effect,
- (5) missing apparitions.

### 4.4.1 (1) The Kresák and Kresáková $H_{10}$ weights

Kresák and Kresáková provide weights for every  $H_{10}$  value in their catalogue (see equation (3.10)). Figure (4.2) shows the variation in these  $H_{10}$  weights against the year in which perihelion passage occurred.

It was first thought that this weighting system could be used to produce an error bar for each value of  $H_{10}$ . Unfortunately, a simple interpretation of 0 equals no uncertainty in  $H_{10}$  to 1 equals 100% uncertainty would produce unrealistically large errors. For example, a  $H_{10}$  weight of  $w = 0.5$  would correspond to a  $\pm 50\%$  uncertainty in  $H_{10}$ . Thus, a comet with  $H_{10} = 7.0$  would have an uncertainty of  $\pm 3.5$  magnitudes. It is concluded that a scaling factor would be required to use

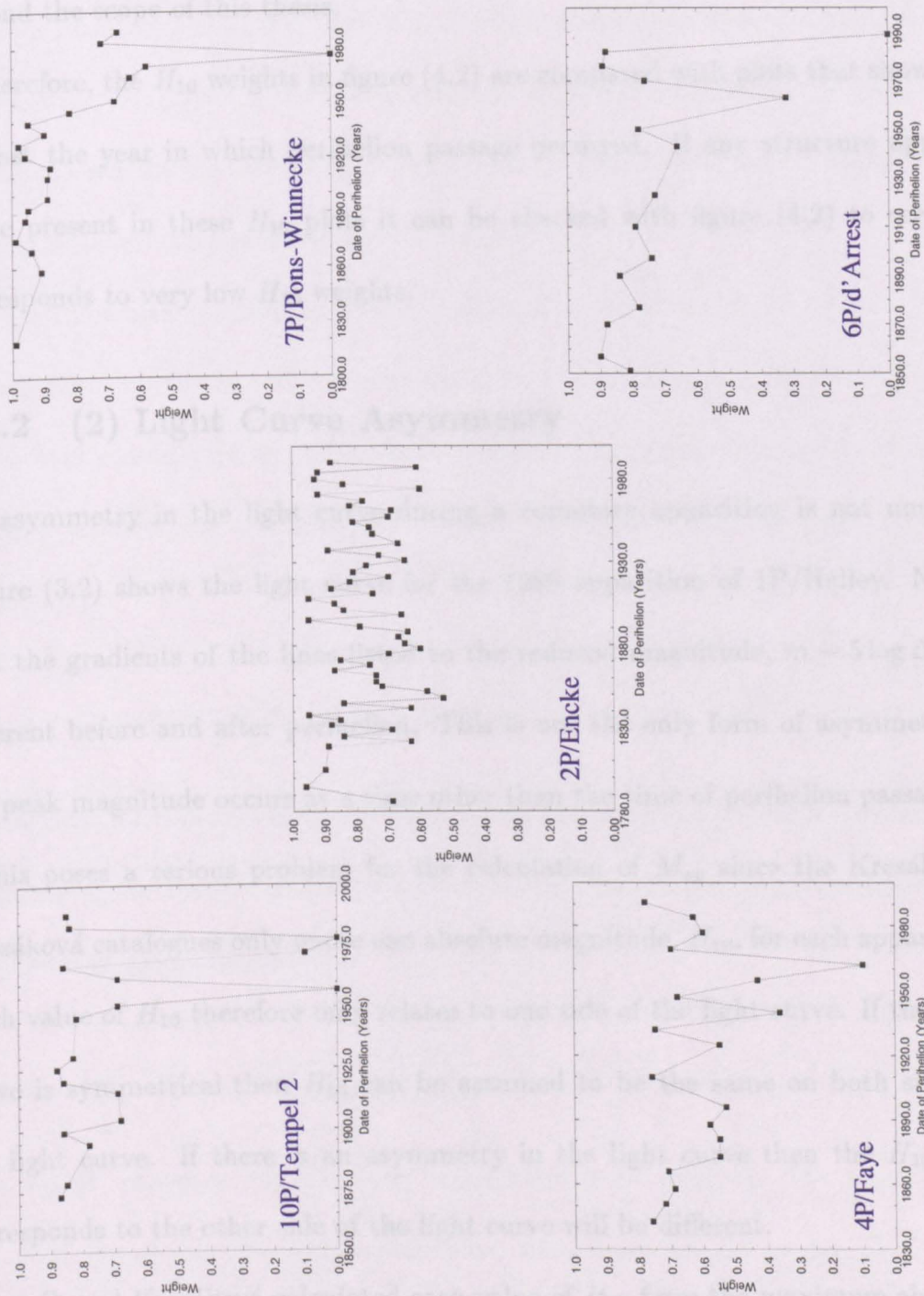


Figure 4.2: The  $H_{10}$  weights calculated by Kresák and Kresáková (1989, 1994) using equation (3.10). Notice that 2P/Encke has a relatively stable orbit and so the weights never fall below 0.5. The weights were used by Kresák and Kresáková to calculate the mean absolute magnitude  $\bar{H}_{10}$  for each comet. Although these weights are not used to find an absolute uncertainty on each value of  $H_{10}$  they are compared with the temporal variation in  $H_{10}$ , such as in figure (4.1), to see if they explain the scatter of the data points.

these weights as uncertainties in individual values of  $H_{10}$ . Unfortunately, this is beyond the scope of this thesis.

Therefore, the  $H_{10}$  weights in figure (4.2) are compared with plots that show  $H_{10}$  against the year in which perihelion passage occurred. If any structure appears to be present in these  $H_{10}$  plots it can be checked with figure (4.2) to see if it corresponds to very low  $H_{10}$  weights.

#### 4.4.2 (2) Light Curve Asymmetry

An asymmetry in the light curve during a cometary apparition is not unusual. Figure (3.2) shows the light curve for the 1986 apparition of 1P/Halley. Notice that the gradients of the lines fitted to the reduced magnitude,  $m - 5 \log \Delta$ , are different before and after perihelion. This is not the only form of asymmetry as the peak magnitude occurs at a time other than the time of perihelion passage.

This poses a serious problem for the calculation of  $M_{ap}$  since the Kresák and Kresáková catalogues only quote one absolute magnitude,  $H_{10}$ , for each apparition. Each value of  $H_{10}$  therefore only relates to one side of the light curve. If the light curve is symmetrical then  $H_{10}$  can be assumed to be the same on both sides of the light curve. If there is an asymmetry in the light curve then the  $H_{10}$  that corresponds to the other side of the light curve will be different.

Kresák and Kresáková calculated each value of  $H_{10}$  from the maximum absolute brightness reached by the comet during each orbit. If this one  $H_{10}$  value is used to calculate the mass of dust released from both the pre-perihelion and post-perihelion parts of the cometary orbit then the final value of  $M_{ap}$  will be an over-estimate if the light curve is asymmetrical.

### 4.4.3 (3) $\pm 0.5$ Magnitude Error Bars

While it is not expected that each  $H_{10}$  absolute magnitude would in reality have a constant uncertainty (i.e. see the Kresák and Kresáková weighting system) it was considered worthwhile assigning a large error to each  $H_{10}$  absolute magnitude to see if it accounts for the scatter in the data.

A  $\pm 0.5$  magnitude uncertainty was assigned to each value of  $H_{10}$ . From the top of each error bar to the bottom corresponds to a  $\times 2.5$  change in brightness. These errors bars should give an indication of what observational uncertainty would be required to eliminate any evidence of structure in plots such as those shown in figure (4.1).

### 4.4.4 (4) The Holetschek Effect

The Holetschek effect, discussed in section (3.2.2) is examined to see if the observing geometry of the Earth-comet-Sun system is sufficient to produce structure in the  $H_{10}$  absolute magnitude plots.

### 4.4.5 (5) Missed Apparitions

The list of cometary  $H_{10}$  absolute magnitudes is incomplete. For some of the expected apparitions there are no recorded magnitudes for the comet. Table (4.1) summarises how many apparitions are missing.

Table (4.3) shows an estimate, to the nearest year, for the dates when these apparitions were missed. There are many reasons for missing apparitions. The comet may have been faint for a physical reason, perhaps it became dormant, or the observing conditions may have been poor, e.g. the geometry of the Sun-comet-

2P/Encke	6P/d'Arrest	4P/Faye	7P/Pons-Winnecke	10P/Tempel 2
1789,1792,1798, 1801,1808,1811, 1814,1944	1864,1884,1904, 1917,1930,1937, 1957	1903,1917	1863,1880,1903, 1957	1883,1888,1909, 1935,1940

Table 4.3: An estimate of the date, to the nearest year, in which expected apparitions of the comets were missing. The dates were calculated by using the orbital period of the comet just before the missing apparition. The dates for the 6P/d'Arrest missing apparitions were taken from Carusi et al. (1991).

Earth system can be such that faint comets are missed (see section (3.2.2)). Even sociological reasons, such as wars, may have considerably reduced the number of people observing comets at that particular time and caused gaps in the data set.

Table (4.1) shows that missed apparitions can form a significant percentage of the total number of perihelion passages expected. For example, nearly 32% of the expected number of apparitions between 1851 and 1981 for 6P/d'Arrest were missed. Therefore, the significance of missing apparitions in the analysis of the secular variation in  $H_{10}$  is considered for each comet.

### Can the Data be Trusted?

As it's not possible to recreate the light curve of every apparition it's probably not possible to significantly improve on the  $H_{10}$  absolute magnitudes calculated by Kresák and Kresáková. However, since the absolute magnitudes were calculated using the maximum absolute brightness of each comet *and* are empirically corrected by Kresák and Kresáková, it is not unreasonable to expect to see real trends in the  $H_{10}$  data.

## 4.5 The $M_{ap}$ Computer Program

### 4.5.1 Overview and Assumptions

A computer program was created that takes the absolute magnitude,  $H_{10}$ , the perihelion distance,  $q$  (AU) and the eccentricity,  $e$ , as the input and calculates the total mass of dust in grams released during one orbit,  $M_{ap}$ , for an individual comet. This computer program is hereafter referred to as the ' $M_{ap}$  program'.

The  $M_{ap}$  program<sup>1</sup> calculates the instantaneous dust mass-loss rate,  $\dot{m}_i$  ( $\text{gs}^{-1}$ ), at intervals of 1 day from when the comet is at perihelion until it reaches 2.8 AU. Figure (4.3) shows a diagram of the situation.  $\dot{m}_i$  is calculated for the position of the comet at the start of each day and is assumed to be valid for the whole of that day. Each value of  $\dot{m}_i$  is then multiplied by the number of seconds in a day and summed to produce the total mass of dust released during one half of the cometary orbit. If the outgassing from the comet is symmetrical about perihelion then this value is doubled to produce the total mass of dust released during one orbit.

The  $M_{ap}$  program includes several assumptions about short period comets:

1. Cometary activity is completely driven by the sublimation of water snow.
2. Short period comets are inactive at heliocentric distances greater than 2.8 AU.
3. The instantaneous dust mass-loss rate,  $\dot{m}_i$  is proportional to  $\frac{1}{r^2}$ , where  $r$  is the heliocentric distance of the comet in AU (this means that  $n = 4$ ).

The water content in cometary nuclei is normally inferred from the observations of O, H and OH in the cometary coma. These are assumed to result from the

---

<sup>1</sup>A computer program, rather than an analytical solution, was required to calculate the orbital position of the comet from perihelion to a heliocentric distance of 2.8 AU in daily intervals.

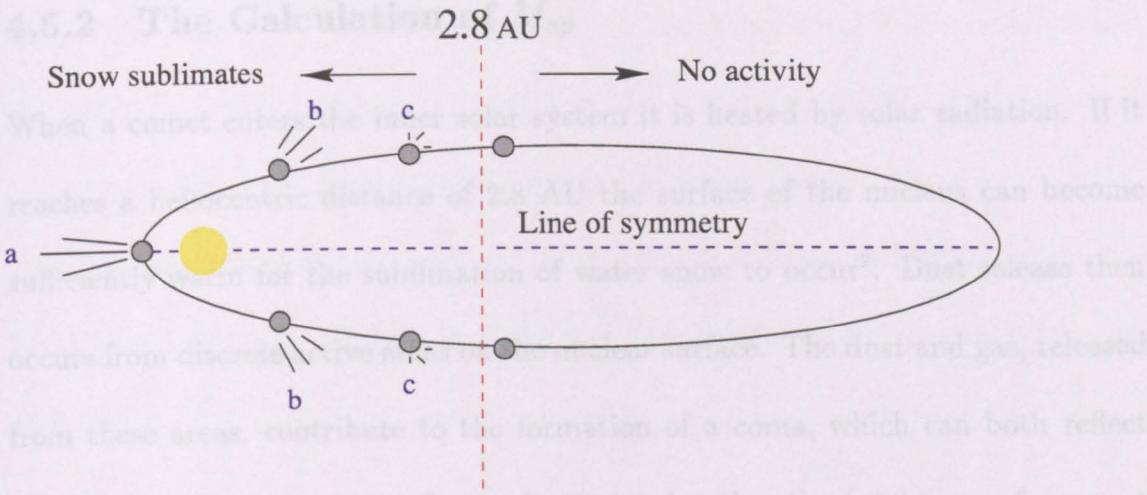


Figure 4.3: The model apparition. In this model water snow is the only material that sublimates and consequently the nucleus becomes active within a heliocentric distance of 2.8 AU. The mass of dust that is released from the comet is calculated in daily intervals for one half of the orbit. If outgassing is symmetrical about perihelion then the masses of dust that are lost in the mirror image of the orbit, *i.e.* at points b and c, are the same.

photodissociation of the fragile water molecules that outgas from the nucleus (see chapter(2)).

As water snow is the principle constituent then the sublimation of this snow should occur within 2.8 AU (see chapter (2)). Water sublimation has been inferred at distances greater than 2.8 AU by A'Hearn et al. (1984) from observations of OH in comet C/1980 E1 Bowell at a heliocentric distance of 5.25 AU. This emission was, however, attributed to grains that were already present in the coma and not to sublimation from the cometary nucleus.

The assumption that  $\dot{m}_i \propto \frac{1}{r^2}$  is a result of assuming that the amount of material released by the nucleus into the coma is proportional to the flux of incident sunlight (Hughes 1989b).

### 4.5.2 The Calculation of $M_{ap}$

When a comet enters the inner solar system it is heated by solar radiation. If it reaches a heliocentric distance of 2.8 AU the surface of the nucleus can become sufficiently warm for the sublimation of water snow to occur<sup>2</sup>. Dust release then occurs from discrete active areas on the nuclear surface. The dust and gas, released from these areas, contribute to the formation of a coma, which can both reflect sunlight and fluoresce. As a first order approximation the brightness of a comet should be related to the amount of dusty material released from the nucleus.

#### 1P/Halley as the Standard Comet

1P/Halley was used as the standard comet in this model. Specifically, the water outgassing rate at perihelion for its 1986 apparition,  $\dot{Q}_h$ , was used in the calculation of  $\dot{m}_i$  for each comet (see equation (4.6) below). It was, therefore, necessary to scale this constant for each comet. Thus,

$$\dot{m}_i = C \left( \frac{q_h}{q_c} \right)^2 \frac{B_c}{B_h} \left( \frac{q_c}{r} \right)^2 \quad (4.6)$$

Here,  $B_h$  and  $B_c$  are the brightness of 1P/Halley and the comet being examined,  $q_h$  is the perihelion distance of 1P/Halley during its 1986 apparition and the constant,  $C$ , is the mass of dust released by 1P/Halley per second at the perihelion distance

---

<sup>2</sup>Modifying the blackbody temperature for an object with an albedo,  $A$ , produces  $T = \left( \frac{L_\odot(1-A)}{4\pi r^2 \epsilon \sigma} \right)^{0.25}$ . Here,  $L_\odot$  is the Solar luminosity ( $3.9 \times 10^{26} \text{ W}$ ),  $r$  is the heliocentric distance of the object in metres,  $\epsilon$  is the emissivity of the object (presumed to have a value of unity) and  $\sigma$  is the Stephan-Boltzmann constant ( $5.7 \times 10^{-8} \text{ W m}^{-2} \text{ K}^{-4}$ ). Thus, if  $A = 0.05$  (see section (2.3.2)) then at 2.8 AU the temperature of this object is  $T = 233 \text{ K}$ . Note that the *actual* temperature of the cometary nucleus at 2.8 AU does not feature in any of the models presented in this thesis.

of  $q_h$ . The ratio  $\left(\frac{q_h}{q_c}\right)^2$  scales the constant to the comet's perihelion distance and the ratio  $\frac{B_c}{B_h}$  scales it to the brightness of the comet (which may be brighter or fainter because of a difference in the size of the active areas).

If these brightness values are calculated when the comet is at 1 AU from the Earth and 1 AU from the Sun they can be related to the absolute magnitudes,  $H_c$  and  $H_h$  by,

$$H_c - H_h = -\frac{5}{2} \log \frac{B_c}{B_h} \quad (4.7)$$

Substituting equation (4.7) into equation (4.6) produces,

$$\dot{m}_i = C \left(\frac{q_h}{q_c}\right)^2 10^{-\frac{2}{5}(H_c - H_h)} \left(\frac{q_c}{r}\right)^2 \quad (4.8)$$

Here,  $C$  is defined as,

$$C = \dot{Q}_h m_h \xi \quad \text{gs}^{-1}, \quad (4.9)$$

where  $\dot{Q}_h$  is the rate at which water is released from the nucleus of 1P/Halley at perihelion for the 1986 apparition,  $1 \times 10^{30}$  molecules  $s^{-1}$  (Feldman et al. 1986). This is converted into a mass by multiplying by  $m_h$ , the molecular weight of water,  $\sim 2.99 \times 10^{-23}$ g. Finally, this is multiplied by the dust to snow mass ratio,  $\xi$ , to produce a mass loss rate. Hughes (1996a) considered the mass ratio of dust to

snow for bodies formed in the proto-planetary cloud and concluded that the water snow to dust mass ratio was 2.2:1 for cometary nuclei, *i.e.*  $\xi = \frac{1}{2.2}$ .

The absolute magnitude,  $H_h$  and the perihelion distance,  $q_h$ , were set to the 1986 values for 1P/Halley. Thus,  $H_h = 2.5$  (Kresák & Kresáková 1989) and  $q_h = 0.587104$  AU (Marsden & Williams 1996). Equation (4.8) can then be approximated to,

$$\dot{m}_i \approx 4.68 \times 10^7 \frac{1}{r^2} 10^{-\frac{2}{5}H_c} \text{ gs}^{-1}, \quad (4.10)$$

where  $H_c$  is the  $H_{10}$  absolute magnitude for a comet on an orbit with perihelion at  $q_c$  (AU) and which is currently at a heliocentric distance of  $r$  (AU).

The instantaneous dust mass release rate,  $\dot{m}_i$ , is then calculated, at daily intervals, from perihelion up to 2.8 AU. The absolute magnitude,  $H_{10}$ , only applies to either the pre or post perihelion part of the light curve. Ideally the total dust mass released by the comet would be found by,

$$M_{ap} = 86400 \cdot \sum_{i=1}^{N_d} \dot{m}_i^{pre} + 86400 \cdot \sum_{i=1}^{N_d} \dot{m}_i^{post} \text{ g}, \quad (4.11)$$

where  $\dot{m}_i^{pre}$  is the instantaneous mass loss rate using the  $H_{10}$  value from the pre-perihelion part of the light curve and  $\dot{m}_i^{post}$  is the corresponding value using the post-perihelion value of  $H_{10}$ .  $N_d$  is the number of days taken by the comet to travel from perihelion to a heliocentric distance of 2.8 AU. The value of 86400 is the number of seconds in a day.

As Kresák and Kresáková only provide the  $H_{10}$  value for *either* the pre-perihelion or post-perihelion part of the light curve. The light curve is presumed to be symmetrical for the calculation of  $M_{ap}$ .

Equation (4.11) then becomes,

$$M_{ap} = 172800 \cdot \sum_{i=1}^{N_d} \dot{m}_i, \quad g \quad (4.12)$$

where  $\dot{m}_i$  is found from either the pre-perihelion or post-perihelion value of  $H_{10}$ .

## 4.6 The Orbital Parameters

The  $M_{ap}$  computer program takes the perihelion distance,  $q$  and the eccentricity,  $e$ , as input to define the cometary orbit. It is therefore worthwhile examining how these orbital parameters vary over each apparition for the 5 comets. Figure (4.4) shows the temporal variation in perihelion distance, eccentricity and orbital period for each comet.

As an approximation these comets can be divided into three groups:

### 1. Stable orbits.

Only **2P/Encke** falls into this category. From 1786 to 1994, the orbital period has only varied by 0.03 of a year from 3.28 years to 3.31 years. The perihelion distance has varied by 0.02 AU from 0.33 AU to 0.35 AU. The eccentricity has varied by 0.01 from 0.84 to 0.85. This stability is be-

cause 2P/Encke is always more than 1 AU within the orbit of Jupiter (see figure (4.5)). Therefore, unlike most short period comets, 2P/Encke is effectively decoupled from major gravitational perturbations by Jupiter.

## 2. Fairly stable orbits.

From 1843 to 1991, the orbital period of **4P/Faye** has varied by 0.27 years from 7.32 years to 7.59 years. The perihelion distance has varied by 0.16 AU from 1.59 AU to 1.75 AU. The eccentricity has varied by 0.03 from 0.55 to 0.58.

From 1873 to 1994, the orbital period of **10P/Tempel 2** has varied by 0.32 years from 5.16 years to 5.48 years. The perihelion distance has varied by 0.17 AU from 1.31 AU to 1.48 AU. The eccentricity has varied by 0.04 from 0.52 to 0.56.

## 3. Highly variable orbits.

**7P/Pons-Winnecke** shows the largest progressive variation in its orbital period, perihelion distance and eccentricity. From 1819 to 1996, the orbital period increased by 0.81 of a year from a period of 5.56 years in 1819 to 6.37 years by 1996. The perihelion distance increased by almost 0.5 AU from 0.77 AU in 1819 up to 1.26 AU in 1996. Correspondingly, the eccentricity fell from 0.75 in 1819 down to 0.63 in 1996.

The orbit of **6P/d'Arrest** has also significantly changed over time. From 1851 to 1995, the orbital period has varied by 0.5 of a year from 6.23 years up to 6.72 years. The perihelion distance has varied by 0.23 AU from 1.16 AU to 1.39 AU. The eccentricity has varied by 0.06 from 0.61 to 0.67.

### **Is a Changing Orbit Important for the $M_{ap}$ Calculation?**

Since  $M_{ap}$  is a function of the orbital parameters ( $q$  and  $e$ ), which vary from apparition to apparition, as well as  $H_{10}$ , it is worthwhile looking for differences between the shape of the  $H_{10}$  against time plots and the corresponding  $M_{ap}$  against time plots. Thus, in the following sections, the  $H_{10}$  and  $M_{ap}$  plots are compared for each comet.

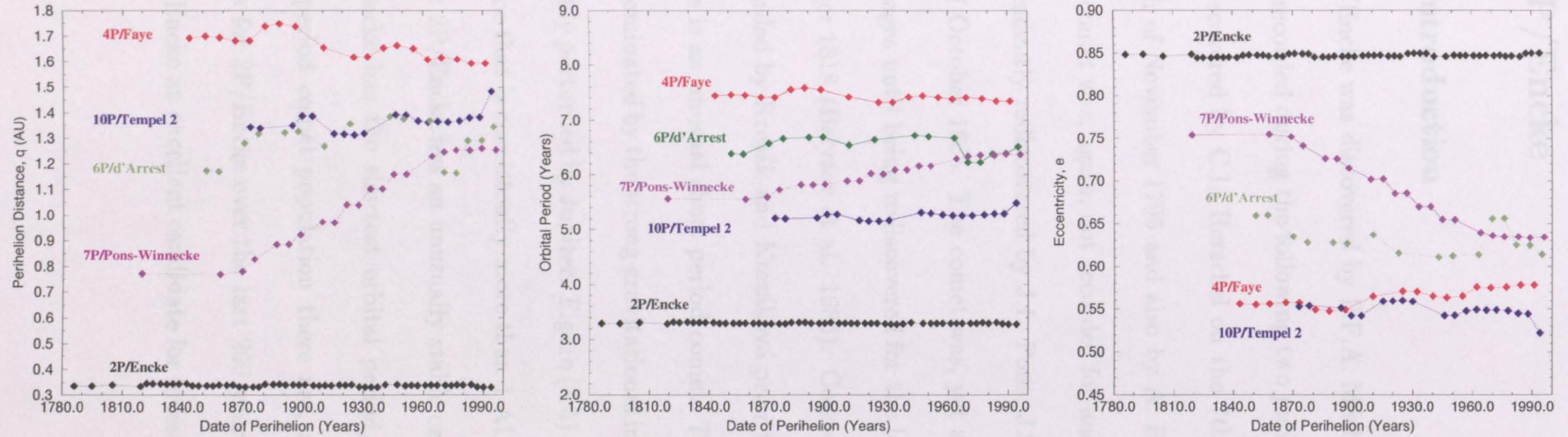


Figure 4.4: The temporal variation in perihelion distance,  $q$  (AU), orbital period,  $P$  (years) and eccentricity,  $e$ , for the 5 comets (Marsden & Williams 1996).

The 5 comets encompass a wide range of different short period orbits ( $P < 15$  years):

2P/Encke is effectively de-coupled from the gravitational influence of Jupiter and consequently is on a very stable orbit.

6P/d'Arrest has had several close encounters, within 0.5 AU, with Jupiter and so displays relatively large variations in its orbit. 7P/Pons-Winnecke shows a progressive increase in its orbital period, perihelion distance and a corresponding progressive decrease in its eccentricity. Comets 4P/Faye and 10P/Tempel 2 fall somewhere between the large variations of 7P/Pons-Winnecke and 6P/d'Arrest and the stable situation of 2P/Encke.

Note that the dotted lines are only used as a guide and are not meant to indicate a linear variation between apparitions.

## 4.7 2P/Encke

### 4.7.1 Introduction

Comet 2P/Encke was discovered by P.F.A. Méchain on the 17th of January 1786. It was not recorded during the following two perihelion passages and was independently rediscovered by C.L. Herschel on the 7th of November 1795, by T. Carle on the 11th of November 1795 and also by A. Bouvard on the 14th of November 1795. The comet was, again, not recorded for another two perihelion passages and was independently rediscovered by J.L. Pons, J.S.G. Huth and A. Bouvard all on the 20th of October 1805. The comet was, yet again, missed for three more perihelion passages until being rediscovered for the last time by J.L. Pons on the 26th of November 1818 (Belyaev et al. 1986). Consequently, there are only three  $H_{10}$  values recorded by Kresák and Kresáková prior to 1819.

2P/Encke is an unusual short period comet. The short period class of comets is normally dominated by the strong gravitational influence by Jupiter. But 2P/Encke is only weakly perturbed by Jupiter. Figure (4.5) shows that 2P/Encke has an aphelion distance that is consistently more than 1 AU within the orbit of Jupiter. This means that 2P/Encke has an unusually stable orbit, as can be seen in figure (4.4).

As 2P/Encke has the shortest orbital period,  $\sim 3.3$  years, of any member of the short period comet population there are, as a consequence, more recorded apparitions for 2P/Encke over the last 200 years than for any other comet. This makes 2P/Encke an excellent candidate for investigating the decay of the cometary nucleus.

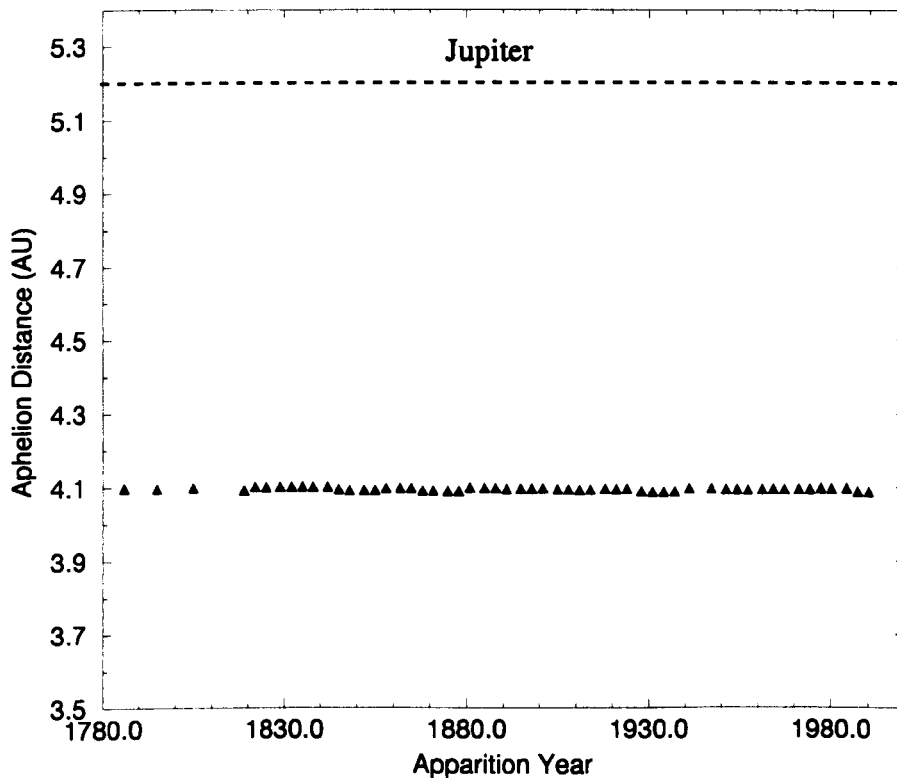


Figure 4.5: The variation in aphelion distance for 2P/Encke over the last 200 years. The blue line shows the semi-major axis of Jupiter. The orbit of 2P/Encke is over 1 AU within the orbit of Jupiter which means that 2P/Encke is only weakly perturbed by the Jovian gravitational field. Consequently, 2P/Encke has an orbit that varies little when compared with the other short period comets investigated in this chapter (see figure (4.4)).

The aphelion distances were taken from the *Catalogue of Cometary Orbits* (Marsden & Williams 1996).

## 4.7.2 Pre-1786 Perihelion Passages

Two important and yet unanswered questions about 2P/Encke are:

1. How did the comet come to be on such a stable orbit?
2. Why was the comet not seen before 1786?

Steel and Asher (1996) performed numerical integrations on test-particles on orbits similar to 2P/Encke. They concluded that the current orbit of 2P/Encke may have been produced by non-gravitational forces 4 times as strong as those currently acting on the comet. The non-gravitational forces would have progressively reduced the semi-major axis of the cometary orbit. Thus, the cometary orbit would have changed from one strongly influenced by the Jovian gravitational field to the effectively decoupled orbit of today.

The comet may have been dormant or difficult to observe prior to 1786. Kamel (1991) suggested that before 1786 the comet was “only bright when close to the Sun or located in the Southern Sky”. The lack of recorded apparitions is in conflict with any extrapolation from the linear regression used in figure (4.1). The linear regression fitted to the 2P/Encke  $H_{10}$  data (see table (4.2)) would indicate that the comet was almost 5 magnitudes brighter only 50 years prior to 1786! This demonstrates the limitation of inferring anything about cometary decay from linear regression fits.

In figure (4.6a) the  $H_{10}$  values appear to occupy a band and there is a peak in this band from 1860 to 1900. This band shape is the result, at least in part, of the 2P/Encke light curve asymmetry.

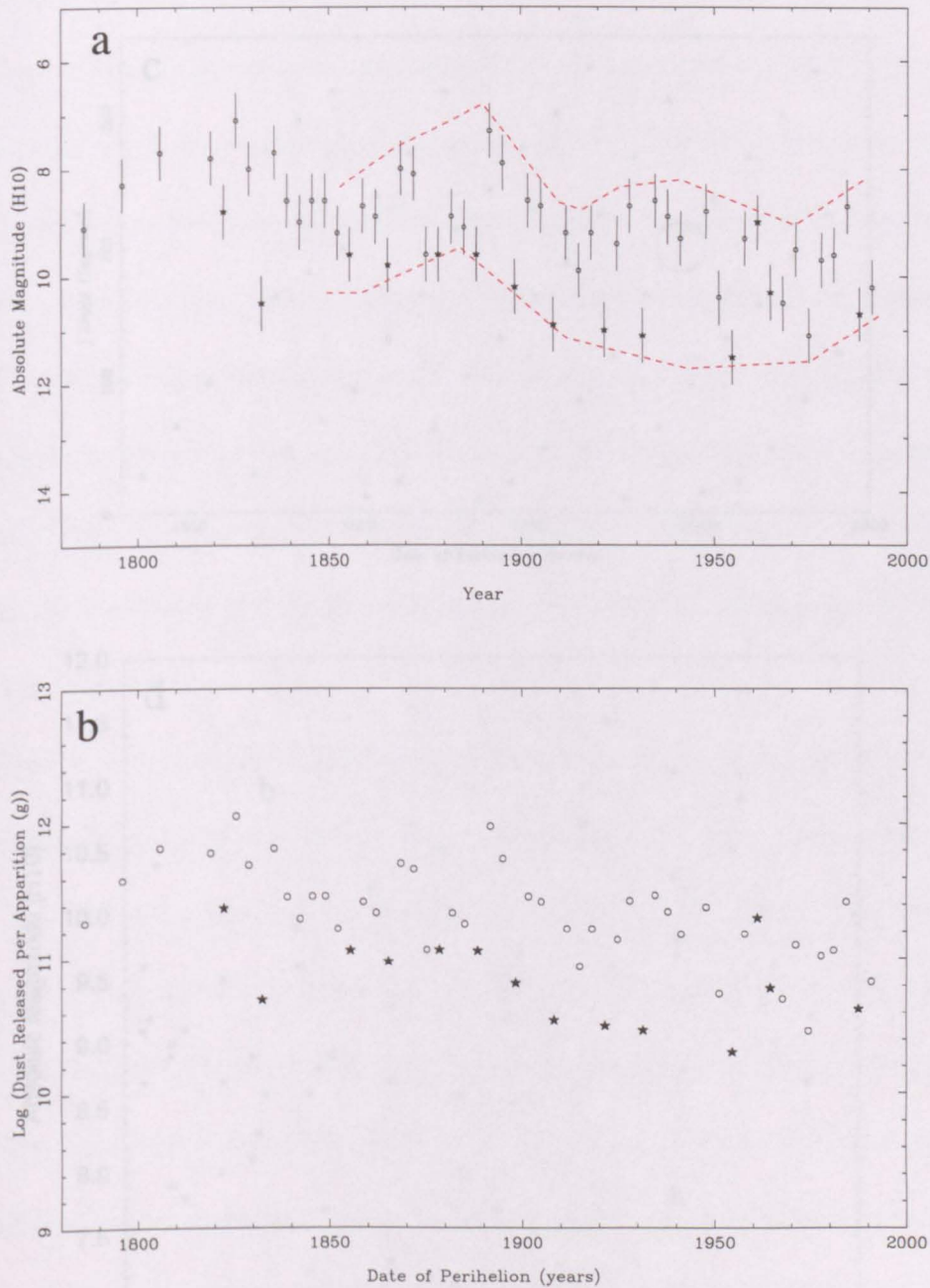


Figure 4.6: **2P/Encke**. Plot (a) shows the variation in  $H_{10}$  against the year in which perihelion passage occurred. The symbol  $\star$  refers to values of  $H_{10}$  calculated from the post-perihelion part of the light curve and the symbol  $\circ$  refers to values of  $H_{10}$  calculated from the pre-perihelion part of the light curve. The red dotted line is a free-hand sketch to show that the data forms the shape of a band. In plot (b) the mass of dust released per apparition,  $M_{ap}$ , is calculated by presuming the light curve is symmetrical about perihelion, i.e. pre and post-perihelion values of  $H_{10}$  are the same.

4.7.3 Light Curve Asymmetry

The asymmetry in the 2P/Encke light curve is a result of the geometry of the orbit only. 14 out of the 15 points are post-perihelion observations (i.e. fainter than the pre-perihelion observations) and it is possible that the asymmetry is due to the post-perihelion activity was low or if the orbit is not exactly circular.

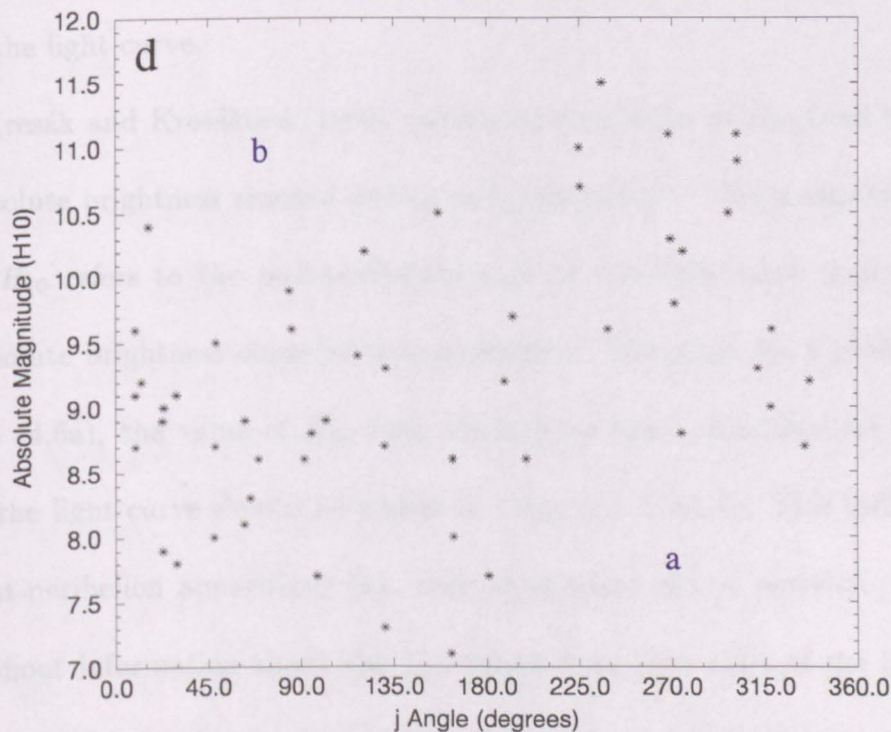
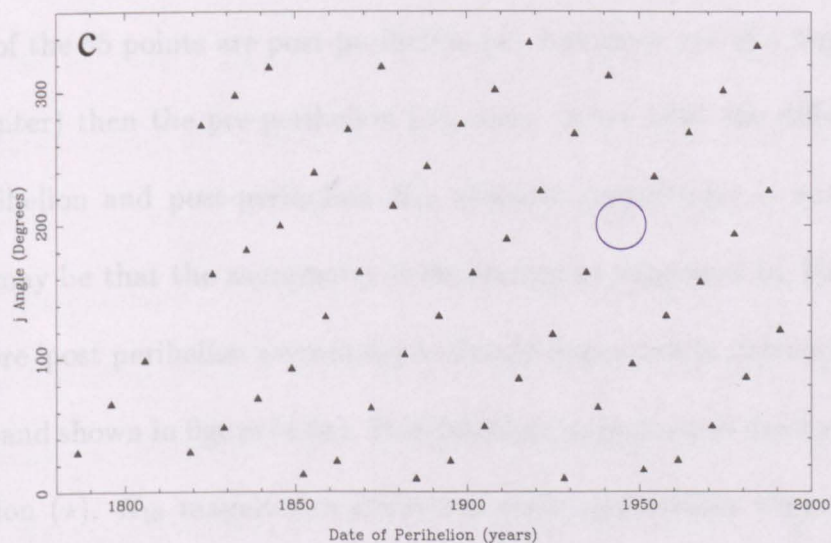


Figure 4.6: [Continued] Plot (c) shows the  $j$  angle against the year in which perihelion passage occurred. The regular pattern is due to the unusually stable orbit of 2P/Encke which results in a regular observing geometry. The circle indicates the estimated  $j$  angle for a missed apparition that was expected to have occurred in 1944. Plot (d) shows the  $j$  angle against  $H_{10}$ . Missing data were not considered to be important for 2P/Encke and so the lack of points in regions (a) and (b) may indicate a systematic error in the calculation of  $H_{10}$ .

### 4.7.3 Light Curve Asymmetry

The asymmetry in the 2P/Encke light curve is well known. In figure (4.6a) only 14 out of the 55 points are post-perihelion ( $\star$ ), but these are of a higher magnitude (*i.e.* fainter) than the pre-perihelion ( $\circ$ ), data. After 1960 the difference between pre-perihelion and post-perihelion  $H_{10}$  absolute magnitudes is not so noticeable and it may be that the asymmetry is decreasing as suggested by Kamel (1991).

The pre/post perihelion asymmetry is clearly important in determining the shape of the band shown in figure (4.6a). It is therefore important to determine if the post-perihelion ( $\star$ ),  $H_{10}$  magnitudes really represent apparitions where the cometary activity was low or if the difference is simply a result of measuring different portions of the light curve.

Kresák and Kresáková (1989) calculated each value of  $H_{10}$  from the “maximum absolute brightness reached during each apparition”. This means that if the value of  $H_{10}$  refers to the post-perihelion part of the light curve then the maximum absolute brightness occurred post-perihelion. Therefore, for a given point on figure (4.6a), the value of  $H_{10}$  that would have been calculated for the other side of the light curve should be higher in value (*i.e.* fainter). This indicates that the post-perihelion apparitions ( $\star$ ), were apparitions of low activity. Unfortunately, without information about the  $H_{10}$  values from both sides of the light curve, the actual difference in activity between the  $\star$  and  $\circ$  apparitions cannot be found.

#### 4.7.4 Missing Apparitions, Holetschek Effect and the $H_{10}$ Weights

From 1786 to 1990 8 apparitions were missed. Most of these were during the late 18th and early 19th centuries when the comet was first being identified and not known to be periodic. After 1819 all apparitions have been recorded except for one that would have occurred in about the year 1944. This means that over the time period considered, 12.7% of the apparitions are missing. As these missing apparitions are mostly confined to the earliest period shown in figure (4.6a) missing apparitions are not considered to be the cause of any structure in the plot.

In figure (4.6c) the stability of the the 2P/Encke orbit produces the regular pattern in the  $j$  angle over time (see section (3.2.2) for the calculation of  $j$ ). The location of the missing 1944 apparition can easily be estimated and is indicated by the circle. At this apparition the  $j$  angle would have been approximately  $200^\circ$ . This would mean that the comet appeared to be close to the Sun during its perihelion passage and would be difficult to detect. However, figure (4.6c) shows that other apparitions that had  $j = 200^\circ$  were not missed, and so the 1944 apparition may have been missed for sociological reasons.

In figure (4.6d) the absolute magnitude,  $H_{10}$  is plotted against the  $j$  angle. There are gaps in the data in regions (a) and (b). The reason for these is not known but since missing apparitions are not considered important the features should be real and may indicate a systematic error in the  $H_{10}$  calculations.

The stability of the 2P/Encke orbit means that the Kresák and Kresáková  $H_{10}$  weights do not vary as much as for the other 4 comets. Figure (4.2) shows that the 2P/Encke  $H_{10}$  weights never fall below 0.5. There are no low weights which could

account for any structure in the figure (4.6a).

#### 4.7.5 The Mass of Dust Released per Apparition, $M_{ap}$

Figure (4.6b) shows the variation in  $\log M_{ap}$  during the last 200 years for 2P/Encke. For this plot no attempt has been made to account for the light curve asymmetry. Thus, each value of  $H_{10}$  in figure (4.6a) is presumed to refer to both sides of the light curve for that particular apparition.

In figure (4.7a) each value of  $\log M_{ap}$  is given an error bar corresponding to an uncertainty in  $H_{10}$  of  $\pm 0.5$  magnitudes (see section (4.4.3)). A linear regression was applied to the data set assuming all points had equal weighting (*i.e.* the same as in table (4.2)). With these error bars, 32 of the points (58%) lie more than  $1\sigma$  from the line. This suggests that either  $\pm 0.5$  magnitudes is an underestimate of the error or that the scatter is due to a physical reason. Clearly, the light curve asymmetry (*i.e.* the difference between the  $\star$  and the  $\circ$  points in figure (4.7a)) plays a role and so some attempt needs to be made to correct the data for this asymmetry.

Using the values of  $M_{ap}$  from figure (4.6a), 2P/Encke released a total of  $(2.7 \pm 0.2) \times 10^{13}$  g of dust over 55 apparitions. For the 55 apparitions considered here, the mean mass of dust released per apparition was  $\bar{M}_{ap} = (4.8 \pm 0.4) \times 10^{11}$  g. See table (4.5) for a comparison with the other 5 comets.

The mean dust release rate,  $\bar{M}_{ap}$  can be converted into a mean layer loss rate for the cometary nucleus. Using the dust to snow mass ratio of 1:2.2, the total mean mass lost from the comet is  $15.4 \times 10^{11}$  g per apparition. For a mean cometary density of  $0.5 \text{ g cm}^{-3}$  (see section (2.3.2)), this corresponds to a volume loss of  $3.1 \times 10^{12} \text{ cm}^3$  per apparition. This volume should be approximately equal to

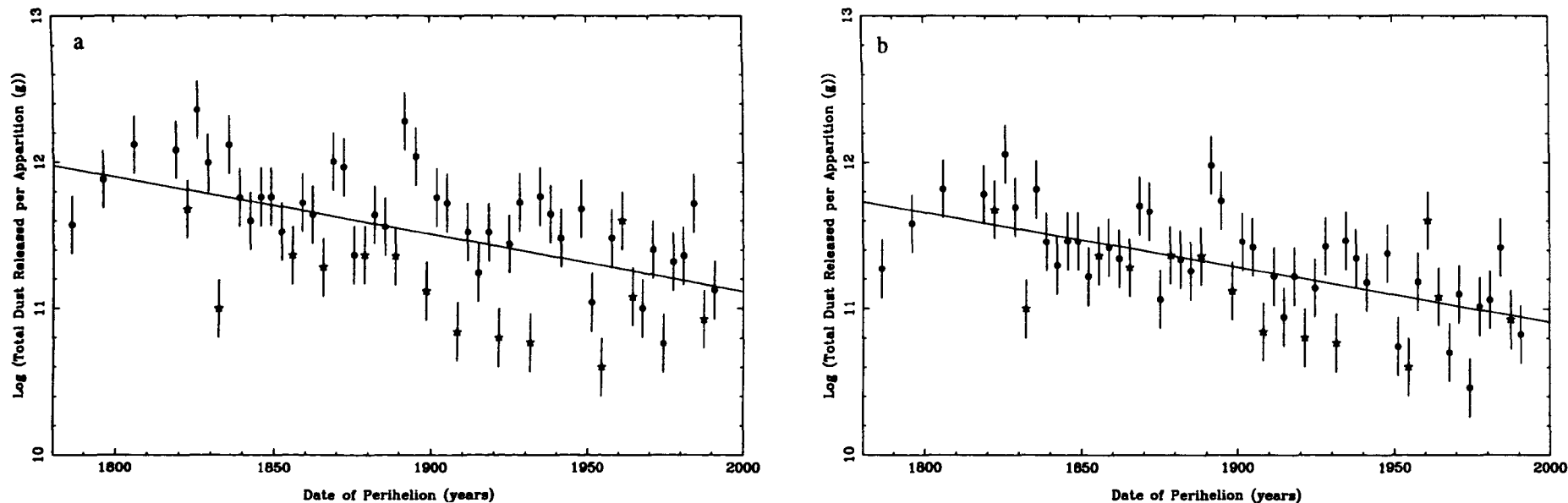


Figure 4.7: In plot (a) the linear regression used in figure (4.1) for 2P/Encke is compared with the calculated uncertainty on  $\log M_{ap}$  assuming an uncertainty of  $\pm 0.5$  in the  $H_{10}$  absolute magnitudes. With these error bars, 32 of the points (58 %) do not agree with the line described by the linear regression. In plot(b) a correction is applied to try to find the minimum thickness of the apparent band shape in plot (a). It is assumed that the light curve is symmetrical for apparitions where the post-perihelion,  $\star$ , value of  $H_{10}$  was calculated. Thus, the  $\star$  symbols are in the same position as in plot (a). For the pre-perihelion values of  $H_{10}$  it is presumed that the comet was completely inactive during the post-perihelion side of the orbit. Therefore, the  $\circ$  values in plot (a) are halved. It is expected that the  $\circ$  values of  $\log M_{ap}$  are underestimated and the  $\star$  values of  $\log M_{ap}$  are overestimated. In plot (b) a new linear regression is applied to the data set. Here, 23 points (42 %) of the points do not agree with the line to the  $1\sigma$  level. It is concluded that either the estimate of the uncertainty on  $H_{10}$  of  $\pm 0.5$  is too small or the data is not well described by a straight line.

$\Delta R \cdot R^2$ , where  $R$  is the equivalent cometary nucleus radius and  $\Delta R$  is the depth of layer that is lost at each apparition<sup>3</sup>. Thus, if 2P/Encke has an equivalent radius between 1 km and 5 km, then the average depth of layer lost from the nucleus at each apparition should be between  $\sim 3$  m and  $\sim 12$  cm respectively. In section (5.4.2) it will be shown that the typical short period comet is expected to lose a layer of approximately 1 m in depth at each apparition, and so these values are entirely consistent with that hypothesis.

In figure (4.7b) an extreme condition for 2P/Encke is considered. First it is assumed that the  $H_{10}$  value for the post-perihelion,  $\star$ , points is the same on both sides of the light curve. The values of  $M_{ap}$  are therefore kept the same as in figure (4.7a) and should be *overestimates* of the actual values. For the pre-perihelion,  $\circ$ , apparitions the  $H_{10}$  values are presumed to refer to only one side of the light curve. The other side of the light curve is then assumed to be non-existent, *i.e.* no activity post-perihelion. Thus, the  $\circ$  values of  $M_{ap}$  in figure (4.7a) are halved and so the corresponding  $\circ$  values in figure (4.7b) should be *underestimates* of the actual values. Therefore the band in figure (4.7b) should have the minimum possible range in  $H_{10}$ .

A linear regression was applied to the points in figure (4.7b), excluding the error bars.

This is described by,

$$\log M_{ap} = (-0.0037 \pm 0.0007)t + (18.4 \pm 1.3), \quad (4.13)$$

---

<sup>3</sup>Note that this assumes that  $R \gg \Delta R$ , which since 2P/Encke has had at least 55 recorded apparitions without dramatically fading, is probably a reasonable assumption.

where  $t$  corresponds to the year in which perihelion passage occurred.

Equation (4.13) indicates that 2P/Encke is losing, on average, less mass at each apparition. However, equation (4.13) has a coefficient of determination of  $r^2 = 0.36$ , and it is probably not wise to extrapolate from these data very far into the future.

In figure (4.7b) 23 points (42%) still lie more than  $1\sigma$  from the line. Therefore, either  $\pm 0.5$  magnitude is an underestimate of the typical uncertainty on each  $H_{10}$  value or there is a distinct band structure in the  $H_{10}$  data.

## 4.8 6P/d'Arrest

### 4.8.1 Introduction

Comet 6P/d'Arrest was discovered by H.L. d'Arrest on the 28th of June 1851 (Belyaev et al. 1986). From 1851 until 1989 15 apparitions were recorded and 7 have been missed (*i.e.* 32% of the total; see table (4.1) and table (4.3)).

6P/d'Arrest was not a new short period comet at the time of the discovery apparition in 1851. The comet has been identified with 1678 La Hire by Carusi et al. (1991), which is the oldest recorded apparition of a short period comet to date.

Figure (4.4) shows that, of the 5 comets examined in this chapter, 6P/d'Arrest is subject to the second largest variations, after 7P/Pons-Winnecke, in its orbital period, perihelion distance and eccentricity. Since 1851 the orbital period has varied by 0.49 years, the perihelion distance has varied by 0.23 AU and the eccentricity has varied by 0.06.

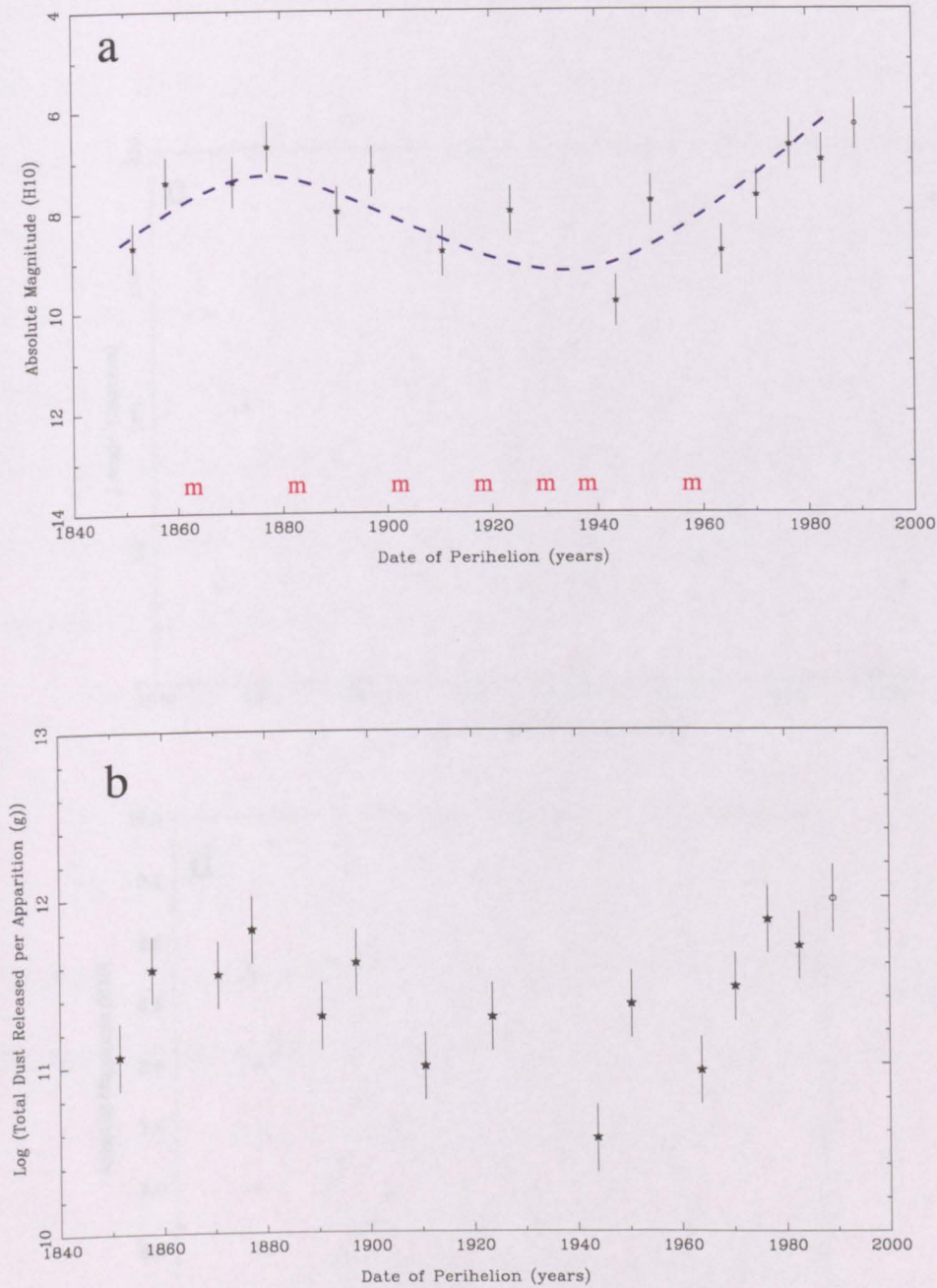


Figure 4.8: **6P/d'Arrest**. Plot (a) shows the variation in  $H_{10}$  against the year in which perihelion passage occurred. The  $\star$  symbols refer to values of  $H_{10}$  calculated from the post-perihelion part of the light curve and the  $\circ$  symbols refer to values of  $H_{10}$  calculated from the pre-perihelion part of the light curve. The red symbol **m** refers to missing apparitions. The blue dotted line indicates that the data appear to form the shape of a sinusoid. In plot (b) the logarithm of the mass of dust released per apparition,  $M_{ap}$ , is calculated by presuming that the light curve is symmetrical about perihelion, *i.e.* pre and post-perihelion values of  $H_{10}$  are the same.

4.8.2  $H_{10}$  Absolute Magnitudes

Figure (4.8a) shows how  $H_{10}$  varies with time. The first impression from this plot is that the absolute magnitudes follow a sinusoidal trend. Figure (4.8a) demonstrates

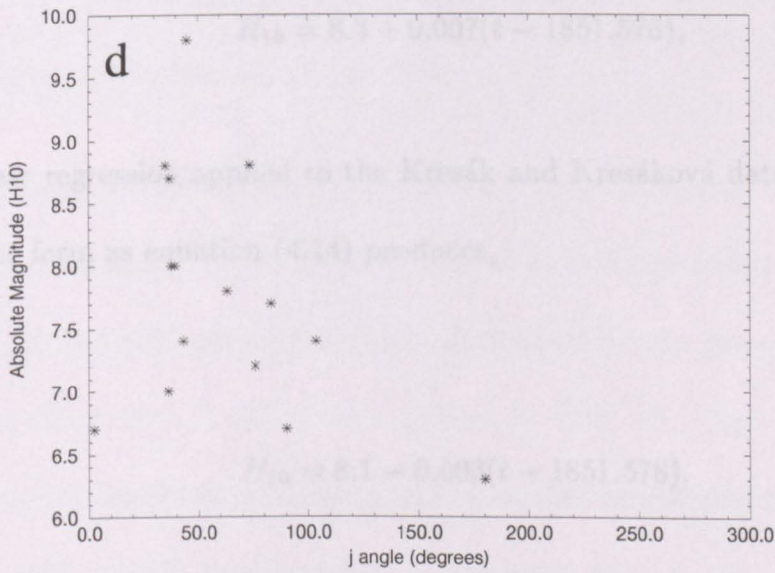
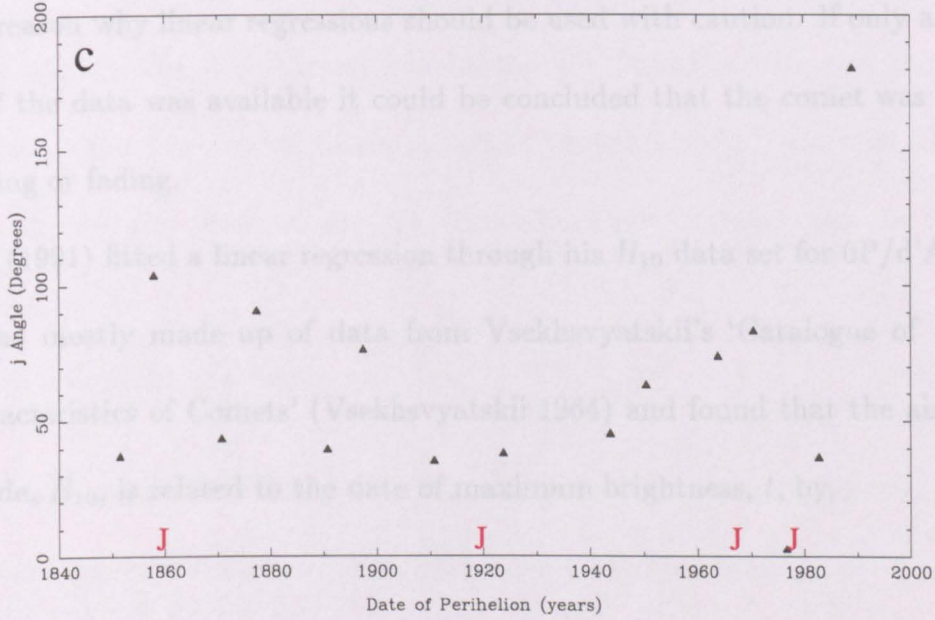


Figure 4.8: [Continued] Plot (c) show the  $j$  angle against the year in which perihelion passage occurred. The red symbol **J** refers to close encounters ( $< 0.5$  AU) with Jupiter. Plot (d) shows the  $j$  angle against  $H_{10}$ .

### 4.8.2 $H_{10}$ Absolute Magnitudes

Figure (4.8a) shows how  $H_{10}$  varies with time. The first impression from this plot is that the absolute magnitudes follow a sinusoidal trend. Figure (4.8a) demonstrates another reason why linear regressions should be used with caution. If only a small subset of the data was available it could be concluded that the comet was *either* brightening or fading.

Svoreň (1991) fitted a linear regression through his  $H_{10}$  data set for 6P/d'Arrest, which was mostly made up of data from Vsekhsvyatskii's 'Catalogue of Physical Characteristics of Comets' (Vsekhsvyatskii 1964) and found that the absolute magnitude,  $H_{10}$ , is related to the date of maximum brightness,  $t$ , by,

$$H_{10} = 8.3 + 0.007(t - 1851.578), \quad (4.14)$$

A linear regression applied to the Kresák and Kresáková data and expressed in the same form as equation (4.14) produces,

$$H_{10} = 8.1 - 0.003(t - 1851.578). \quad (4.15)$$

The linear regression described by equation (4.15) has a coefficient of determination of  $r^2 = 0.02$ . It is concluded that these linear regressions have little physical meaning. From data that follows a sinusoidal trend it is possible to get either a positive gradient (equation (4.14)) or a negative gradient (equation (4.15)), depending on which part of the data set is sampled.

Error bars of  $\pm 0.5$  magnitude are shown for each  $H_{10}$  value in figure (4.8a), and are clearly not sufficient to account for the shape of the curve.

### Light Curve Asymmetry

Carusi et al. describe 6P/d'Arrest as having the "most pronounced recurrent asymmetry of the light curve among all short period comets" and that the absolute brightness and shape of the light curve have not changed over the last 47 apparitions.

They attribute this to either:

- a) the main active area being situated near one of the rotation poles and only being exposed to solar radiation after each perihelion passage,
- b) active areas requiring a longer than average heating time before they start a higher production of gas and dust.

Fortunately, in this model, the asymmetry in the light curve will not affect the main conclusions about the shape of the curve in figure (4.8a) since only 1 value of  $H_{10}$ , (for the 1989 apparition), was calculated from the pre-perihelion section of the light curve.

The main affect of the asymmetry will be on the mass of dust calculated using the  $M_{ap}$  program, as  $H_{10}$  is assumed to be the same on both sides of the light curve. The values calculated from the  $M_{ap}$  programs should therefore be considered as upper limits.

### Missing Apparitions

As 32% of the apparitions from 1851 to 1989 have not been recorded it seems likely that missing data might significantly affect conclusions about the shape of the  $H_{10}$  curve in figure (4.8a). Missing apparitions are indicated in figure (4.8a) by the letter m.

Carusi et al. (1991) state that the 7 missed apparitions (1864, 1884, 1904, 1917, 1930, 1937 and 1957) were missed due to “unfavourable observing geometry”. It is important for an analysis of figure (4.8a) to know the  $H_{10}$  values of the comet at these perihelion passages. It is possible that the data in figure (4.8a) appears sinusoidal simply because of where the missing apparitions would occur on the plot.

### The Holetschek Effect

The remaining apparitions, which are listed in the *Catalogue of Cometary Orbits* (Marsden & Williams 1996), are shown in the  $j$  angle plot in figure (4.8c).

In figure (4.8c) there is not a regular pattern of the  $j$  angles as was the case for 2P/Encke in figure (4.6c). This is due to close approaches of the comet with Jupiter that perturbed the comet onto different orbits.

Carusi et al. defined close approaches between 6P/d’Arrest and Jupiter as those encounters that come within 0.5 AU of the planet. They found 8 close approaches to Jupiter and one close approach to Mars. Four of these Jovian close approaches apply to the data set used here. They occurred in 1861 (0.3474 AU), 1920 (0.4965 AU), 1968 (0.4078 AU) and in 1979 (0.2987 AU) and are indicated by the letter J in figure (4.8c). Although the 1920 approach was not the closest to Jupiter this date appears to be the time after which the  $j$  angle becomes more unpredictable (see

figure (4.8c)). Unfortunately, because of the missing apparitions, the pattern which seems to exist before 1920 may be fortuitous.

The relationship between the  $j$  angle and  $H_{10}$  is shown in figure (4.8d). The data points fill only the region  $j < 200^\circ$ . This is in part due to the smallness of the sample (15 apparitions) and the bias towards post-perihelion data. The only point that has a  $j$  angle greater than  $180^\circ$  is the 1989 pre-perihelion value of  $H_{10}$ .

### The Kresák and Kresáková $H_{10}$ Weights

Only 2 of the recorded apparitions have  $H_{10}$  values that are weighted below 0.5. The 1963 value of  $H_{10}$  has a weight of 0.32 and the 1989 apparitions has a  $H_{10}$  weight of 0.0. Neither of these points are crucial for determining the shape of the curve in figure (4.8a).

### 4.8.3 The Mass of Dust Released per Apparition, $M_{ap}$

To calculate the mass of dust released at each apparition,  $M_{ap}$ , the light curve was assumed to be symmetrical. These  $M_{ap}$  values are therefore upper limits on the mass of dust released at each apparition.

The shape of the  $\log M_{ap}$  curve in figure (4.8b) is the same as the  $H_{10}$  curve in figure (4.8a). This indicates that the variation in the orbit of the comet has not had a significant effect on the mass of dust released.

The mass of dust released per apparition,  $M_{ap}$ , varies from  $3.6 \times 10^{10}$  g in 1943 to  $9.7 \times 10^{11}$  g in 1989. The total mass of dust released during the 15 apparitions is  $(1.1 \pm 0.5) \times 10^{13}$  g. See table (4.5) for a comparison with the other comets.

Using the mean mass of dust released per apparition,  $\bar{M}_{ap} = 7.0 \times 10^{11}$  g, and the

dust to snow mass ratio of 1:2.2, 6P/d'Arrest released a combined (snow and dust) mean mass of  $22.4 \times 10^{11}$  g per apparition. This corresponds to a mean volume loss of  $4.5 \times 10^{12}$   $\text{cm}^3$  per apparition. If the equivalent radius of the nucleus is between 1 km and 5 km then this volume loss corresponds to an mean layer loss of between  $\sim 4.5$  m ( $R = 1$  km) and  $\sim 18$  cm ( $R = 5$  km) from the cometary nucleus.

#### 4.8.4 Discussion

A first glance at the absolute magnitude data for 6P/d'Arrest appears to show a sinusoidal trend in  $H_{10}$  over time. But a further analysis of the data set shows that simple linear regressions should be used with caution. It would be easy, for example, to only sample the years 1885 to 1945 and conclude that the comet is rapidly increasing in brightness, while from 1945 to 1989 the conclusion would be that the comet is rapidly fading.

Pre/Post-perihelion asymmetry in the light curve is important for 6P/d'Arrest but since all but one absolute magnitude is post-perihelion,  $\star$ , the asymmetry should not be the cause of the shape of the curve in figure (4.8a).

The missing apparitions, forming nearly a third of the total number of perihelion passages from 1851-1989, are likely to be significant for the shape of the curve. It would be interesting to see if the sinusoidal shape remained if these data could be introduced.

## 4.9 10P/Tempel 2

### 4.9.1 Introduction

10P/Tempel 2 was discovered by E.W.L. Tempel on the 3rd of July 1873 (Belyaev et al. 1986). The changes in the orbital period, perihelion distance and eccentricity are of a similar magnitude to those for 4P/Faye (see figure (4.4)). Since 1873 the orbital period has only varied by 0.32 years, the perihelion distance has varied by 0.17 AU and the eccentricity has varied by 0.04.

### 4.9.2 $H_{10}$ Absolute Magnitudes, Light Curve Asymmetry, the Holetschek Effect and $H_{10}$ Weights

10P/Tempel 2 is perhaps the least remarkable of all the comets considered in this chapter. Figure (4.9) shows that there are no obvious trends in the  $H_{10}$  against time plot.

In figure (4.9a) 5 values of  $H_{10}$  were calculated from the pre-perihelion part of the light curve and are indicated by the symbol  $\circ$ , the other 13  $H_{10}$  values, indicated by a  $\star$ , were calculated from the post-perihelion part of the light curve. There is no obvious structure in figure (4.9a) that is the result of using either pre-perihelion or post-perihelion  $H_{10}$  values. From a total of 23 possible apparitions, during the period 1873 to 1988, 5 (22%) were missed.

In figure (4.9c) the  $j$  angle is plotted against the year in which perihelion passage occurred. In figure (4.9d) the absolute magnitude,  $H_{10}$ , is plotted against the  $j$  angle. Neither of these plots show any obvious features that would indicate that figure (4.9a) is influenced by the Holetschek effect.

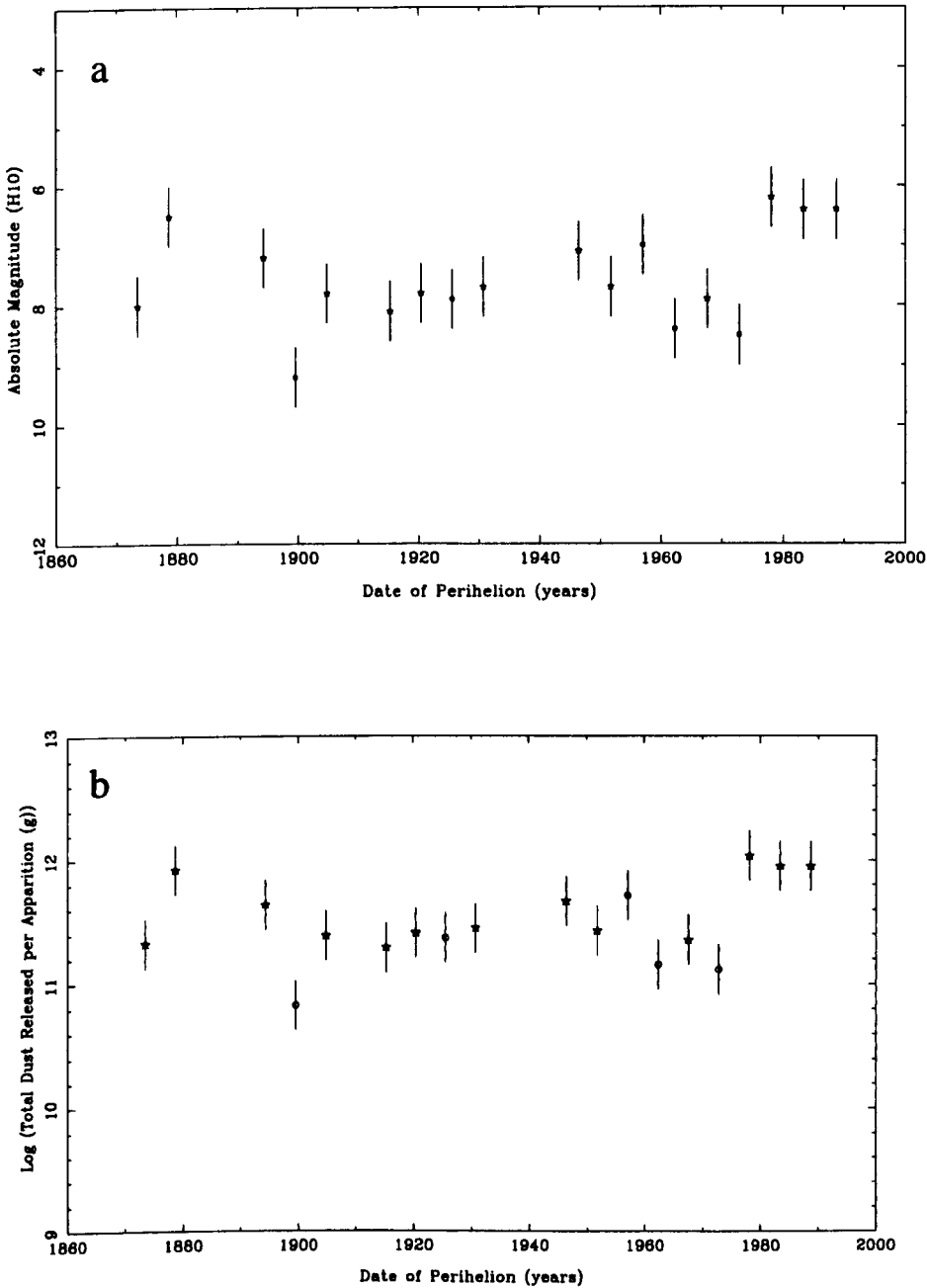


Figure 4.9: 10P/Tempel 2. Plot (a) shows the variation in  $H_{10}$  against the year in which perihelion passage occurred. The symbol  $\star$  refers to values of  $H_{10}$  calculated from the post-perihelion part of the light curve and the symbol  $\circ$  refers to values of  $H_{10}$  calculated from the pre-perihelion part of the light curve. In plot (b) the logarithm of the mass of dust released per apparition,  $M_{ap}$  is calculated by presuming the light curve is symmetrical about perihelion, *i.e.* pre and post-perihelion values of  $H_{10}$  are the same.

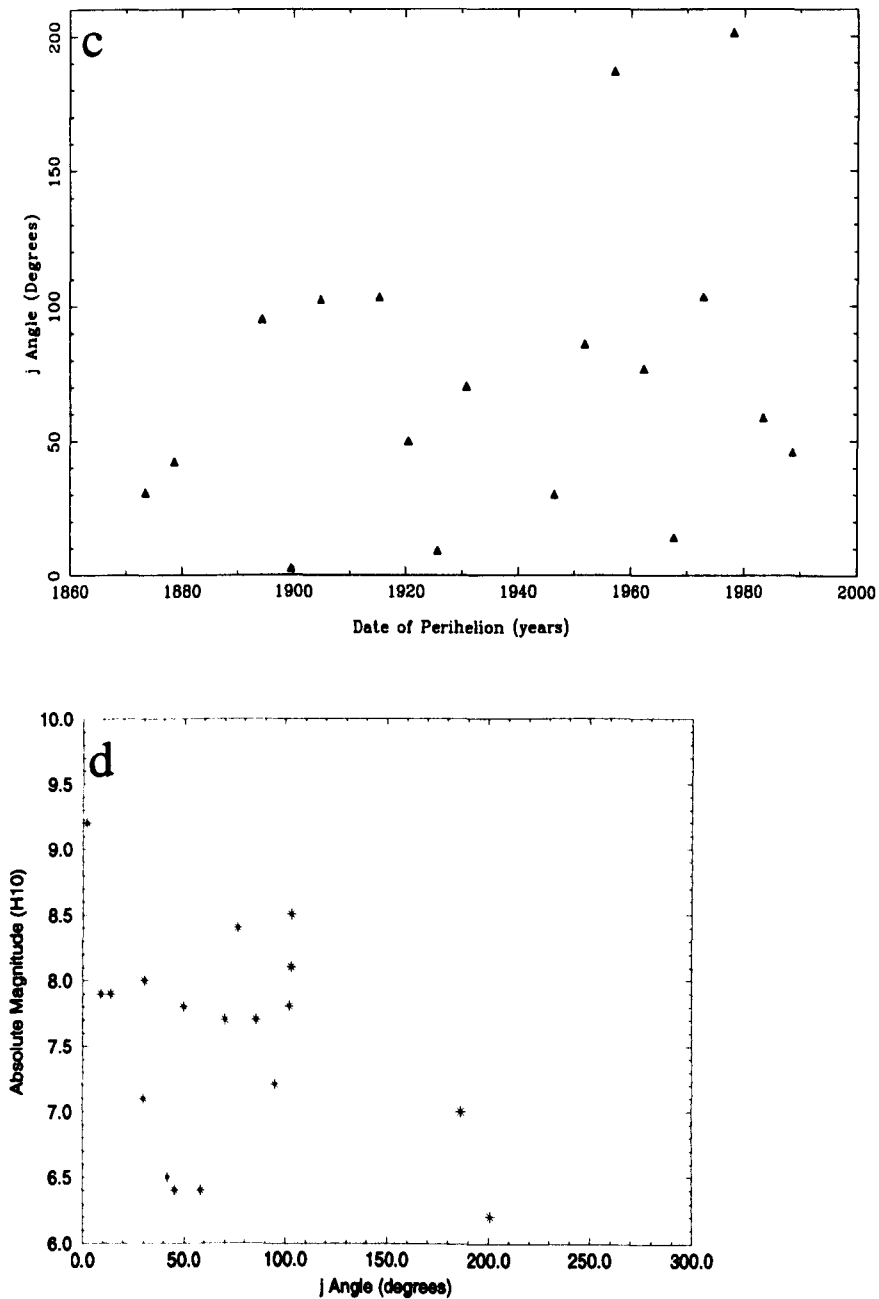


Figure 4.9: [Continued] Plot (c) show the  $j$  angle against the year in which perihelion passage occurred. Plot (d) shows the  $j$  angle against  $H_{10}$ .

Only 3 apparitions have  $H_{10}$  weights smaller than 0.5. In 1972 the  $H_{10}$  weight fell to 0.10 while in 1957 and 1978 the weight dropped to 0.00. Figure (4.9b) shows the variation in  $\log M_{ap}$  with the year in which perihelion passage occurred. During 18 apparitions 10P/Tempel 2 released  $(1.5 \pm 0.7) \times 10^{13}$  g (for errors of  $\pm 0.5$  magnitudes). This corresponds to an average of  $(8.2 \pm 0.2) \times 10^{11}$  g of dust released per apparition. See table (4.5) for a comparison with the other comets.

This corresponds to a combined (water and dust) mean mass release rate of  $26.2 \times 10^{11}$  g per apparition, or  $5.2 \times 10^{12}$   $cm^3$  ( $\bar{\rho} = 0.5$   $gcm^{-3}$ ) lost from the nucleus per apparition. For an equivalent radius of 5.9 km (see below), the mean depth of layer lost from the nucleus is  $\sim 15$ cm.

### 4.9.3 Active Areas

A'Hearn et al. (1989) used a thermal model of asteroids for 10P/Tempel 2 and calculated a visual geometric albedo of  $0.022_{-0.006}^{+0.004}$  and an equivalent radius of  $5.90_{-0.68}^{+0.24}$  km. If this radius is used in equation (4.1) then the percentage of the nucleus surface that is active can be calculated for each apparition. This is plotted in figure (4.10a). In figure (4.10b) the logarithm of the active fraction,  $f$ , is plotted with error bars assuming an uncertainty in  $H_{10}$  of  $\pm 0.5$  magnitudes.

These plots indicate that the percentage of the nucleus surface for 10P/Tempel 2 that is active is low. This percentage reached a maximum of 1.8 % in 1978 and a minimum of 0.1 % in 1899. The maximum change *between two consecutive apparitions* was from 0.2% to 1.8% between 1972 and 1978 (see table (4.6)), *i.e.* a  $\times 9$  change in the size of the active areas. Table (4.6) lists the extremes in the percentage of the nucleus surface that was active.

A'Hearn et al. combined "the outgassing rate observed in the comet and the size of the nucleus to estimate the fraction of the surface of the nucleus which is active". For an outgassing rate of  $3 \times 10^{16}$  molecules  $cm^{-2}s^{-1}$  they found a *maximum* active area size of  $11 \text{ km}^2$  which corresponded to 3% of the nucleus surface. They concluded that a good estimate of this percentage for 10P/Tempel 2 is  $\sim 1\%$ . Thus, unless the 5 missing apparitions coincided with periods of unusually high activity, 10P/Tempel 2 has had activity restricted to only a few percent of the nucleus surface during the period 1873 to 1988.

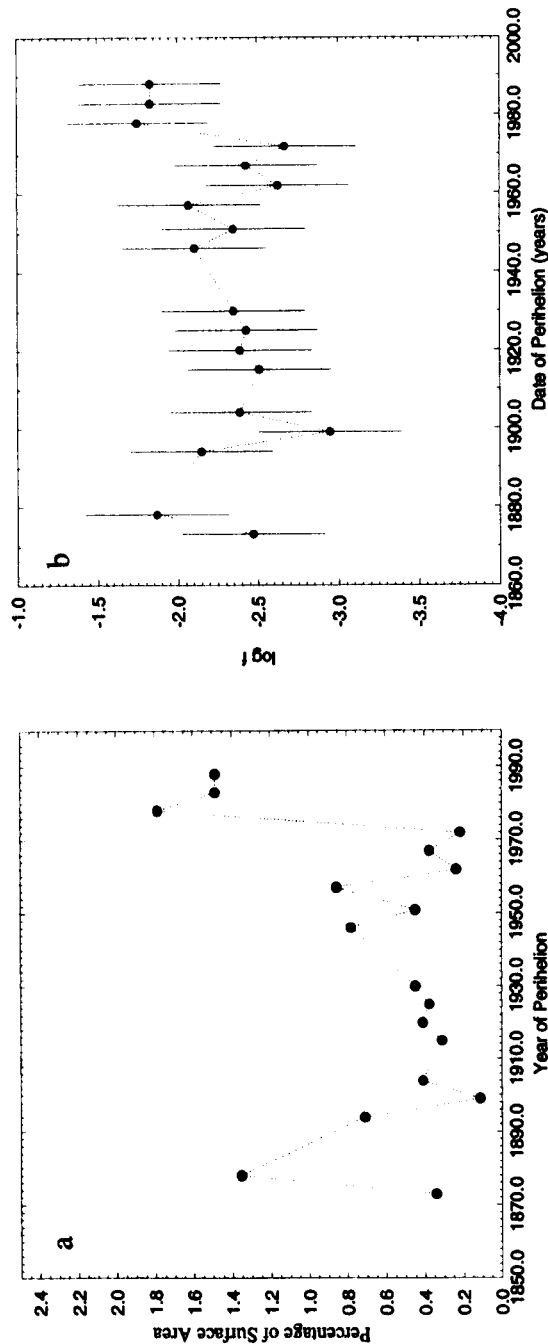


Figure 4.10: The percentage of the 10P/Tempel 2 nucleus surface that was active is shown in plot (a) and the logarithm of the active fraction,  $\log f$ , used in equation (4.1) is shown in plot (b). The error bars were calculated by assuming that the uncertainty in  $H_{10}$  was  $\pm 0.5$  magnitudes. The percentage of the nucleus surface that was active did not get above 2.0%, and so it may be reasonable to consider 10P/Tempel 2 to be in a steady-state period in its activity.

## 4.10 7P/Pons-Winnecke

### 4.10.1 Introduction

Comet 7P/Pons-Winnecke was discovered by J.L. Pons on the 12th of June 1819, lost for 6 returns and then rediscovered by F.A.T. Winnecke on the 9th of March 1858 (Belyaev et al. 1986).

Figure (4.4) shows that, of the 5 short period comets examined in this chapter, 7P/Pons-Winnecke is subject to the largest variations in its orbital period, perihelion distance and eccentricity.

During the period 1819 to 1996 the orbital period progressively increased from 5.56 years to 6.37 years. The perihelion distance has increased by almost 0.5 AU from 0.77 AU in 1819 to 1.26 AU in 1996. Correspondingly, the eccentricity has fallen from 0.75 in 1819 down to 0.63 in 1996.

These large changes made Sekanina (1989) conclude that the varying orbital parameters “are bound to alter substantially the insolation distribution over the nucleus surface and thus the comet’s long term pattern of activity”. This conclusion is not supported in this analysis.

### 4.10.2 $H_{10}$ Absolute Magnitudes, Light Curve Asymmetry and Missing Apparitions

The  $H_{10}$  data in figure (4.11a) does not appear to follow any progressive trend, such as the apparent sinusoidal curve seen in the 6P/d’Arrest plot in figure (4.8a). Clearly, the error bars need to be substantially larger than  $\pm 0.5$  to explain the scatter of these  $H_{10}$  values or the variation in  $H_{10}$  is real.

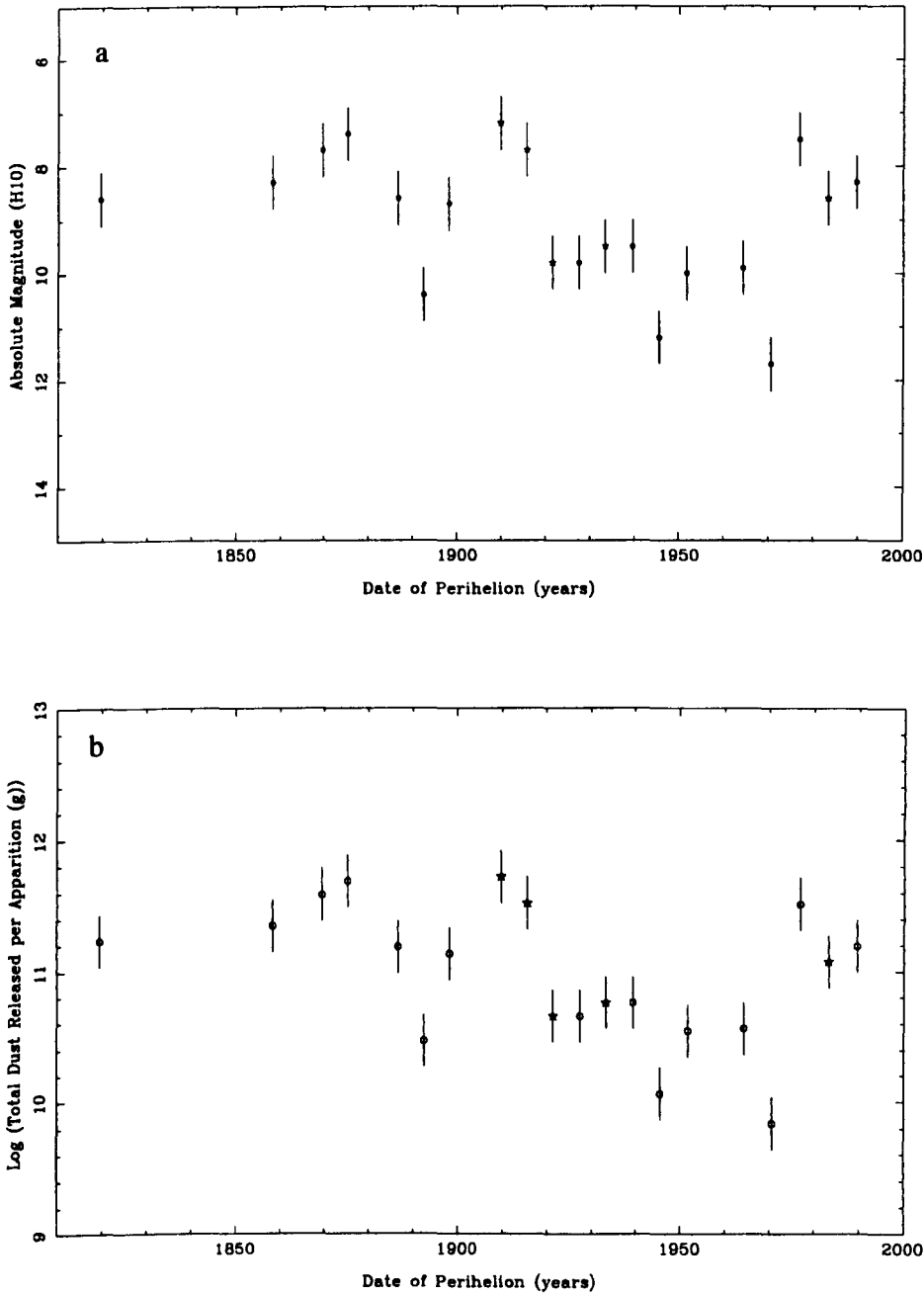


Figure 4.11: **7P/Pons-Winnecke**. Plot (a) shows the variation in  $H_{10}$  against the year in which perihelion passage occurred. The symbol  $\star$  refers to values of  $H_{10}$  calculated from the post-perihelion part of the light curve and the symbol  $\circ$  refers to values of  $H_{10}$  calculated from the pre-perihelion part of the light curve. In plot (b) the logarithm of the mass of dust released per apparition,  $M_{ap}$ , is calculated by presuming the light curve is symmetrical about perihelion, *i.e.* pre and post-perihelion values of  $H_{10}$  are the same.

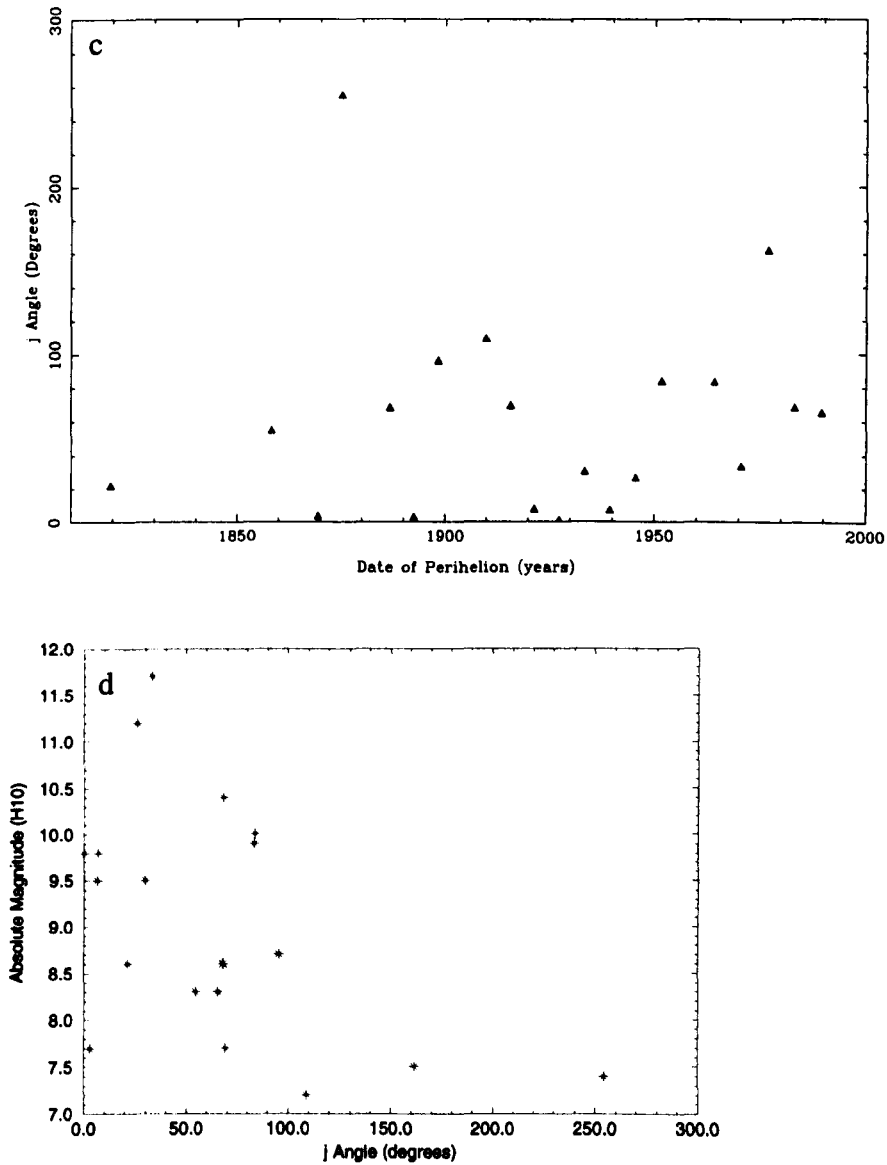


Figure 4.11: [Continued] Plot (c) show the  $j$  angle against the year in which perihelion passage occurred. Plot (d) shows the  $j$  angle against  $H_{10}$ .

In figure (4.11a) only 5 apparitions have a  $H_{10}$  value calculated from the post-perihelion light curve. These 5 points do not create any obvious structure in the plot and so light curve asymmetry is considered unimportant for conclusions about the shape of the curve in figure (4.11a).

During the period 1819 to 1989, 4 perihelion passages were missed (see table (4.1)). This constitutes 17% of the number of perihelion passages expected during this time. The estimated missed perihelion passages are listed in table (4.3).

### **The Holetschek Effect and the $H_{10}$ Weights**

The variation in the orbit of 7P/Pons-Winnecke from apparition to apparition means that the observing geometry is not regular. Figure (4.11c) shows the  $j$  angle against the year in which perihelion passage occurred. Figure (4.11d) shows  $H_{10}$  against the  $j$  angle. Neither indicate that the shape of the data in figure (4.11a) is a result of variable observing geometry.

The first 13 recorded apparitions from 1851 until 1939 have the largest  $H_{10}$  weights, never falling below 0.85 (see figure (4.2)). After 1939 the weights decrease in value, although only the 1976 apparition has a weight as low as 0.0 and is the only one to have a weight less than 0.5. This 1976 apparition is not sufficient to alter the main conclusions about figure (4.11a). The  $H_{10}$  weights at the time of the close approaches with Earth are shown in table (4.4). All these apparitions have a  $H_{10}$  weight,  $W > 0.8$ .

Apparition (Year)	Minimum Distance from Earth (AU)	$H_{10}$ Weight
1819	0.1318	0.99
1869	0.2341	0.94
1892	0.1236	0.95
1921	0.1412	0.96
1927	0.0394	0.98
1939	0.1073	0.95
1945	0.4541	0.82

Table 4.4: Close approach distances,  $\Delta < 5$  AU, between 7P/Pons-Winnecke and the Earth taken from Sekanina (1989). The  $H_{10}$  weights are taken from the Kresák and Kresáková catalogue (1989).

### 4.10.3 The Mass of Dust Released per Apparition, $M_{ap}$

7P/Pons-Winnecke has released enough dust over its lifetime to have a meteor stream associated with it, the June Boötids, which can be seen from June 27 to July 5 (e.g. Beech (1998)). Table (4.5) shows that the comet released an average of  $\bar{M}_{ap} = (3.4 \pm 0.4) \times 10^{11}$  g per apparition, which makes 7P/Pons-Winnecke the smallest contributor of dust, from the five comets considered in this chapter.

For a dust to snow mass ratio of 1:2.2, this corresponds to a combined (snow and dust) mean mass release rate of  $10.9 \times 10^{11}$  g per apparition. For a mean density of  $0.5 \text{ g cm}^{-3}$ , this is a mean volume loss of  $2.2 \times 10^{12} \text{ cm}^3$  per apparition. For an equivalent nucleus radius of 2 km (see below) this corresponds to a mean layer loss of about  $\sim 14$  cm per apparition.

Note that the conclusion by Sekanina that the varying orbital parameters will significantly affect the mass of dust released by the nucleus is not supported by this model. Figure (4.4) shows the increasing trend in perihelion distance over time. But in figure (4.11b) the shape of the  $\log M_{ap}$  curve does not appear any different to the shape of the  $H_{10}$  plot shown in figure (4.11a).

#### 4.10.4 Active Areas

Sekanina (1989) assumed an albedo of 0.04 and calculated an equivalent diameter of about 4.0 km for 7P/Pons-Winnecke. This value is used in equation (4.1) to find the variation in the percentage of the nucleus surface that is active at each apparition (see figure (4.12a)).

Figure (4.12b) shows the variation in the logarithm of the fraction of the nucleus surface that is active, i.e.  $\log f$  from equation(4.1). These plots indicate that 7P/Pons-Winnecke has had a low level of activity during the period 1819 to 1989. These results indicate that the percentage of the nucleus surface that was active reached a maximum of 5.6 % in 1909 and a minimum of 0.09 % in 1970. The maximum change *between two consecutive apparitions* was from 1.4 % to 5.6 % (a  $\times 4$  change in the total area covered by the active areas) between 1898 and 1909 (see table (4.6)). Sekanina (1989) estimated, from the water production rates, that  $2 \text{ km}^2$  of the nucleus surface was active during the 1927 apparition of the comet, and concluded that this corresponds to 3% – 5% of the cometary nucleus surface. In this analysis a value of 0.5% was calculated for the 1927 apparition, however activity of the order of 3% – 5% of the nucleus surface is probably not unusual for 7P/Pons-Winnecke.

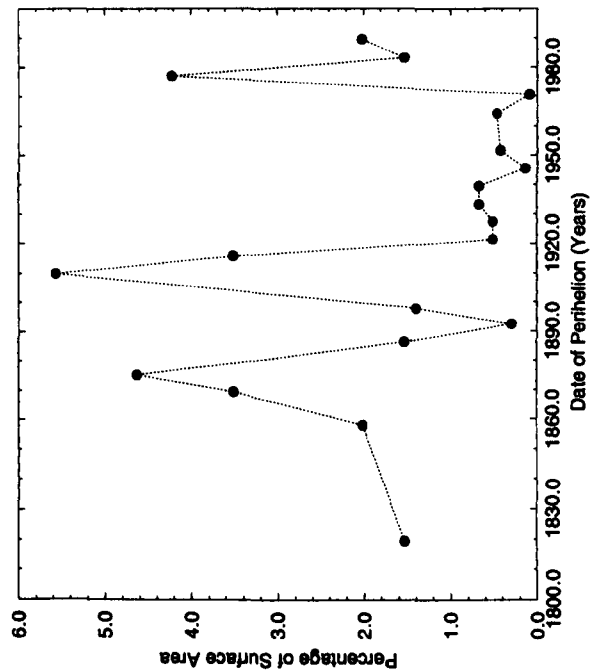
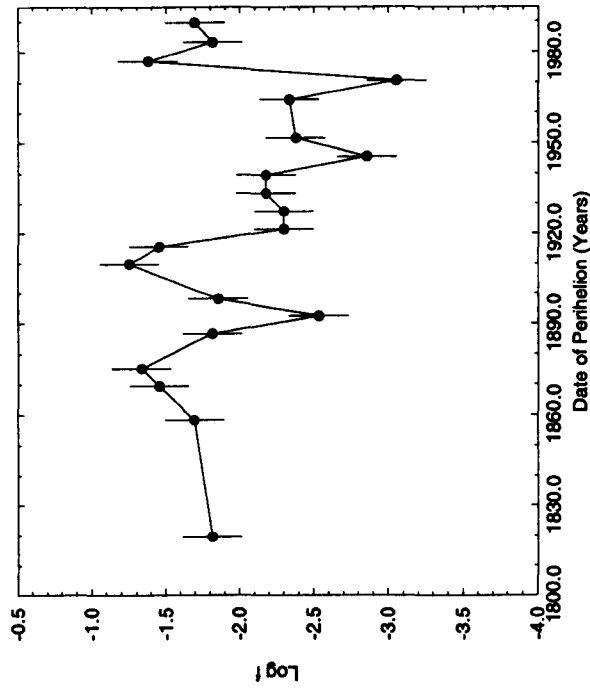


Figure 4.12: The percentage of the 7P/Pons-Winnecke nucleus surface that was active is shown in plot (a) and the logarithm of the active fraction,  $\log f$ , used in equation (4.1) is shown in plot (b). The error bars were calculated by assuming that the uncertainty in  $H_{10}$  was  $\pm 0.5$  magnitudes.

## 4.11 4P/Faye

### 4.11.1 Introduction

Comet 4P/Faye was first discovered by H.A. Faye on the 23rd of November 1843 (Belyaev et al. 1986). Figure (4.4) shows that the orbital period, eccentricity and perihelion distance for 4P/Faye have not been subject to changes as drastic as those for 6P/d'Arrest or 7P/Pons-Winnecke. Since 1843, the orbital period has varied by 0.27 years, the perihelion distance has varied by 0.16 AU and the eccentricity has varied by 0.03.

### 4.11.2 $H_{10}$ Absolute Magnitudes, Light Curve Asymmetry and Missing Apparitions

Of the 5 comets considered here, the  $H_{10}$  data for P/Faye provides the best evidence for a possible progressive variation in the physical brightness of a comet over several apparitions. Figure (4.13a) shows the variation in  $H_{10}$  over 19 apparitions of the comet. The  $\pm 0.5$  magnitude uncertainties are clearly not large enough to account for the scatter in the pre-1910 region.

Figure (4.13a) indicates that, pre-1910, the comet was unusually active. It then faded to a 'steady state' situation in the post-1910 era.

The 10 pre-perihelion,  $\circ$ , and 9 post-perihelion,  $\star$ , absolute magnitudes in figure (4.13a) appear to be well mixed and there is no obvious structure in the plot that can be attributed to the light curve asymmetry. In the 'steady state', i.e. post-1910 region, the mean of the 6 pre-perihelion absolute magnitudes is  $7.2 \pm 0.5$ . This agrees with the mean for the 5 post-perihelion 'steady state' absolute mag-

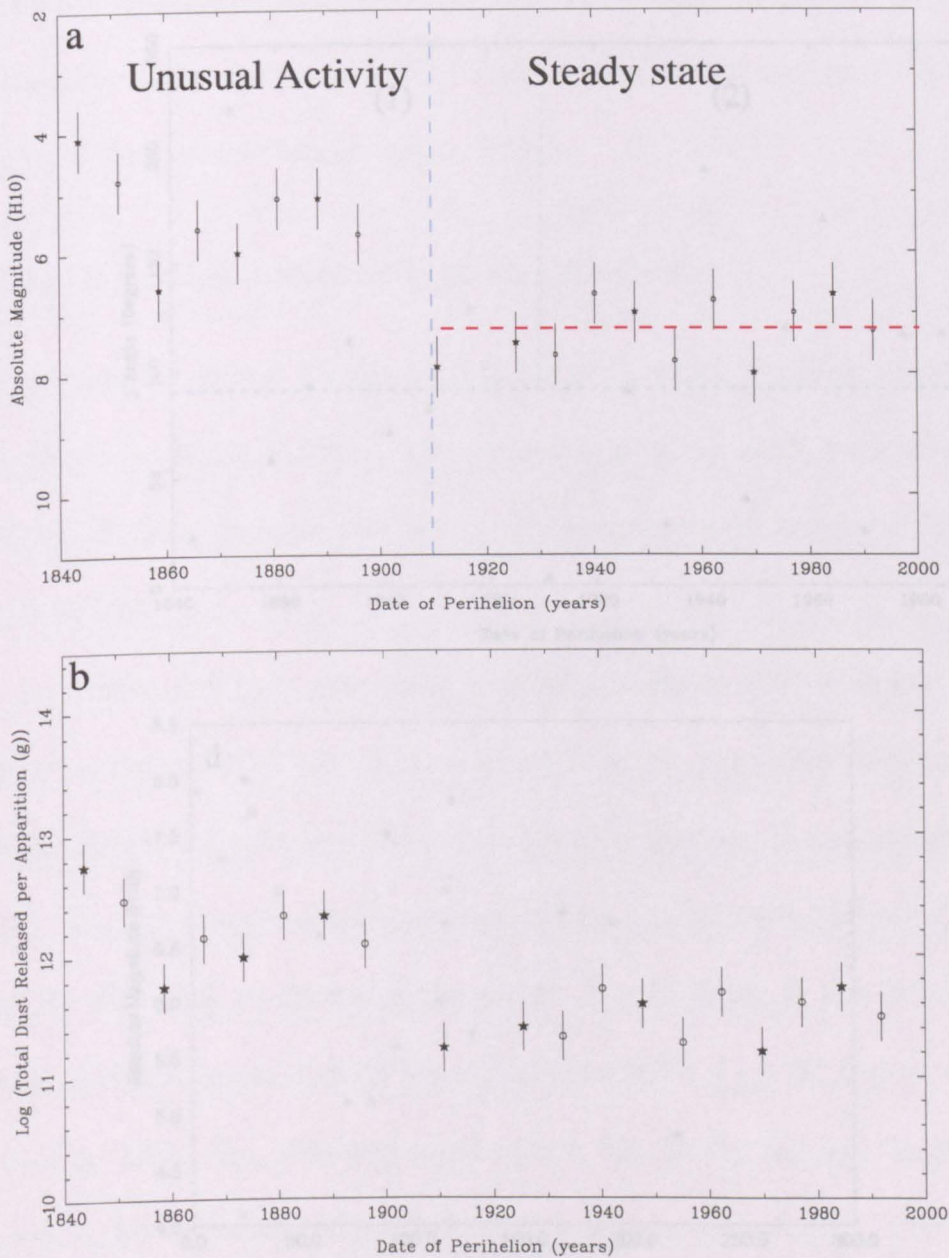


Figure 4.13: **4P/Faye**. Plot (a) shows the variation in the absolute magnitude,  $H_{10}$ , over 19 cometary apparitions. The interpretation is that, pre-1910, the comet progressively faded, albeit in a non linear way, down to a steady state situation in the post-1910 region. In plot (b) the logarithm of the mass of dust released per apparition,  $\log M_{ap}$  is calculated by presuming the light curve is symmetrical about perihelion, *i.e.* pre and post-perihelion values of  $H_{10}$  are the same.

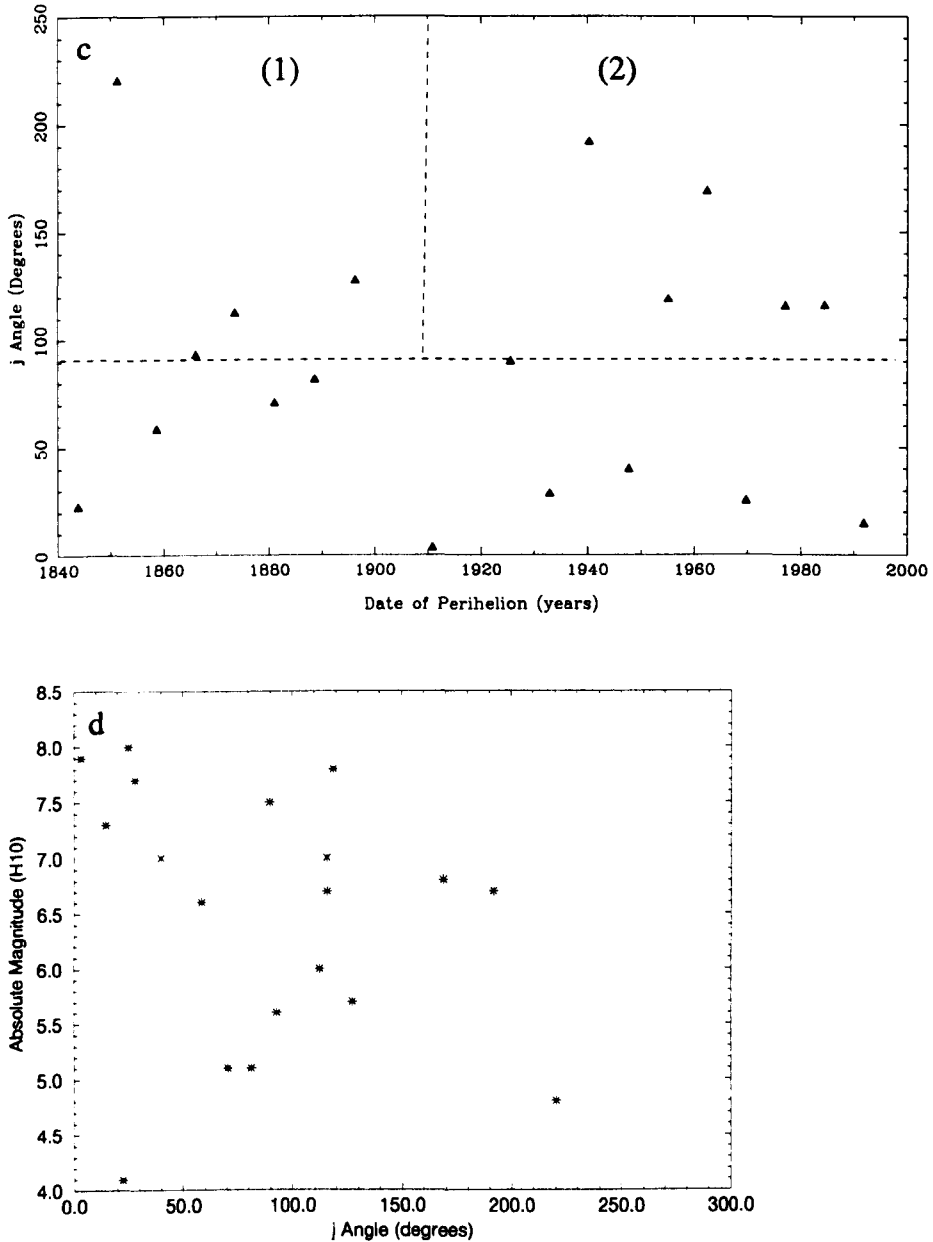


Figure 4.13: [Continued] Plot (c) show the  $j$  angle against the year in which perihelion passage occurred. The plot is divided into 2 regions: (1) Pre-1910,  $90^\circ > j > 270^\circ$  and (2) Post-1910,  $90^\circ > j > 270^\circ$  to see if the Holetschek effect can explain the difference in the  $H_{10}$  values for the two periods of time. Plot (d) shows the  $j$  angle against  $H_{10}$ .

nitudes of  $7.4 \pm 0.6$ . There is no reason to conclude that light curve asymmetry affects the shape of steady state region in figure (4.13a).

Only two apparitions in 1903 and 1917 were missed during the period 1843-1991 (see table (4.1) and table (4.3)). These would not be enough to account for the general form of the data in figure (4.13a).

### The Holetschek Effect and the $H_{10}$ Weights

The variation in the  $j$  angle with the year in which perihelion passage occurred is shown in figure (4.13c). The variation in the  $j$  angle with  $H_{10}$  is shown in figure (4.13d). Neither plot shows any structure similar to the  $H_{10}$  plot in figure (4.13a).

In section (3.2.2) it was noted that as  $j$  tends to  $180^\circ$  it should be harder to observe the comet. Thus, in figure (4.13c) the  $90^\circ < j < 270^\circ$  section of the plot is highlighted and split into the unusual activity region (1) and steady state region (2). It might be expected that that the unusual activity region (2) is the result of the difficulty in observing the comet. But from the 8, pre-1910,  $H_{10}$  absolute magnitudes 4 points, (i.e. 50 %), fall into the  $90^\circ < j < 270^\circ$  region, while from the 11, post-1910,  $H_{10}$ , absolute magnitudes 6, (i.e. 55 %), fall into the  $90^\circ < j < 270^\circ$  region. Therefore, the Holetschek effect cannot account for the differences between the pre and post-1910 data.

The variation in  $H_{10}$  weight as a function of the year in which perihelion passage occurred is shown in figure (4.2). The weights suggest the opposite of what would be expected if the scatter in the unusual activity region in figure (4.13a), was due to observational uncertainty. The pre-1910 weights do not fall below 0.5 and have

a mean value of 0.64. The post-1910 weights *do* fall below 0.5 for 3 apparitions (1940,1955 and 1962) and have a mean value of 0.58. This indicates that the absolute magnitudes in the pre-1910, unusual activity, region should be more certain than in the post-1910, steady-state, region.

### 4.11.3 The Mass of Dust Released per Apparition, $M_{ap}$

The logarithm of the mass of dust released per apparition,  $M_{ap}$ , is shown in figure (4.13b). The shape from figure (4.13a) is still present, indicating that the variation in the cometary orbit was not significant.

If the 4P/Faye light curve has been symmetrical over all of the recorded apparitions then 4P/Faye released a greater mass of dust in 19 apparitions than in the 55 recorded apparitions of 2P/Encke (see table (4.5)). The first 8, pre-1910, apparitions in figure (4.13b) released 82.3% of the total dust mass, while post-1910 the comet settled down to release  $3.6 \times 10^{12}$  g of dust over 11 apparitions. The mean mass of dust released post-1900 was  $\bar{M}_{ap} = 3.3 \times 10^{11}$  g per apparition.

The mean mass of dust released during all 19 apparition was  $\bar{M}_{ap} = 21.6 \times 10^{11}$  g. This corresponds to a combined (water and dust) mean mass release rate of  $69.1 \times 10^{11}$  g per apparition, or a volume of  $1.4 \times 10^{13}$   $cm^3$  ( $\bar{\rho} = 0.5$   $gcm^{-3}$ ) lost from the nucleus per apparition. For an equivalent radius of 2.68 km (see below), the mean depth of layer lost from the nucleus was  $\sim 1.9$  m.

### 4.11.4 Active Areas

Gil-Hutton and Licandro (1994) calculated an equivalent radius of  $4.7 \pm 1.1$  km for the nucleus of 4P/Faye by assuming an albedo of  $\leq 0.05$ . Lamy and Toth (1995)

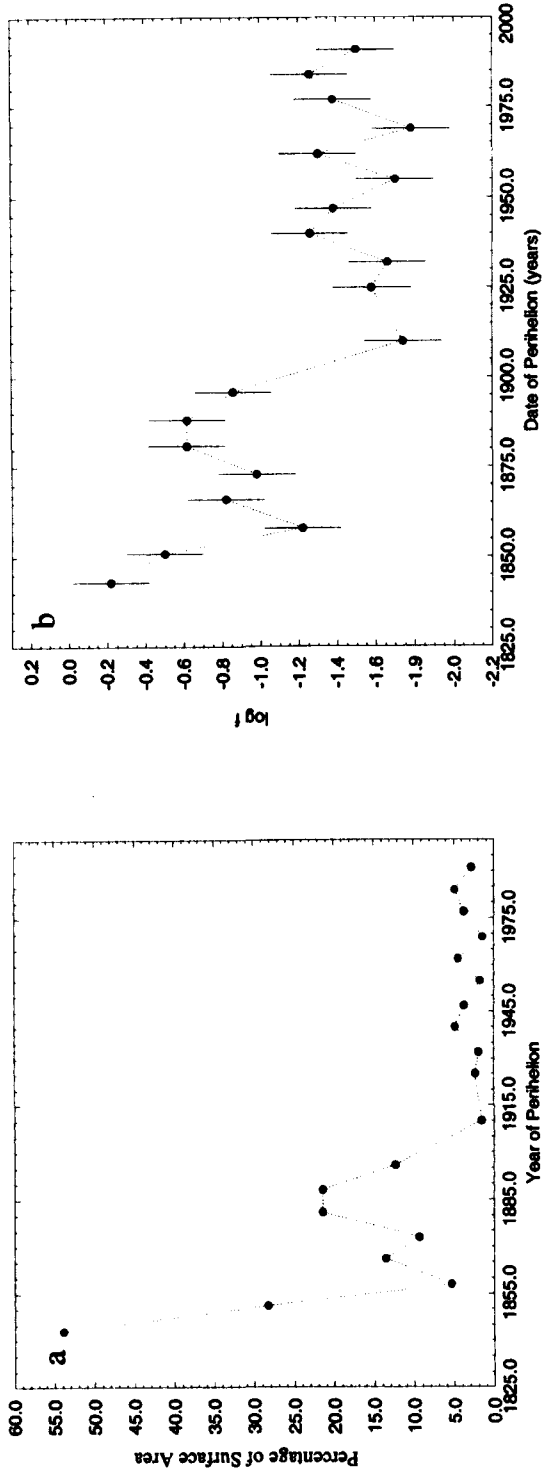


Figure 4.14: The percentage of the 4P/Faye nucleus surface that was active is shown in plot (a) and the logarithm of the active fraction,  $f$ , used in equation (4.1) is shown in plot (b). The error bars were calculated by assuming that the uncertainty in  $H_{10}$  was  $\pm 0.5$  magnitudes.

made an “unambiguous detection” of the cometary nucleus, with the Hubble Space Telescope, and by assuming an albedo of 0.04 found that the nucleus has a mean radius of  $2.68 \pm 0.05$  km. This later, more accurate value, is used to calculate the fraction of the nucleus surface that is active at each apparition.

The increase in  $H_{10}$  magnitude (*i.e.* drop in brightness) from 4.1 in 1843 to 7.9 in 1910 is significant if  $\pm 0.5$  magnitude error bars are reasonable. Using equation (4.2) this dip corresponds to a change in the equivalent radius from 10.7 km to 1.9 km. This corresponds to an unrealistic average loss of about 1 km from the radius per apparition. Therefore, assuming a constant value of  $f$  is not valid for this comet and a variable value of  $f$  should be used, *i.e.* equation (4.1).

In figure (4.14a) the Lamy and Toth radius of 2.68 km is used in equation (4.1) to calculate the percentage of the nucleus surface that was active at different apparitions. The logarithm of the fraction of the nucleus surface that was active,  $\log f$ , is shown in figure (4.14b)

Figure (4.14a) indicates that pre-1910 the percentage of the nucleus surface that was active varied from 54% (during 1843), down to a steady state situation where the percentage did not get above 5%. The minimum percentage was 1.5 % in 1969 and the maximum change in the percentage of the nucleus surface that was active between two consecutive apparitions was from 28 % to 54 % (a  $\times 2$  change in the size of the active areas) and occurred during the period 1843 to 1851 (see table (4.6)).

Gil-Hutton and Licandro (1994) calculated the production rate of water for the 1991 apparition of 4P/Faye and, for a radius of  $4.7 \pm 1.1$  km calculated that  $3\% \pm 2\%$  of the nucleus surface was active, this agrees, albeit fortuitously, with the value of

Comet	$N_{ap}$	$M_{Total} (\times 10^{13} \text{g})$	$\bar{M}_{ap} (\times 10^{11} \text{g})$
2P/Encke	55	$2.7 \pm 0.2$	$4.8 \pm 0.4$
6P/d'Arrest	15	$1.1 \pm 0.5$	$7.0 \pm 0.2$
4P/Faye	19	$4.1 \pm 1.9$	$21.6 \pm 0.5$
7P/Pons-Winnecke	20	$0.7 \pm 0.3$	$3.4 \pm 0.4$
10P/Tempel2	18	$1.5 \pm 0.7$	$8.2 \pm 0.2$

Table 4.5: For each comet, the total mass of dust released,  $M_{Total}$ , over all of the apparitions recorded in the Kresák and Kresáková catalogues is listed. The mean mass of dust released per apparition,  $\bar{M}_{ap}$  is also recorded and indicates that 4P/Faye is a prolific contributor of dust. The uncertainty is calculated by assuming an uncertainty in the  $H_{10}$  values of  $\pm 0.5$ .

Comet	Min %	Max %	Min $\Delta\%$	Max $\Delta\%$
4P/Faye	$1.5^{+0.9}_{-0.5}$ (1969)	$54^{+32}_{-20}$ (1843)	0.00 (1881-1888)	28 % to 54 % (1843-1851)
7P/Pons-Winnecke	$0.09^{+0.05}_{-0.03}$ (1970)	$6^{+3}_{-3}$ (1909)	0.00 (1921-1927, 1933-1939)	1.4 % to 5.6 % (1898-1909)
10P/Tempel 2	$0.1^{+0.2}_{-0.1}$ (1899)	$2^{+3}_{-1}$ (1978)	0.00 (1983-1988)	0.2 % to 1.8 % (1972-1978)

Table 4.6: The extremes in the percentage of the nucleus surface that is active. Min % and Max % are the minimum and maximum percentage of the nucleus surface that was actively releasing gas and dust. The year in which this occurred is given in parenthesis and the uncertainty comes from assuming  $\Delta H_{10} = 0.5$ . Min  $\Delta\%$  and Max  $\Delta\%$  are the maximum and minimum variations in the percentage of the nucleus surface that was active *between two consecutive apparitions*, excluding the uncertainty in the calculation of  $f$ . The years during which the change occurred are also given in parenthesis.

$3^{+2}_{-1}\%$  calculated here for the 1991 apparition.

## 4.12 Summary

1. The 2P/Encke light curve asymmetry is very important when considering the secular variation in the  $H_{10}$  absolute magnitudes for this short period comet. The  $H_{10}$  plot shown in figure (4.6a) appears to form the shape of a band. This is due to the difference in pre/post-perihelion values of  $H_{10}$ . There is

tentative evidence that a band shape (thinner than the one in figure (4.6a)) may be real.

2. The  $H_{10}$  plot for 6P/d'Arrest, shown in figure (4.8a), appears sinusoidal. This is likely to be a result of the missing data which corresponds to 32% of the apparitions expected from 1851 to 1989. This is a good example of why linear regressions must be applied with caution to absolute magnitude data.
3. There are no obvious progressive trends in the  $H_{10}$  data for 7P/Pons-Winnecke and 10P/Tempel 2.
4. The  $H_{10}$  plot for 4P/Faye, shown in figure (4.13a), shows the best evidence for progressive variations in cometary absolute magnitudes. This is interpreted as a period of unusual activity, where up to  $54_{-20}^{+32}$  of the surface of the nucleus was active. This was followed by a steady-state period post-1910, during which time the percentage of the surface that was active stayed below 5%.

# Chapter 5

## A Decaying Short Period Comet Population

### 5.1 Introduction

Active comets decay at each perihelion passage. The mass released from a comet is not replenished and so, unless new comets are perturbed onto short period orbits, the total number of comets in the inner Solar System population must decrease.

In this chapter a model population of short period comets is created. A distribution of the sizes of cometary nuclei is produced which is based on the size distribution of the present short period comet population. A simplified assumption about cometary decay is made and each comet in the population is allowed to decay according to this model. The population is then examined at different stages of its decay.

An important parameter in cometary physics is the mass (or size) distribution index. This parameter defines how the masses (or sizes) of cometary nuclei are dis-

tributed within a population of comets, *i.e.* is most of the population mass in the form of a few very massive cometary nuclei, or are there many small-mass comets? The mass distribution index is defined and calculated for the decaying model population at different times and the effect that a decaying cometary population has on the mass distribution index is examined.

## 5.2 The Size Distribution of Cometary Nuclei

### 5.2.1 The Size Range of Short Period Comets

To produce a model population of comets and observe how the sizes of those comets change with time it is first necessary to produce reasonable values for the current dimensions of short period cometary nuclei. To deduce the size of a cometary nucleus is not an easy task. When a comet is active a coma of dust and gas is produced which acts to obscure the nucleus. Unless the comet is dormant (see section (2.5.2)) it is normally inactive because it is too cold for snow at, or near, the surface of the cometary nucleus to sublimate. This normally occurs at large heliocentric distances, *i.e.* water snow sublimation is significant at heliocentric distances within 2.8 AU. If the nucleus contains substances that are more volatile than water snow, such as CO then sublimation can occur at larger heliocentric distances. Hale-Bopp, for example, was observed to be outgassing CO at a heliocentric distance of 7 AU (Biver et al. 1996). As cometary nuclei have a mean albedo of  $0.05 \pm 0.04$  (Hartmann et al. 1987) and have diameters of only a few kilometres, calculations of the size of these objects, at large heliocentric distances, can be difficult.

The best way to find the size of a cometary nucleus is to send a space probe to

make observations at close range. 1P/Halley was observed by *Giotto* at a distance of  $591.5 \text{ km} \pm 2 \text{ km}$  and the nucleus was found to have semi-major axes of  $8 \text{ km}$  by  $4.1 \text{ km}$  by  $4.2 \text{ km}$  (Keller et al. 1987). Unfortunately, this is the only comet where this technique has been used. Consequently, other methods need to be used.

### 5.2.2 Measuring the Size of a Bare Nucleus

If a cometary nucleus does not have a significant coma and is observed at a large heliocentric distance (*i.e.* when sublimation of the snow has ceased) and if the albedo of the object is known then the size of the nucleus can be found.

Following Russell (1916), the Bond definition of the albedo,  $A$ , for a spherical object is,

$$AR^2 = r^2 M_o \Delta^2 \cdot 2 \int_0^\pi \phi(\alpha) \sin \alpha \, d\alpha \quad (5.1)$$

Here,  $R$  is the equivalent radius of the object, *i.e.* the radius of a sphere with the same surface area as the cometary nucleus.  $r$  is the heliocentric distance of the object in AU.  $M_o$  is the ratio of the apparent brightness of the object, at full phase, to that of the Sun when the object is at a distance  $\Delta$ (AU) from the Earth.  $\phi(\alpha)$  is the brightness of the object at a phase angle  $\alpha$ , where the object at full phase has a brightness of unity.

### 5.2.3 Measuring the Size of an Active Nucleus

Unfortunately, the bare cometary nucleus has not been seen for most comets. A method is therefore required to calculate the equivalent radius of an active, coma-obscured, nucleus.

Hughes (1988b) assumed that the brightness of a comet,  $B$ , is proportional to the surface area of the nucleus that is active,

*i.e.*,

$$B \propto fR^2, \quad (5.2)$$

where  $R$  is the equivalent radius of the nucleus in km and  $f$  is the fraction of the nucleus surface that is actively emitting gas and dust.

Hughes (1989a) used the above relationship and produced an equation that relates the equivalent radius of a cometary nucleus,  $R$ , the absolute magnitude,  $H_{10}$ , and the active fraction of the nucleus surface,  $f$ . This had the form of,

$$\log R(\text{km}) = 1.114 - 0.5 \log f - 0.2H_{10} \quad (5.3)$$

Hughes found the constant, 1.114, from the average fraction of the nucleus surface that has been active for 1P/Halley during the last 2000 years ( $\bar{f} = 0.034$ ), the average absolute magnitude during this time ( $\bar{H}_{10} = 5.5 \pm 0.7$ ) and the equivalent nucleus radius ( $R = 5.6$  km), measured during the *Giotto* mission.

To produce an estimate of the radii of cometary nuclei, weighted mean absolute

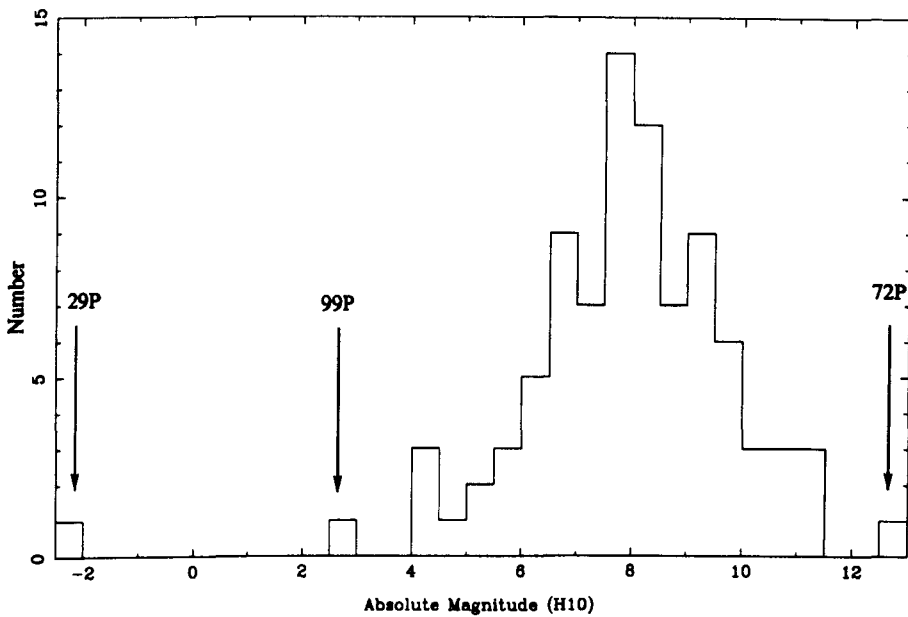


Figure 5.1: The weighted mean absolute magnitude,  $H_{10}$ , for the 90 short period comets in the Kresák and Kresáková catalogues that have had more than one apparition recorded. The individual values of  $H_{10}$  used to calculate  $\bar{H}_{10}$  were estimated from either the pre-perihelion or post-perihelion light curve. The mean absolute magnitude for 29P/Schwassmann-Wachmann 1 is not included in further analysis since the comet has had several outbursts and so equation (5.4) is not valid for this comet.

magnitudes,  $\bar{H}_{10}$ , were taken from the Kresák and Kresáková catalogues (1989, 1994) and used in equation (5.3). Figure (5.1) shows the distribution of mean absolute magnitudes for the 90 short period comets in the catalogues that have had more than one apparition.

By assuming that 1P/Halley is a typical comet and that its equivalent radius has not significantly altered during this time Hughes concluded that the active fraction of the nuclear surface can be approximated to a constant value of  $\bar{f} = 0.034$ . Consequently, equation (5.3) becomes,

$$\log R(\text{km}) = 1.848 - 0.2H_{10} \quad (5.4)$$

A constant value of  $f$  is unlikely to be realistic (see chapter (4)), but in this chapter it was not necessary to produce the exact radii of individual short period comets but instead to ascertain the *characteristic sizes* of short period cometary nuclei. Therefore, equation (5.4) was used to calculate the nucleus size of all the comets in the population.

The mean absolute magnitudes,  $\bar{H}_{10}$ , were taken for the 90 non-defunct short period comets of more than one apparition from the Kresák and Kresáková catalogues. These were used to find an upper limit to the size of short period cometary nuclei.

Using equation (5.4) produces a range of sizes from 0.21 km for 72P/Denning-Fujikawa ( $\bar{H}_{10} = 12.6$ ) up to 194.1 km for 29P/Schwassmann-Wachmann 1 ( $\bar{H}_{10} = -2.2$ ). The latter radius should be compared with the maximum radius of the nucleus found by Meech (1993) of  $15.4 \pm 0.2$  km. All of the apparitions of 29P/Schwassmann-Wachmann 1 were given a  $H_{10}$  weighting of 0.0 in the catalogues (see chapter (4)), as this comet has been subject to several outbursts. Therefore, 29P/Schwassmann-Wachmann 1 was excluded from the model population of short period comets.

The next brightest comet is 99P/Kowal 1 ( $\bar{H}_{10} = 2.7$ ) and puts the upper size of short period cometary nuclei at 20.3 km. This value was considered a more appropriate upper limit on the equivalent radii of short period comets for the model developed in this chapter.

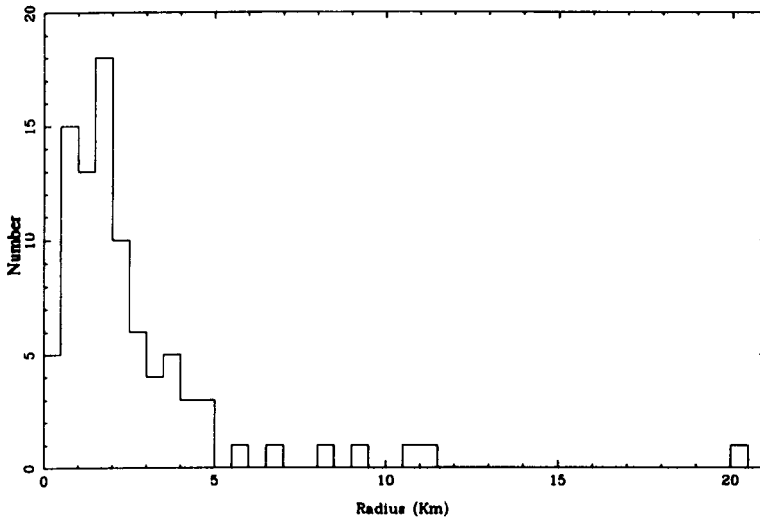


Figure 5.2: The short period comet nucleus size distribution. From equation (5.4) 29P/Schwassmann-Wachmann 1 has an unlikely equivalent radius of 194.1 km and so is not shown here. Note that equation (5.4) indicates that most comets in the distribution have an equivalent radius less than 5 km. The bin size is  $\Delta R = 0.5$  km.

#### 5.2.4 Producing the Size Distribution

Equation (5.4) and the values of  $\bar{H}_{10}$  in the Kresák and Kresáková catalogues can be used to produce a list of cometary radii for the current population of short period comets. Figure (5.2) shows the distribution of radii for 89 of the short period comets.

The 89 short period comet magnitudes used in this chapter can be contrasted with a total of 185 short period comets quoted in the *Catalogue of Cometary Orbits* (Marsden & Williams 1996). The extra short period comets are both those that have had only one apparition recorded and those that are now classified as defunct. Equation (5.4) was thought to be less reliable for these comets and so they are excluded from this model population.

It is also expected that the data set becomes more incomplete with increasing

cometary perihelion distance (see section (6.5.1)). Unfortunately, accounting for the missing comets was beyond the scope of this chapter. Thus, rather than use the incomplete size distribution shown in figure (5.2), a model population was created from the key characteristics of the current short period comet population. These key characteristics are the range of cometary nucleus sizes (the upper limit of 20 km calculated here) and the shape of the size distribution for the *largest* short period cometary nuclei.

### 5.2.5 Describing the Distribution by a Power Law

If  $\bar{H}_{10}$  magnitudes can be converted into masses then a quantity called the *mass distribution index*,  $s$ , can be calculated. This index can be used to produce a *size distribution* for the model cometary population.

The mass distribution index (defined in section (5.2.8)) is a parameter which has been used to define how the total mass of a given population is distributed among the members of that population. It is an important quantity in the physics of minor Solar System bodies as it acts as an indication of the process by which the bodies formed and evolved (see Hughes (1982)).

The mass distribution index is defined, such that a value of  $s < 2$  indicates that most of the total mass of the cometary population is in the form of a few massive cometary nuclei. Such a low value might also indicate that comets formed by the accretion of small mass bodies. Daniels and Hughes (1981) modelled the formation of a cometary nucleus by the accretion of particles and found that their model produced an index of  $s = 1.65 \pm 0.11$ .

A value of  $s > 2$  would indicate that the majority of the total mass of the cometary

population is in the form of many small mass cometary nuclei. Such a high value of  $s$  would indicate that comets formed, or evolved, by a fragmentational process, in which larger mass bodies broke up into the current cometary nuclei.

To date, no cometary mass has been measured and so the mass distribution index is usually found from cometary magnitude data.

### 5.2.6 The Cumulative Number, $N(\bar{H}_{10})$

The cumulative number of comets with an absolute magnitude less than (*i.e.* brighter than)  $\bar{H}_{10}$  is often plotted against  $\bar{H}_{10}$  (*e.g.* see Hughes and Daniels (1980)), and assumed to agree with an equation of the form,

$$N = ba^{\bar{H}_{10}}, \quad (5.5)$$

Here,  $b$  and  $a$  are taken to be constants.

Equation (5.5) can be expressed in a logarithmic form as,

$$\log N(\bar{H}_{10}) = \bar{H}_{10} \log a + \log b \quad (5.6)$$

The values of  $\log a$  and  $\log b$  can be found from a cumulative plot of the  $\bar{H}_{10}$  data.

This method is discussed in more detail in section (5.3).

The mean absolute magnitude,  $\bar{H}_{10}$  is proportional to the logarithm of the cometary brightness,  $B$ , such that,

$$\bar{H}_{10} = -\frac{5}{2} \log B + C_1, \quad (5.7)$$

where  $C_1$  is a constant. If the cometary brightness is assumed to be proportional to the surface area of the cometary nucleus, then the mass of the cometary nucleus,  $M$ , would be proportional to  $B^{\frac{3}{2}}$  and equation (5.7) becomes,

$$H_{10} = -\frac{5}{3} \log M + C_2, \quad (5.8)$$

where  $C_2$  is a constant.

### 5.2.7 The Cumulative Number, $N(M)$

Combining equation (5.5) and equation (5.8) produces the cumulative number,  $N(M)$ , of comets with masses greater than  $M$ ,

$$N(M) = C_3 a^{-\frac{5}{3} \log M}, \quad (5.9)$$

where  $C_3$  is a constant. By defining  $a = 10^p$  equation (5.9) becomes,

$$N(M) = C_3 10^{\log(M^{-\frac{5}{3}p})} = C_3 M^{-\frac{5}{3}p} \quad (5.10)$$

### 5.2.8 The Definition of the Mass Distribution Index

Following Hughes (1980),  $\zeta(M)$  is the number of comets with masses between  $M$  and  $M \pm \delta M$  and is defined by,

$$\zeta(M) = AM^{-s} dM, \quad (5.11)$$

where  $s$  is the mass distribution index and  $A$  is a constant.

The cumulative number,  $N(M)$ , of comets with masses greater than  $M$  is then,

$$N(M) = \int_M^{\infty} AM^{-s} dM = \frac{AM^{-(s-1)}}{1-s} = C_4 M^{1-s}, \quad (5.12)$$

where  $s > 1$  and  $N(M)$  in equation (5.12) is the same as in equation (5.10).

Thus,

$$N(M) = C_4 M^{1-s} = C_3 M^{-\frac{5}{3}p}, \quad (5.13)$$

where  $C_4$  is a constant. Since  $C_4 = C_3$  then,

$$1 - s = -\frac{5}{3}p = -\frac{5}{3} \log a \quad (5.14)$$

*i.e.*

$$s = 1 + \frac{5}{3} \log a \quad (5.15)$$

### 5.2.9 Relating the Mass of the Nucleus to the Effective Radius

The mass of the nucleus,  $M$ , is proportional to  $R^3$  and so equation (5.12) becomes,

$$N(R) = C_5 R^{3(1-s)} \quad (5.16)$$

and

$$\log N(R) = 3(1 - s) \log R + \log C_5, \quad (5.17)$$

where  $C_5$  is a constant. Thus, if a plot of the form  $\log N(R)$  against  $\log R$  is produced then the gradient is  $3(1 - s)$  and can be used to find the mass distribution index. Conversely, if a mass distribution index is known then this can be used to produce the cometary nucleus size distribution for the model population.

Note that equation (5.17) indicates that the  $\log N(R)$  against  $\log R$  should be linear. In practice this occurs only for the larger members of the population. This problem is discussed in section (5.3).

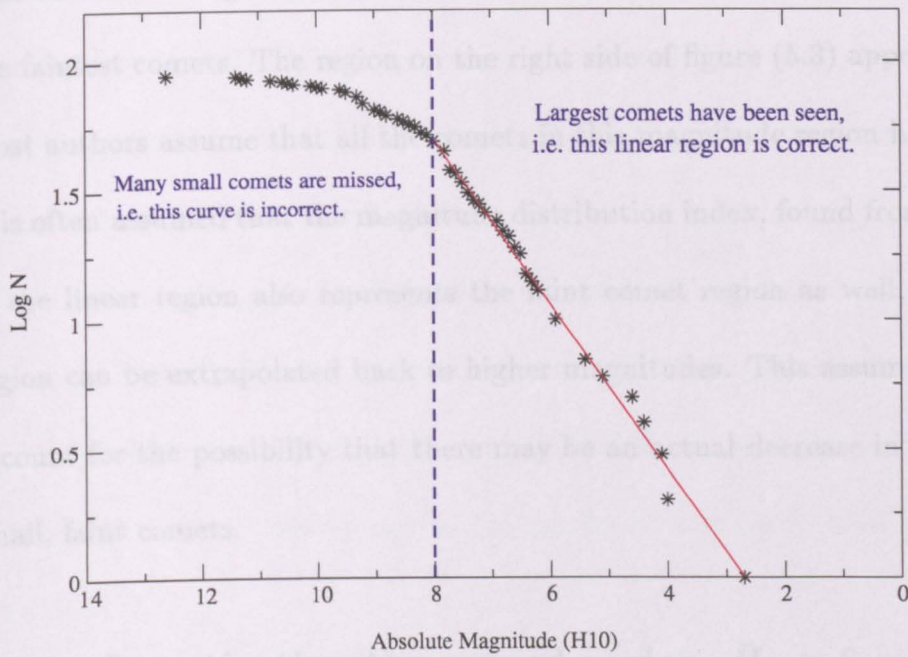


Figure 5.3: The mean absolute magnitudes,  $\bar{H}_{10}$ , of the 89 short period comets plotted in cumulative form. Each point on the plot corresponds to the logarithm of the total number of comets brighter than or equal to the magnitude at that point. The point at which the linear region ends is at  $\bar{H}_{10} = 8.0 \pm 0.5$ . The normal interpretation is that comets with  $\bar{H}_{10} > 8.0$  are being missed rather than an actual decrease in the number of small comets.

A linear regression analysis<sup>3</sup> for this data set (see red line) implies a mass distribution index<sup>4</sup> of  $s = 1.54 \pm 0.01$ , which agrees with the model value of  $s = 1.65 \pm 0.11$  calculated by Hughes (1989a).

### 5.3 Are the Faintest Comets Missing?

Using equation (5.6) the mass distribution index,  $s$ , can be calculated from mean cometary absolute magnitudes. These  $\bar{H}_{10}$  values can be plotted in cumulative form to produce a curve like the one shown in figure (5.3).

This technique has been used by Hughes & Daniels (1980) and has undergone a

<sup>3</sup>Note that, since the data points are not independent of each other (i.e. it's a cumulative plot) a linear regression analysis does not produce a good estimate of the uncertainty in  $s$ .

<sup>4</sup>This value of the mass distribution index was not used to produce the model cometary population. However, varying the value of  $s$  slightly does not significantly change the main conclusions in this chapter.

more rigorous treatment by Donnison (1990). In the past the assumption has been that the curved region in figure (5.3) is a result of our inability to observe all of the faintest comets. The region on the right side of figure (5.3) appears linear and most authors assume that all the comets in this magnitude region have been seen. It is often assumed that the magnitude distribution index, found from the gradient of the linear region also represents the faint comet region as well, *i.e.* the linear region can be extrapolated back to higher magnitudes. This assumption does not account for the possibility that there may be an actual decrease in the number of small, faint comets.

### 5.3.1 Investigating the curved region, $\bar{H}_{10} > 8$

Equation (5.4) implies that the faintest comets are the smallest comets. Hughes (1985) concluded that 1P/Halley, based on the mass of its meteor stream, has had 2300 perihelion passages on its present orbit. Based on the size of the nucleus and the rate at which mass is lost from the cometary nucleus, Hughes concluded that the comet will survive for a similar number of perihelion passages as long as it remains on its current orbit. Thus, Hughes refers to short period comets as “middle aged”. It seems reasonable to conclude, therefore, that many of the short period comets in the current population will have had at least a few hundred perihelion passages.

The line dividing the curved and linear regions in figure (5.3) is at  $\bar{H}_{10} = 8.0 \pm 0.5$ . Using equation (5.4) this corresponds to a nuclear radius of  $1.8 \pm 0.4$  km. Hughes (1985) concluded that 1P/Halley lost the equivalent of 2 m from its nuclear surface during the 1910 perihelion passage (see section (5.4.2)). Short period comets have

radii of the order of a few kilometres and after several hundred apparitions it is expected that some of the smallest comets will have decayed away completely. Therefore, it is worthwhile investigating the curved, high magnitude region to see if it represents the actual distribution of the fainter comets or whether it is just an artifact of insensitive observations.

The apparent magnitude of a comet can be high (*i.e.* faint) either because the comet is physically faint or because the comet does not pass close to the Earth. It is sensible therefore to limit the analysis of the curvature in figure (5.3) to a region of the Solar System close enough to the Sun for all the short period comets to have been detected.

### Missing Comets

Fernández (1992) investigated the number of short period comets with  $H_{10} < 11$  that have been discovered over the last 200 years. He concluded that the “discovery completeness” for  $q \leq 1.0$  AU and  $H_{10} < 11$  short period comets is very high. He suggested that the sample of short period comets with  $q \leq 1.5$  AU and  $H_{10} < 11$  is “approaching completeness” and that for  $q > 2$  AU discovery completeness is very low.

If the sample of short period comets is known to be complete and a knee appears in a cumulative plot, such as in figure (5.3), then the lack of fainter comets must be real and not due to observational insensitivity.

Figure (5.4) shows cumulative plots and non-cumulative distributions for both  $q \leq 1.5$  AU and  $q \leq 1.0$  AU short period comets taken from the Kresák and Kresáková catalogues. Unfortunately, restricting the perihelion distance to such

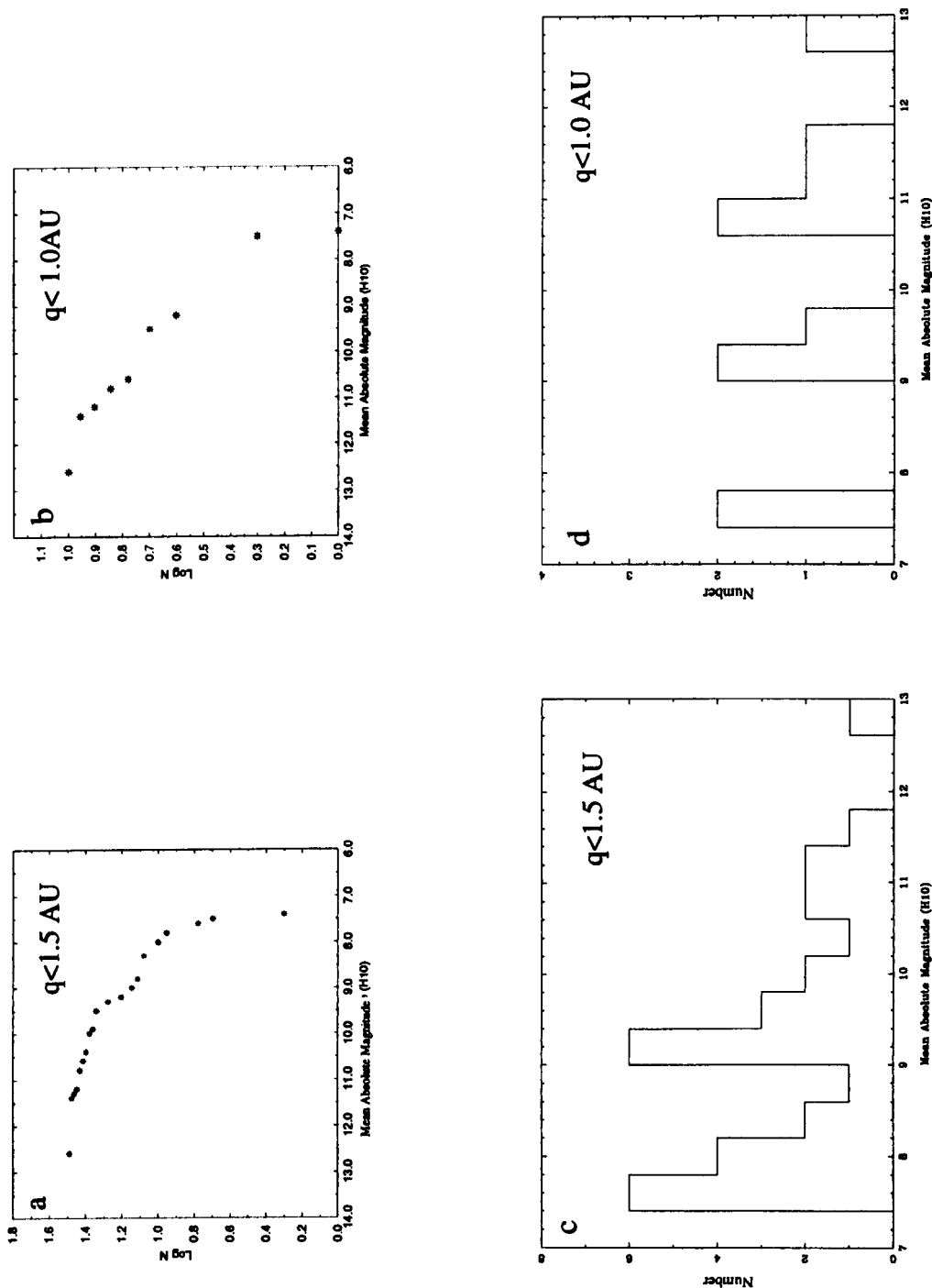


Figure 5.4: Plot (a) and plot (b) show the logarithm of the cumulative number of short period comets,  $N(\bar{H}_{10})$ . Each point indicates the logarithm of the number of comets with  $\bar{H}_{10}$  less than or equal to that particular value. Plot (a) shows the cumulative number for short period comets with  $q \leq 1.5 \text{ AU}$  and plot (b) shows the corresponding curve for  $q \leq 1.0 \text{ AU}$  short period comets.

Plot (c) and plot (d) show the  $\bar{H}_{10}$  distributions for both the  $q \leq 1.5 \text{ AU}$  sample of comets and the  $q \leq 1.0 \text{ AU}$  sample of comets.

The bi-modal nature of the distribution in plot (c) may either be due to the incompleteness of the sample or indicate a real lack of short period comets of  $7.8 \leq \bar{H}_{10} \leq 9.0$ . Plot (d) indicates that the range of  $\bar{H}_{10}$  values does not reduce when the perihelion distance is limited from 1.5 AU to 1.0 AU.

Note that a knee at  $\bar{H}_{10} = 8.0 \pm 0.5$  would not be inconsistent with either plot (a) or plot (b).

small ranges significantly reduces the sample size. If the restriction  $q \leq 1.5$  AU is applied, then the number of comets in the sample is reduced to 31. For the  $q \leq 1.0$  AU limit, the sample size is reduced to only 10 short period comets.

The cumulative plot for the  $q \leq 1.5$  AU sample, shown in figure (5.4a) is clearly curved and the distribution, in non-cumulative form, shown in figure (5.4c) is bimodal. This may be a result of the incompleteness of the sample or it may indicate a physical lack of comets with mean absolute magnitudes  $7.8 \leq \bar{H}_{10} \leq 9$ . Since the  $\bar{H}_{10}$  data is restricted to  $q \leq 1.5$  AU, incompleteness of the data set is not thought to be likely.

The cumulative plot for the  $q \leq 1.0$  AU sample is shown in figure (5.4b). Figure (5.4d) shows that the number of comets in each magnitude range is approximately evenly spaced. Note that, although the sample size has been reduced, the values of  $\bar{H}_{10}$  still cover the same range as in the case of the  $q \leq 1.5$  AU sample, *i.e.*  $7.4 \leq \bar{H}_{10} \leq 13.0$ .

It is not possible to be conclusive about the existence of small comets from these data. The  $q \leq 1.5$  AU sample produces a clear curved shape in figure (5.4a) but the data set may not yet be complete for comets of  $\bar{H}_{10} < 11$ . Unfortunately, the  $H_{10} < 11$  limit applied to the  $q \leq 1.0$  AU sample reduces the data set to only 7 comets. While the comets do seem to be spread evenly along the range of magnitudes in figure (5.4d) it would be unwise to draw conclusions about the entire short period comet population from such a small sample.

## 5.4 A Decaying Cometary Population

A model population of short period comets was produced and allowed to decay over a number of apparitions. Each comet in the population loses a surface layer of depth 1 m from the nucleus at each perihelion passage (see section (5.4.2) for the calculation of this value).

This implies a model where:

1. the orbit of each comet is the same.
2. cometary outbursts, splitting or other irregular events do not occur.

Of the 153 comets of  $P \leq 15$  years shown in figure (2.1), 73 (i.e. 48%) have orbital periods within the narrow range of 6.5 years to 8.8 years. This gives some justification to assumption (1).

Unfortunately, assumption (2) is difficult to justify. There have only been 200 years of serious scientific observations of comets and this is not long enough to observe significant cometary decay (see chapter (4)). Irregular events such as outbursts and splitting will shorten the lifetime of the comet, while dormant phases will prolong the lifetime of the comet (Kresák 1987). It is not yet possible to say if these events are more important when it comes to prolonging, or shortening, the lifetime of a comet than the gradual sublimation of the nucleus snow over many apparitions. The role of these effects in determining cometary lifetimes is beyond the scope of this thesis. Therefore, the model presented here should be considered as a simple approximation of cometary decay.

5.4.1 The ‘Apparition Zero’ Model Population of Comets

The initial model population, hereafter referred to as the ‘Apparition Zero’ population, consists of 2214 short period comets with a distribution of radii such that

The number of comets in this model population is a result of assuming that

1. the largest comet in the population has a radius of 100 km,
2. a mass distribution index of  $s = 1.67$  characterises the small comet region.

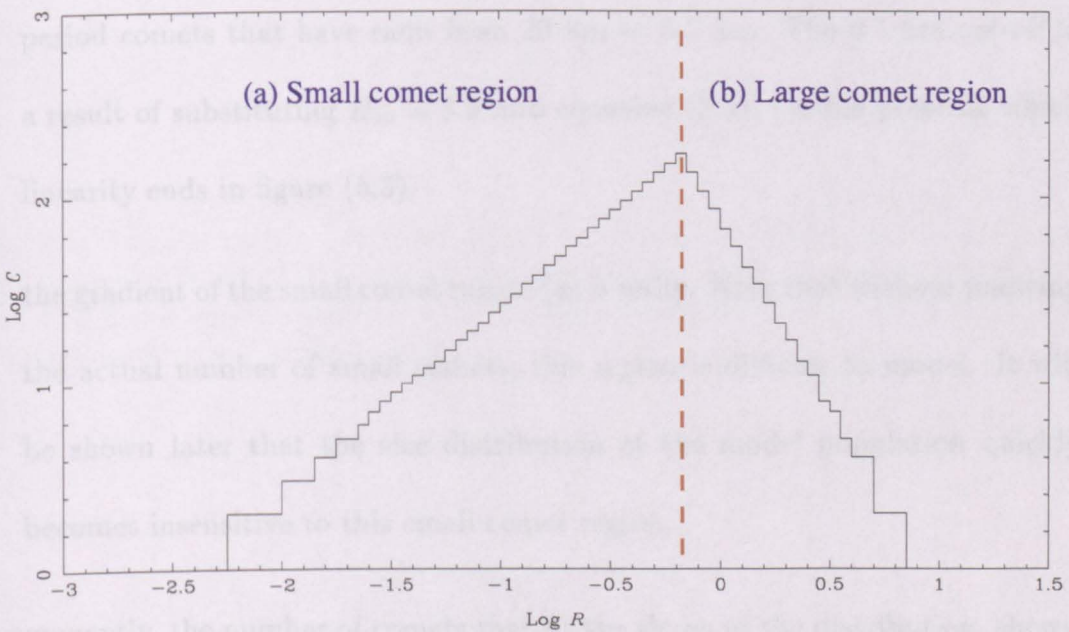


Figure 5.5: The ‘Apparition Zero’ distribution for the model population of short period comets.  $R$  is the nuclear radius in kilometres and  $C$  is number of comets in each bin. The large comet region (b) is characterised by a mass distribution index of  $s = 1.67$ . The small comet region (a) was set such that the slope on this plot was unity. Although the exact shape of this region is somewhat arbitrary it will be seen later that the model is not sensitive to the initial shape of the small comet region. The bin size is  $\Delta[\log R] = 0.05$

Hughes (1990a) concluded that the mass lost from the cometary nucleus per apparition is proportional to the radius  $r_0$  of the nucleus and the perihelion distance  $q$  of the comet. Hughes also stated that work done by Wallis and Weidmann (1986) showed that,

### 5.4.1 The ‘Apparition Zero’ Model Population of Comets

The initial model population, hereafter referred to as the ‘Apparition Zero’ population, consists of 2214 short period comets and is shown in figure (5.5).

The number of comets in this model population is a result of assuming that,

1. the largest comet in the population has a radius of 20 km.
2. a mass distribution index of  $s = 1.67$  (Hughes (1989a)) is valid for short period comets that have radii from 20 km to 0.7 km. The 0.7 km cut-off is a result of substituting  $H_{10} = 8.0$  into equation (5.4), i.e. the point at which linearity ends in figure (5.3).
3. the gradient of the small comet region (a) is unity. Note that without knowing the actual number of small comets, this region is difficult to model. It will be shown later that the size distribution of the model population quickly becomes insensitive to this small comet region.

Consequently, the number of comets that fit the shape of the distribution, shown in figure (5.5), is 2214. In this chapter it is the shape of the size distribution that is considered important, as this will determine the mass distribution index. The number of comets in the model population is not important.

### 5.4.2 The Layer Loss Rate

Hughes (1989a) concluded that the mass lost from the cometary nucleus per apparition is proportional to the surface area of the nucleus and the perihelion distance of the comet. Hughes also stated that work done by Wallis and Wickramasinghe showed that,

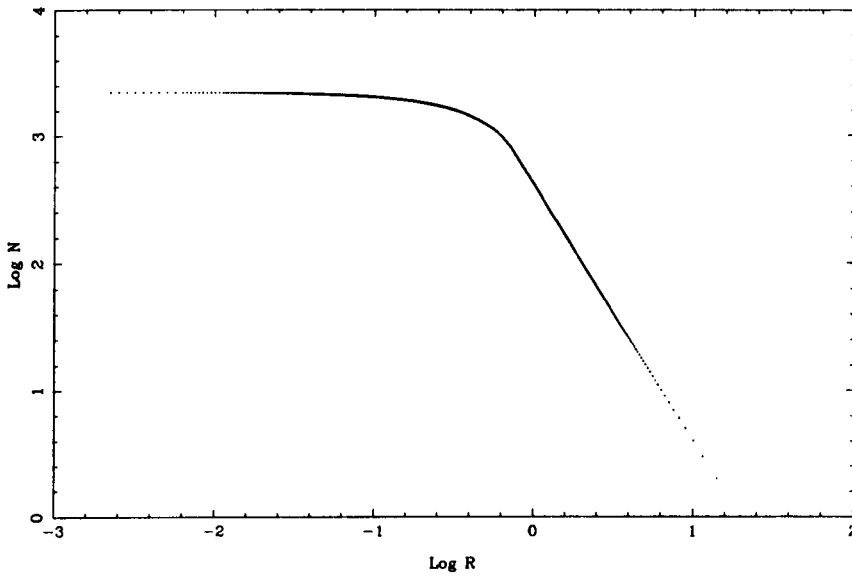


Figure 5.6: The ‘Apparition Zero’ model population in cumulative form. The small comet region in figure (5.5) produces the knee shape when plotted in cumulative form. The linear region corresponds to a mass distribution index of  $s = 1.67$ , i.e. the large comet region in figure (5.5).

$$M_{ap} \propto 4\pi R^2 q^{-k \pm 1.5}, \quad (5.18)$$

where  $k$  is a constant. Hughes (private communication) suggested that since  $m_i \propto \frac{1}{r^2}$  (i.e.  $k = 2$ ) then,

$$M_{ap} \propto 4\pi R^2 q^{-\frac{1}{2}}, \quad (5.19)$$

would be a reasonable approximation.

The value of  $M_{ap}$  is also proportional to the volume of the layer that is lost from the nucleus. To a first order approximation, and for  $R \gg \Delta R$ ,

$$M_{ap} \propto R^2 \Delta R, \quad (5.20)$$

where  $\Delta R$  is the depth of layer lost from the cometary nucleus.

Combining equation (5.19) and equation (5.20) thus produces,

$$\Delta R \propto q^{-\frac{1}{2}} \quad (5.21)$$

Comet 1P/Halley effectively lost 2 metres at the 1910 apparition (Hughes 1985) and reached a perihelion distance of 0.59 AU. The mean perihelion distance for short period comets is about 1.9 AU and so the mean short period comet loses  $2\left(\frac{0.59}{1.9}\right)^{\frac{1}{2}} = 1.1$  m. Consequently, in this model each comet loses a layer 1 metre thick from its nucleus per apparition.

Note that this estimate of a layer loss rate of 1 metre per apparition is not crucial for the following analysis. The main assumption is that the average comet loses a *typical depth* from its nucleus per apparition. Values different to 1 metre per apparition will only tend make the comets decay at a faster or slower rate, but will not change the shapes of the size distributions in the following analysis.

### 5.4.3 The Large Comet Region

Figure (5.7) shows the evolution of the ‘apparition zero’ population over 2000 apparitions into the future and 1200 apparitions in the past. Future apparitions are indicated by a ‘+’ symbol and past apparitions are indicated by a ‘-’ symbol.

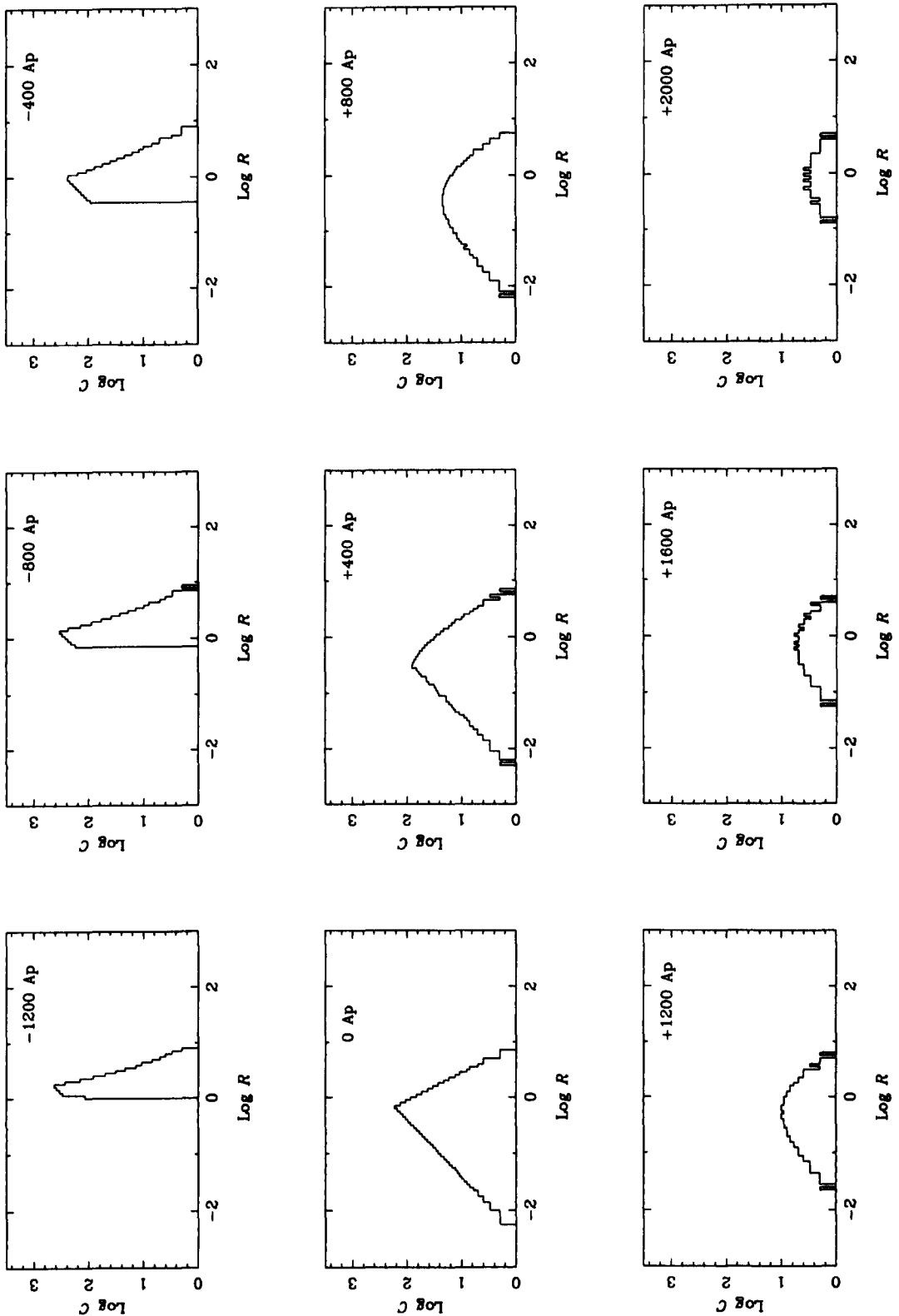


Figure 5.7: Each comet in the ‘Apparition Zero’ population, shown in figure (5.5), loses 1m from the radius of the nucleus at each apparition. Each comet in the model population has the same orbital period and passes perihelion at the same time. The population is shown at intervals of 400 apparitions both in the future (+ symbol) and in the past (- symbol).

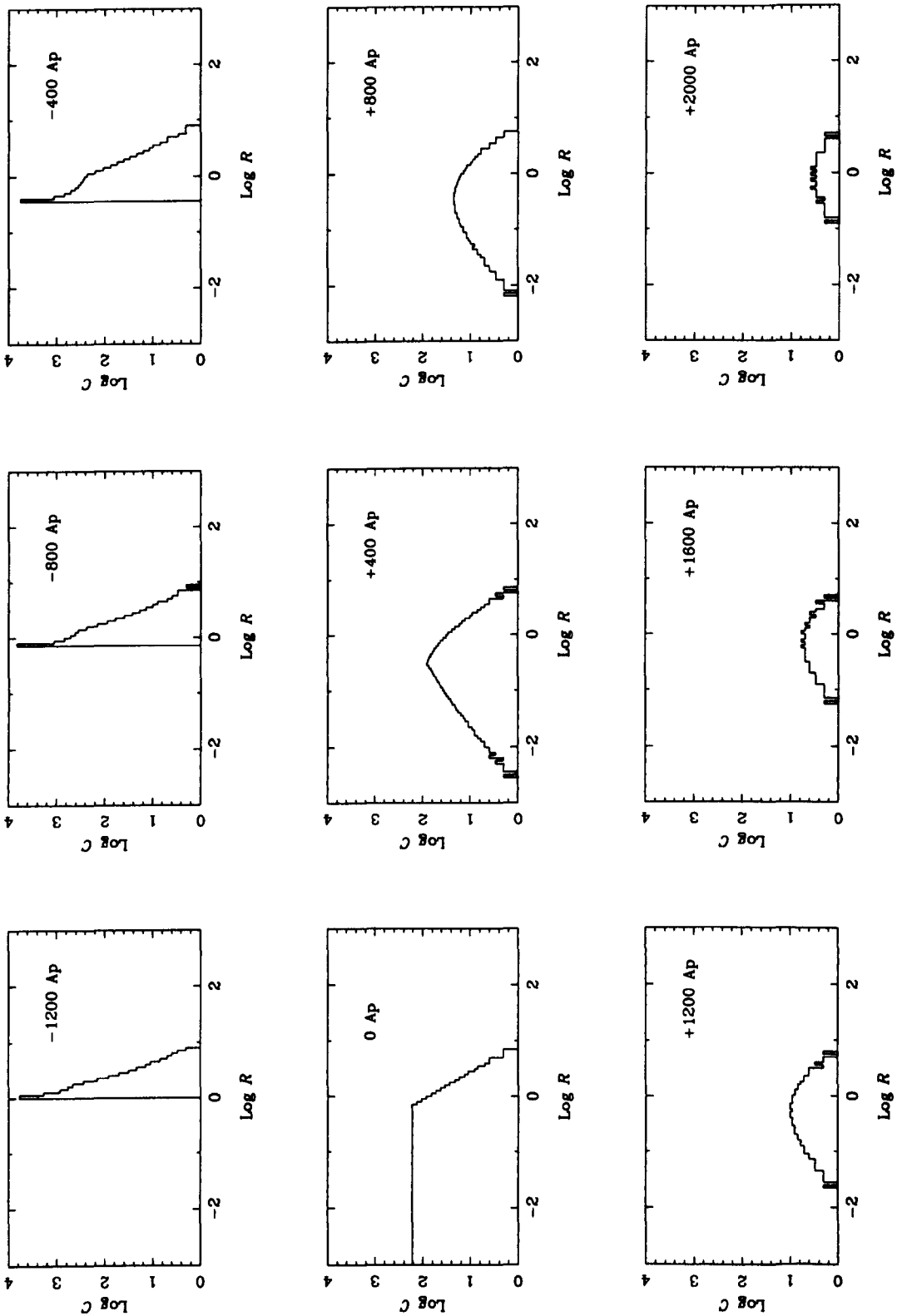


Figure 5.8: The decaying distribution for a different apparition zero. Here the number of small comets does not fall off for  $\text{log } R < -0.15$ . The comets in this region quickly decay and by +710 apparitions the distribution is the same as in figure (5.7).

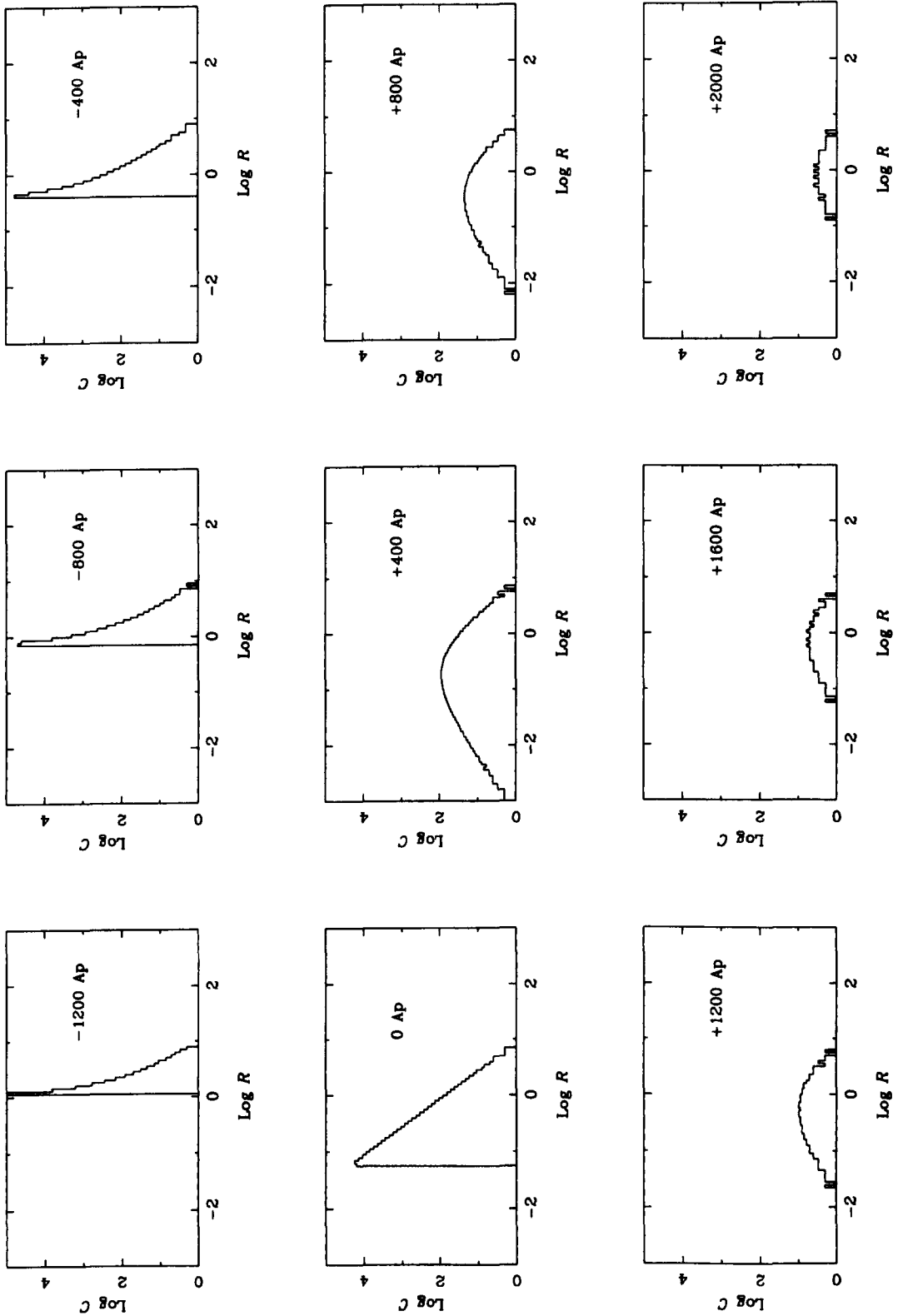


Figure 5.9: Another apparition zero. The large comet, linear region, is extended such that the population consists of 50000 comets. Again, the comets in the  $\log R < -0.15$  region quickly decay away and by +710 apparitions the distribution is the same as in figure (5.7).

As the population decays the distribution becomes more semi-circular in shape. The shape is a result of the disappearance of the smallest comets. The plots are logarithmic and this means that, the smaller the comet, the faster it will move to the left of the plot as it decays.

At a layer loss rate of 1 m per apparition the entire small comet region,  $R < 0.71$  km, disappears after 710 apparitions. The shape of the distribution is then entirely dictated by the decay of the large comets. This means that other apparition zero populations, that started with different numbers of small comets would be indistinguishable from these distributions after 710 apparitions.

Figure (5.8) and figure (5.9) show the decay of two new apparition zero populations that have different numbers of small comets. Note that in both cases the distributions are identical after +710 apparitions.

#### 5.4.4 How Does $s$ Vary as the Population Decays?

It is interesting to see what the interpretation would be if each of the distributions shown in figure (5.7) were actually the observed distribution of the current population. How representative would the analysis discussed in section (5.3) be of the actual population?

The  $\log R > 0.2$  region in figure (5.7) for each apparition was considered to be sufficiently linear for the value of  $s$  to be calculated from the gradient. For each of the plots in figure (5.7) a corresponding cumulative plot was produced as described in section (5.3). Figure (5.10) shows an example of one of these plots. Linear regressions were used to find the best line through the points. As the population decays the use of this technique becomes more difficult since the large comet region

eventually becomes non-linear.

Following equation (5.17), the gradient of each of the lines,  $g$ , such as in figure (5.10), is related to the mass distribution index,  $s$ , by,

$$s = 1 - \frac{g}{3} \quad (5.22)$$

For each of the distributions in figure (5.7) a value of  $s$  was calculated, and these are plotted in figure (5.11).

As comets decay in this model the mass distribution index for comets with  $R > 1.58$  km (*i.e.*  $\log R > 0.2$ ), decreases with apparition number in a non-linear way. As an aid to the diagram a second-order polynomial was fitted to the data and has the form,

$$s = 1.68 - 1.67 \times 10^{-4} A + 3.04 \times 10^{-8} A^2 \quad (5.23)$$

where  $s$  is the mass distribution index and  $A$  is the apparition number (see figure (5.11)).

The mass distribution index decreases with increasing apparition number. This means that most of the total mass of the population is in the form of the more massive comets.

Apparition*	Population size <sup>b</sup>	N <sup>c</sup> used to find $s^d$	Percent <sup>e</sup>
-1200	2214	1457	65.8
-1000	2214	670	30.3
-800	2214	293	13.2
0	2214	162	7.3
+800	1438	163	7.2
+1200	643	71	11.0
+1500	260	32	18.3
+1800	110	40	25.2
+2100	10	31	30.4

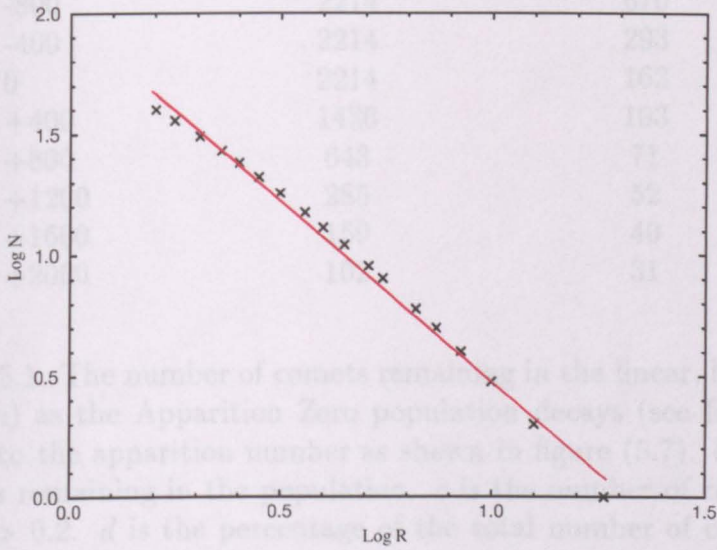


Figure 5.10: A cumulative plot for the +800 Ap distribution shown in figure (5.7). Cumulative plots were produced for each of the distributions for the region  $\log R > 0.2$ . This region appears linear for all of the apparitions shown in figure (5.7). A linear regression was applied to the data and from the gradient,  $3(1 - s)$ , the mass distribution index can be calculated.

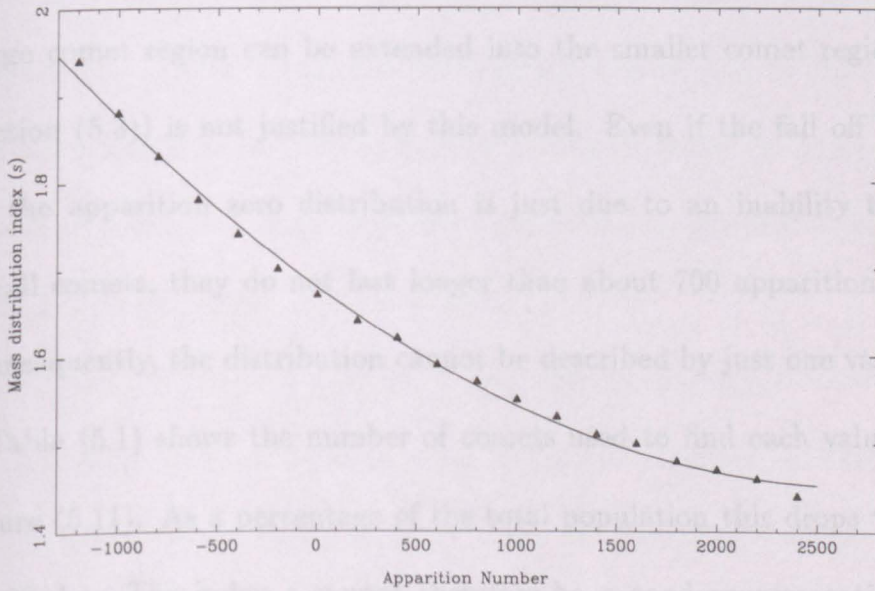


Figure 5.11: The mass distribution index decreases as the population decays. Since  $s$  becomes considerably less than 2, this indicates that the total mass of the population becomes dominated by only a few comets.

Apparition <sup>a</sup>	Population size <sup>b</sup>	$N^\circ$ used to find $s^c$	Percent <sup>d</sup>
-1200	2214	1457	65.8
-800	2214	670	30.3
-400	2214	293	13.2
0	2214	163	7.4
+400	1426	103	7.2
+800	643	71	11.0
+1200	285	52	18.3
+1600	159	40	25.2
+2000	102	31	30.4

Table 5.1: The number of comets remaining in the linear, large comet region ( $R > 0.2$  km) as the Apparition Zero population decays (see figure (5.7)). Column  $a$  refers to the apparition number as shown in figure (5.7).  $b$  is the total number of comets remaining in the population.  $c$  is the number of comets left in the region  $\log R > 0.2$ .  $d$  is the percentage of the total number of comets remaining in the region  $\log R > 0.2$ .

### 5.4.5 The Limitation of Using the Mass Distribution Index

The analysis of the mass distribution index described in section (5.4.4) has a distinct limitation as it only describes a small region of the population, those comets that can be most easily observed, *i.e.*  $R > 1.58$  km. The traditional view that the linear large comet region can be extended into the smaller comet region (discussed in section (5.3)) is not justified by this model. Even if the fall off in small comets in the apparition zero distribution is just due to an inability to observe these small comets, they do not last longer than about 700 apparitions in this model. Consequently, the distribution cannot be described by just one value of  $s$ .

Table (5.1) shows the number of comets used to find each value of  $s$  shown in figure (5.11). As a percentage of the total population this drops to only 7.2% for +400 Ap. The index  $s$  cannot therefore be a good representation of the whole population.

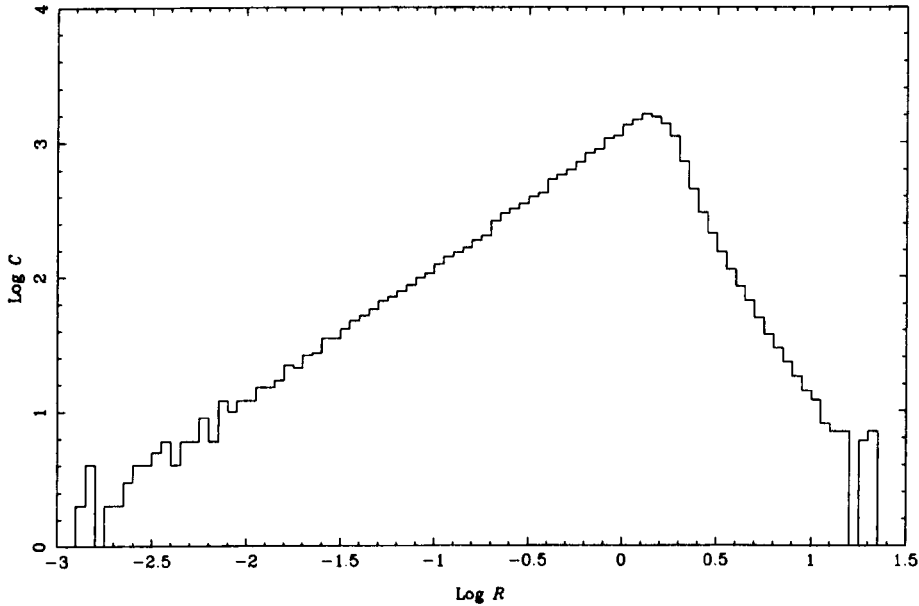


Figure 5.12: A new distribution created by adding apparitions -1200 to 1200 in steps of 200 apparitions from figure (5.7). Note that the shape of the large comet region,  $\log R > -0.15$ , is not quite linear.

#### 5.4.6 Different Populations?

The current population of comets did not arrive in the inner Solar System at the same time. Jupiter is continually capturing comets, and so the current cometary size distribution should be the sum of a range of initial cometary sizes, with each comet at a different stage of decay. Unfortunately, it is not possible to know the initial size distribution of these comets.

Therefore, as a simple exercise, a new size distribution of comets was produced by summing the distributions of 13 populations (based on the apparition zero population in figure (5.5)) at decay times of -1200 Ap, -1000 Ap, -800 Ap, etc. up to +1200 Ap. Figure (5.12) shows the results of these combined distributions. Notice that the large comet region is not quite linear.

## 5.5 Summary

The decay of the short period comet population is more complicated than the model presented here. Comets can be subject to events other than the gradual sublimation of snow, such as dormant phases, outbursts and cometary splitting (see section (2.5)).

Cometary splitting will shorten the lifetime of a comet. 3D/Beila, for example, was recorded as two separate objects, for the 1846 apparition, in the *Catalogue of Cometary Orbits* (Marsden & Williams 1996), after which the two objects were recorded only again during the 1852 perihelion passage. Outbursts will also shorten the lifetime of a comet. Dormant phases during a comet's lifetime will have the opposite effect, as the snow in the nucleus is preserved for longer and will extend the lifetime of a comet.

Unfortunately, if the current ages of comets are similar to the 2300 orbits calculated by Hughes (1985) then the number of observed apparitions of short period comets (up to 55 for 2P/Encke) are not enough to determine the importance of these effects over a typical cometary lifetime.

Even with these uncertainties this analysis has shown that,

1. in a simple model of a population of decaying comets, a real decrease in the number of the smallest comets is expected.
2. in the simple combined distribution in figure (5.12) the large comet region does not remain linear.

Therefore, a simple power law description of the population is too simplistic to describe the whole population. Figure (5.13) shows a diagram of a hypothetical

curve on a  $\log N$  against  $\log R$  plot. The line is expected to be curved due to both a real lack of small comets and insensitive observations. If a power law is used, as an approximation, to describe a region of the comet size distribution, then the range over which it is valid should be made explicit.

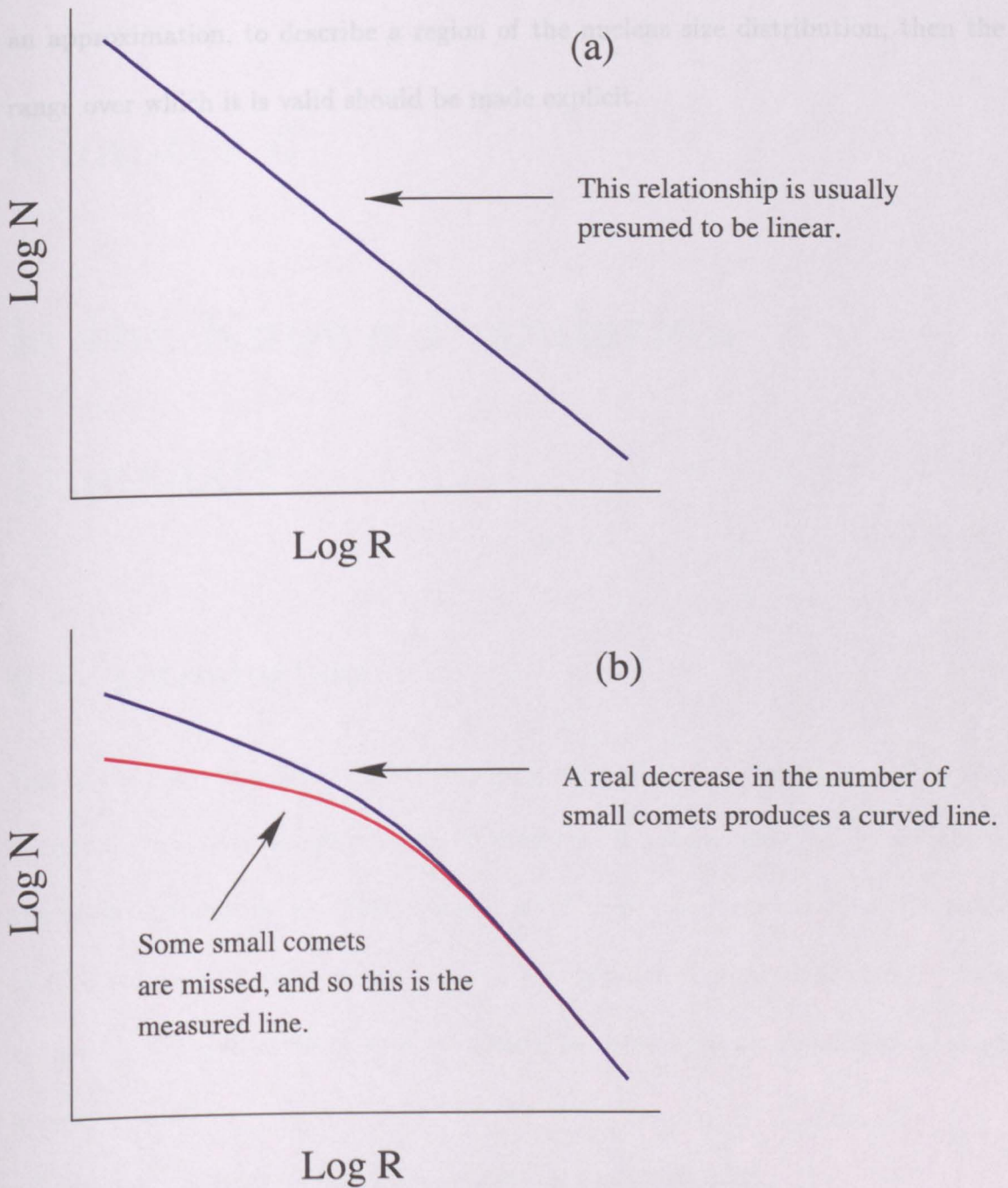


Figure 5.13: The traditional approach is to assume that  $\log N$  is directly proportional to  $\log R$ , as shown in diagram (a). However, in this chapter it is proposed that there should be a real decrease in the number of comets with small nuclei, and that the blue line should be curved as shown in diagram (b). As small faint comets are easier to miss, the actual measured version of the line, shown in red, should be a result of a real lack of small comets *and* insensitive observations.

curve on a  $\log N$  against  $\log R$  plot. The line is expected to be curved due to both a real lack of small comets *and* insensitive observations. If a power law is used, as an approximation, to describe a region of the nucleus size distribution, then the range over which it is valid should be made explicit.

# Chapter 6

## Is the Known Population Unusual?

### 6.1 Introduction

One of the greatest problems when studying the population of short period comets is that there is only one population to examine. A natural question to ask about the known population is: “How unusual is it?”. As this thesis concerns the mass of dust released by short period comets, the question is more specifically: “*How unusual is the rate at which dust is released by today’s known population of short period comets?*”

There are two ways in which the population can be unusual:

1. The number of comets and size distribution index of the current short period comet population could be very different from populations that existed in the past or that will exist in the future.
2. The number of comets and size distribution index of the current short period

comet population may be similar to past and future populations but the orbits that these specific comets have may be unusual, e.g. the largest comets in the population may all have the smallest perihelia, etc.

It is possibility (2) that is examined in this chapter. A model short period comet population is created, based on the mean absolute magnitude data from the Kresák and Kresáková catalogues (1989, 1994). These absolute magnitudes are used in the  $M_{ap}$  program (see chapter (4)) to calculate the average mass of dust released by each comet in the population.

Thus, today's population is defined by a list of  $\bar{H}_{10}$  values, perihelion distances,  $q$ , and eccentricities,  $e$ . This list of  $\bar{H}_{10}$  values is then randomly mixed up and re-assigned back to the fixed list of perihelion distances and eccentricities. This defines a new population of short period comets.

This method is then repeated to create different populations of short period comets. For each population the mass of dust released by each comet per orbit,  $M_{ap}$ , is calculated. These mass loss rates are then summed to produce the total mass of dust released by the population of short period comets,  $M_{pop}$ . These values of  $M_{pop}$  are then compared with the corresponding result for today's known population.

## 6.2 The Assumptions

In order that new short period comet populations can be created two assumptions are made about comets:

1. **The size of the active surface area of a cometary nucleus and the orbit that the nucleus follows significantly affect the amount of dust released by the comet.**

In chapter (5) the equivalent radius of a cometary nucleus,  $R$ , was related to the mean absolute magnitude,  $\bar{H}_{10}$ , and the fraction of the cometary nucleus surface that is active,  $f$ , by,

$$\log R(km) = 1.114 - 0.5 \log f - 0.2\bar{H}_{10} \quad (6.1)$$

If  $f$  is constant then  $\bar{H}_{10}$  is directly related to  $\log R$ . In chapter (5) the value of  $f$  was set to 0.034, this being the value found by Hughes (1989a) from a study of the secular variation in the absolute magnitude of 1P/Halley over 2000 years.

Thus, equation (6.1) becomes,

$$\log R(km) = 1.848 - 0.2\bar{H}_{10}. \quad (6.2)$$

In chapter (4) the absolute magnitude,  $H_{10}$ , and the heliocentric distance,  $r$  (AU), were combined to find the mass of dust,  $\dot{m}_i$ , released by a short period comet per second. The result was,

$$\dot{m}_i \approx 4.68 \times 10^7 \frac{1}{r^2} 10^{-\frac{2}{3}H_c} \text{ gs}^{-1}, \quad (6.3)$$

Introducing the surface area of the nucleus,  $A_s$ , into equation (6.2) and equation (6.3) produces,

$$\dot{m}_i \approx 750 \frac{A_s}{r^2} \text{ g s}^{-1} \quad (6.4)$$

and assumption (1) becomes:

*The size of the entire surface area of a cometary nucleus and the orbit that the nucleus follows significantly affect the amount of dust released by the comet.*

2. **The mass of the cometary nucleus does not significantly affect which orbit the comet is perturbed onto.**

The masses of cometary nuclei are insignificant when compared to the masses of the planets and the Sun. Wyckoff (1982) put the upper limit on the mass of cometary nuclei at  $\sim 10^{19}$ g. In comparison, the masses of the Sun and Jupiter are  $1.99 \times 10^{33}$ g and  $1.90 \times 10^{30}$ g respectively (Allen 1973). Even taking the upper limit for cometary masses means that a cometary nucleus has only  $5.3 \times 10^{-10}\%$  of the Jovian mass.

### **The Implication of the Assumptions**

The assumption that the orbit of the comet is independent of the initial mass of the cometary nucleus means that new populations of comets can be created by simply mixing up the known population, i.e. associating each  $\bar{H}_{10}$  with a different orbit from the list of known short period comets.

This means that the population can be ‘re-run’ to see how typical the known population is at the present time. The long term variation in the population size is not directly considered in this chapter.

### Limitations of the Assumptions

There are distinct dynamical classes of comets, e.g. short period ( $P < 15$  years), intermediate period comets ( $15 > P > 200$  years) and long period comets ( $P > 200$  years). This means that assumptions (1) and (2) should only be applied within one dynamical class. In this chapter the assumptions will be applied to short period comets only.

Active short period comets decay and lose mass at each perihelion passage, it is therefore reasonable to assume that the mean absolute magnitudes of a short period comet population will eventually become a function of perihelion distance. Therefore, in section (6.5) the relationship between the mean absolute magnitude  $\bar{H}_{10}$  and the perihelion distance,  $q$ , for the known short period comet population is examined.

## 6.3 The Model

Before creating new populations of short period comets, a list of the parameters that define the current population needs to be produced. In this model each comet has a perihelion distance,  $q$ , an eccentricity,  $e$  and a mean absolute magnitude,  $\bar{H}_{10}$ . In the  $M_{ap}$  program it is the heliocentric distance,  $r$ , that is important for determining the mass loss rate from the cometary nucleus at a specific point on its orbit. Thus, the orbital inclination,  $i$ , longitude of the ascending node,  $\Omega$ , and the

argument of perihelion,  $\omega$ , are not considered. Using the eccentricity, perihelion distance and mean absolute magnitude the  $M_{ap}$  program (see chapter (4)) calculates the mass of dust released by each comet during one orbit.

### 6.3.1 The Perihelion Distance and Eccentricity

Short period comets have aphelia close to the semi-major axis of Jupiter at 5.2 AU (Allen 1973). Consequently, a close encounter between a comet and Jupiter will tend to perturb the comet onto another orbit. Carusi et al. (1991) concluded that “On the average, a comet of  $P < 10$  years and  $q < 1.5$  AU passes within 1.0 AU from Jupiter once per 40 years and within 0.5 AU once per 90 years [sic]”. Since the Kresák and Kresáková data set (1989, 1994) spans up to  $\sim 200$  years of cometary apparitions it is expected that many of the comets in the list will have had 2 encounters with Jupiter, within 0.5 AU, over the last two centuries.

Calculating the orbit of each comet, at the time that it became a member of the short period population, is beyond the scope of this thesis. Since the aim of this chapter is to see if the *current population* is unusual only the latest value of the perihelion distance and eccentricity for each comet was used. These orbital parameters were taken from the epoch 1996 Nov 13.0 list in the *Catalogue of Cometary Orbits* (Marsden & Williams 1996).

### 6.3.2 The Mean Absolute Magnitude, $\bar{H}_{10}$

The weighted mean absolute magnitudes,  $\bar{H}_{10}$ , were taken from the Kresák and Kresáková catalogues (1989, 1994) (see section (4.4.1) for an explanation of the weighting system). In these catalogues 90 comets with  $P < 15$  years and more

than one recorded apparition are listed. 29P/Schwassmann-Wachmann 1 is given a weighting of 0.0 for each  $H_{10}$  value and so is excluded from this model population. Thus, in this chapter the maximum model population size is restricted to 89 comets. These  $\bar{H}_{10}$  values were substituted into equation (6.3) to calculate the mass loss rate for each comet.

In chapter (4) it was shown that the measured absolute magnitude of a specific short period comet varies from apparition to apparition. This was attributed to observational uncertainty and changes in the total size of the active area on the surface of the cometary nucleus. Unfortunately, there are not enough recorded apparitions for each short period comet to distinguish between steady-state periods in the comet's activity (e.g. see the conclusion about 4P/Faye in section (4.11)) and periods of unusual activity. Thus, the mean absolute magnitude was used in the model presented in this chapter.

### 6.3.3 Creating New Populations

In this chapter the model presented in chapter (4) to calculate the mass of dust released by a comet over one orbit,  $M_{ap}$ , is taken a step further by summing the values of  $M_{ap}$  for each comet to find the total mass of dust released by the cometary population. The total mass of dust released by the population will be referred to as  $M_{pop}$ .

Comets pass perihelion at different times and so to standardise the population each comet in the model has one perihelion passage and the mass of dust released from that orbit contributes to the total of  $M_{pop}$ . The value of  $M_{pop}$  is therefore a theoretical construct and does not reflect the dust mass release rate of the popula-

tion at any particular time.

The technique for creating the new populations can be summarised in 5 steps:

1. The list of mean absolute magnitudes,  $\bar{H}_{10}$ , from the Kresák and Kresáková catalogues (1989, 1994) are matched to the corresponding orbital parameters (q and e) from the Epoch 1996 Nov 13.0 list in the Catalogue of Cometary Orbits 1996 (Marsden & Williams 1996).
2. The  $\bar{H}_{10}$  values are randomly mixed up and re-assigned back to the fixed list of orbital parameters, e.g. the  $\bar{H}_{10}$  of 2P/Encke may be assigned to the orbit of 6P/d'Arrest, etc. In this way a new population is produced.
3. Using the program discussed in chapter (4) the mass of dust released by each comet during one perihelion passage,  $M_{ap}$ , is calculated.
4. The values of  $M_{ap}$  for each comet in the new population are summed to find the mass of dust released by the entire population,  $M_{pop}$ .
5. Steps 2-4 are repeated to create new populations, each with a corresponding value of  $M_{pop}$ .

The list of  $M_{pop}$  values are then plotted as a frequency distribution. The distribution can be considered to be a probability plot, the peak occurring at the most likely value of  $M_{pop}$  for a population of comets restricted to the 89 short period orbits used in this model. The values of  $M_{pop}$  calculated for the new populations can then be compared with the corresponding value of  $M_{pop}$  for the known population of 89 short period comets.

### 6.3.4 The Mass of Dust Released by the Known Population of Short Period Comets

Before examining the new populations of short period comets it is worth finding the typical mass of dust that is released by individual comets in the known population. Using the  $M_{ap}$  program, discussed in chapter (4), for each of the 89 comets in the known population a total value of  $M_{pop} = 4.0 \times 10^{13}$  g was calculated.

The values of  $M_{ap}$  were then compared to find the largest contributors of dust to the population. Table (6.1) lists the top ten contributors of dust (in terms of mass), as well as the ten comets with the smallest mean absolute magnitudes,  $\bar{H}_{10}$  and the ten comets with the smallest perihelia. In general, the comets with the smallest absolute magnitude (*i.e.* physically bright) are also in the top ten dust contributors table. Those comets that have perihelia beyond 2.8 AU do not contribute any dust in this model.

The main conclusion from the results in table (6.1) is that the top ten dust contributing comets form only 11% of the population of 89 comets and yet release 47% of the total mass of dust. That so few comets contribute such a large proportion of the total dust mass indicates that the value of  $M_{pop}$  will be very susceptible to a change in the number of large comets in the population.

### 6.3.5 Short Period Comets with Perihelia greater than 2.8 AU

The comets 90P/Gehrels 1, 36P/Whipple, 82P/Gehrels 3, 74P/Smirnova-Chernykh and 99P/Kowal 1 all have perihelia at heliocentric distances greater than 2.8 AU, yet the small mean absolute magnitudes show that these comets are physically bright (see table (6.2)).

Top Ten Dust Releasing Comets	q	e	$\bar{H}_{10}$	$M_{ap}$ ( $\times 10^{12}$ g)	%
101P/Chernykh	2.35	0.59	4.6	<b>3.38</b>	8.36
47P/Ashbrook-Jackson	2.31	0.40	5.1	<b>2.81</b>	6.94
65P/Gunn	2.46	0.32	5.4	<b>1.90</b>	4.69
31P/Schwassmann-Wachmann 2	2.03	0.42	6.2	<b>1.39</b>	3.43
81P/Wild 2	1.58	0.54	6.5	<b>1.37</b>	3.40
77P/Longmore	2.40	0.34	5.9	<b>1.28</b>	3.15
4P/Faye	1.66	0.57	6.5	<b>1.25</b>	3.08
86P/Wild 3	2.30	0.37	6.2	<b>1.08</b>	2.67
91P/Russell 3	2.51	0.34	5.9	<b>1.04</b>	2.58
53P/Van Biesbroeck	2.40	0.55	5.9	<b>0.99</b>	2.45
<b>Ten Lowest <math>\bar{H}_{10}</math> Values</b>					
99P/Kowal 1	4.68	0.23	<b>2.7</b>	-	-
74P/Smirnova-Chernykh	3.55	0.15	<b>4.0</b>	-	-
82P/Gehrels 3	3.46	0.15	<b>4.4</b>	-	-
<b>101P/Chernykh</b>	2.35	0.59	<b>4.6</b>	3.38	8.36
<b>47P/Ashbrook-Jackson</b>	2.31	0.40	<b>5.1</b>	2.81	6.94
90P/Gehrels 1	2.99	0.51	<b>5.2</b>	-	-
<b>65P/Gunn</b>	2.46	0.32	<b>5.4</b>	1.90	4.69
<b>77P/Longmore</b>	2.40	0.34	<b>5.9</b>	1.28	3.15
<b>91P/Russell 3</b>	2.51	0.34	<b>5.9</b>	1.04	2.58
<b>53P/Van Biesbroeck</b>	2.40	0.55	<b>5.9</b>	0.99	2.45
<b>Ten Smallest Perihelia Comets</b>					
96P/Machholz 1	<b>0.12</b>	0.96	11.2	0.09	0.22
2P/Encke	<b>0.33</b>	0.85	9.2	0.34	0.85
45P/Honda-Mrkos-Pajdušáková	<b>0.53</b>	0.82	10.8	0.06	0.14
27P/Crommelin	<b>0.75</b>	0.92	8.9	0.23	0.57
72P/Denning-Fujikawa	<b>0.79</b>	0.82	12.6	0.01	0.02
73P/Schwassmann-Wachmann 3	<b>0.93</b>	0.69	10.6	0.05	0.12
26P/Grigg-Skjellerup	<b>1.00</b>	0.66	11.4	0.02	0.06
103P/Hartley 2	<b>1.03</b>	0.70	7.4	0.83	2.06
8P/Tuttle	<b>1.03</b>	0.82	7.5	0.68	1.68
15P/Finlay	<b>1.03</b>	0.71	9.5	0.12	0.46

Table 6.1: The top ten contributors of dust (by mass), the ten lowest mean absolute magnitudes ( $\bar{H}_{10}$ ) in the sample (those that are also in the top ten contributors table are shown in **bold**) and the ten comets with the smallest perihelia in the population. Here,  $q$  is the perihelion distance in AU,  $e$  is the eccentricity of the orbit,  $M_{ap}$  is the mass of dust released at a hypothetical apparition where the comet has an absolute magnitude  $\bar{H}_{10}$  and % is the percentage of  $M_{pop}$  released by the comet.

Note that it is the comets with the smallest values of  $\bar{H}_{10}$  that contribute most of the dust, rather than comets with the smallest perihelia. The exception is those comets that have perihelia beyond 2.8 AU, which in this model do not release any dust.

Comet	q (AU)	e	$H_{10}$
90P/Gehrels 1	2.99	0.51	5.2
36P/Whipple	3.09	0.26	6.2
82P/Gehrels 3	3.46	0.15	4.4
74P/Smirnova-Chernykh	3.55	0.15	4.0
99P/Kowal 1	4.68	0.23	2.7

Table 6.2: Short period comets with perihelia greater than 2.8 AU.

This poses a problem for the model since it is assumed that short period comets do not release any dust at heliocentric distances greater than 2.8 AU. Clearly these comets are active and so they must be accounted for.

### Large Comets?

Equation (6.2) relates the mean absolute magnitude of a comet to the equivalent radius of the nucleus. If this equation is valid for these five comets then they are relatively large, ranging from an equivalent radius of 6.4 km for 90P/Gehrels 1, up to 20.3 km for 99P/Kowal 1.

If equation (6.2) is valid for these comets then they should be left in the model. If they are large, contain water snow (*i.e.* equation (6.3) is valid) and are put on orbits with perihelia less than 2.8 AU (see assumption (2) in section (6.2)) then it is likely that they would contribute a significant fraction of the total dust mass released by the population.

### Non-Water Snow Sublimation?

Activity has been observed from several comets at heliocentric distances greater than 2.8 AU. For example, Hale-Bopp was observed to be active at a heliocentric distance of 7 AU and this was attributed to the sublimation of carbon monoxide

snow (Biver et al. 1996). Although Hale-Bopp is not a short period comet it is not unreasonable to assume that some short period comets initially have compositions similar to their long period counterparts. This assumption can be made because the comets in the short period population are likely to have once been long period comets, that have since been captured by Jupiter on to short period orbits. Also, Cochran (1989) examined the production rates of  $C_2$ ,  $C_3$  and  $CN$  for 48 comets and concluded that “most comets observed have undergone a common formation and evolution”.

Unfortunately, if these comets are active because of the sublimation of non-water snow then equation (6.3) is not valid. Although these comets probably also contain water-snow they should be left out of the model population because of the invalidity of equation (6.3).

## Two Different Populations

To account for the difficulty that these five comets pose for the model, two approaches are taken at this point:

1. It is assumed that the five,  $q > 2.8$  AU, comets are large and contain water snow. Consequently, the size of the known model population is maintained at 89 short period comets.
2. It is assumed that the five,  $q > 2.8$  AU, comets are sublimating non-water snow and that this accounts for the values of  $\bar{H}_{10}$ . Although the nuclei may also contain water snow the values of  $\bar{H}_{10}$  are not valid for use in equation (6.3). Consequently, these five comets are excluded from the model and the population size is reduced to 84 short period comets.

## 6.4 The New Populations

A known population of 89 comets can be mixed up to create a maximum number of  $89!$  unique (in terms of which comet is matched to which orbit) new populations. Correspondingly,  $84!$  unique new populations can be created for a known population of 84 comets. To calculate  $M_{pop}$  for all of these different populations would be overly computer intensive. Therefore, only a few thousand possible populations were sampled from the total number of possible populations.

Using a random number generator program the 89, or 84, values of  $\bar{H}_{10}$  were mixed up 3000 times and matched back to the fixed list of  $q$  and  $e$  values.

Each new population must be unique, *i.e.* the same list of comets cannot be matched to the same list of orbits twice. If multiple versions of the same population are created then a frequency distribution of the  $M_{pop}$  values would be distorted. Unfortunately, to compare every comet in each population with every other population would be too computer intensive. Therefore, a simple test of uniqueness was required. Therefore,  $\bar{H}_{10}$  values were taken from three sections of the list and the values in each section were summed. This produced three numbers for each new population that was created. Populations that had the same three numbers as previous populations were then removed.

Unfortunately, this will inevitably mean the loss of some good data. Applying this test for 3000 runs of the 89 comet model produced 2586 new populations of short period comets that were considered unique. In the 84 comet model this number decreased to 2585 unique populations.

Using the dust release model presented in chapter (4) the mass of dust released by each comet,  $M_{dp}$ , was calculated and summed to produce the total mass of dust re-

leased by each of the new populations,  $M_{pop}$ . This corresponded to a total of 230154 comets (89 comets  $\times$  2586 populations) or 217140 comets (84 comets  $\times$  2585 populations) for which  $M_{ap}$  was calculated.

### 6.4.1 The Population of 89 comets

The total mass of dust,  $M_{pop}$ , released by the 2586 populations is shown as a frequency distribution in figure (6.1a).

The sample size is large enough to show several trends:

1.  $M_{pop}$  varies from  $0.6 \times 10^{14}$  g up to  $3.2 \times 10^{14}$  g. Note that this range would be expected to increase with the number of populations in the distribution.
2. The distribution peaks at  $(1.2 \pm 0.1) \times 10^{14}$  g.
3. The value of  $M_{pop}$  for today's known population is  $0.4 \times 10^{14}$  g. Note that this figure is so low that the value lies outside of the distribution shown in figure (6.1a)

The distribution in figure (6.1a) can be interpreted as a probability plot. The peak of the distribution corresponds to the most likely value of  $M_{pop}$  for a population of comets that are limited to the orbits and  $\bar{H}_{10}$  values of the known population.

Figure (6.1b) shows the percentage of  $M_{pop}$  that is contributed by the top ten dust releasing comets in each population. The most likely outcome for these new populations is that 10 comets contribute  $(75 \pm 4)\%$  of  $M_{pop}$ . The value for the known population is very low at 47%. Notice that the asymmetry in figure (6.1b) is in the opposite sense to that in figure (6.1a).

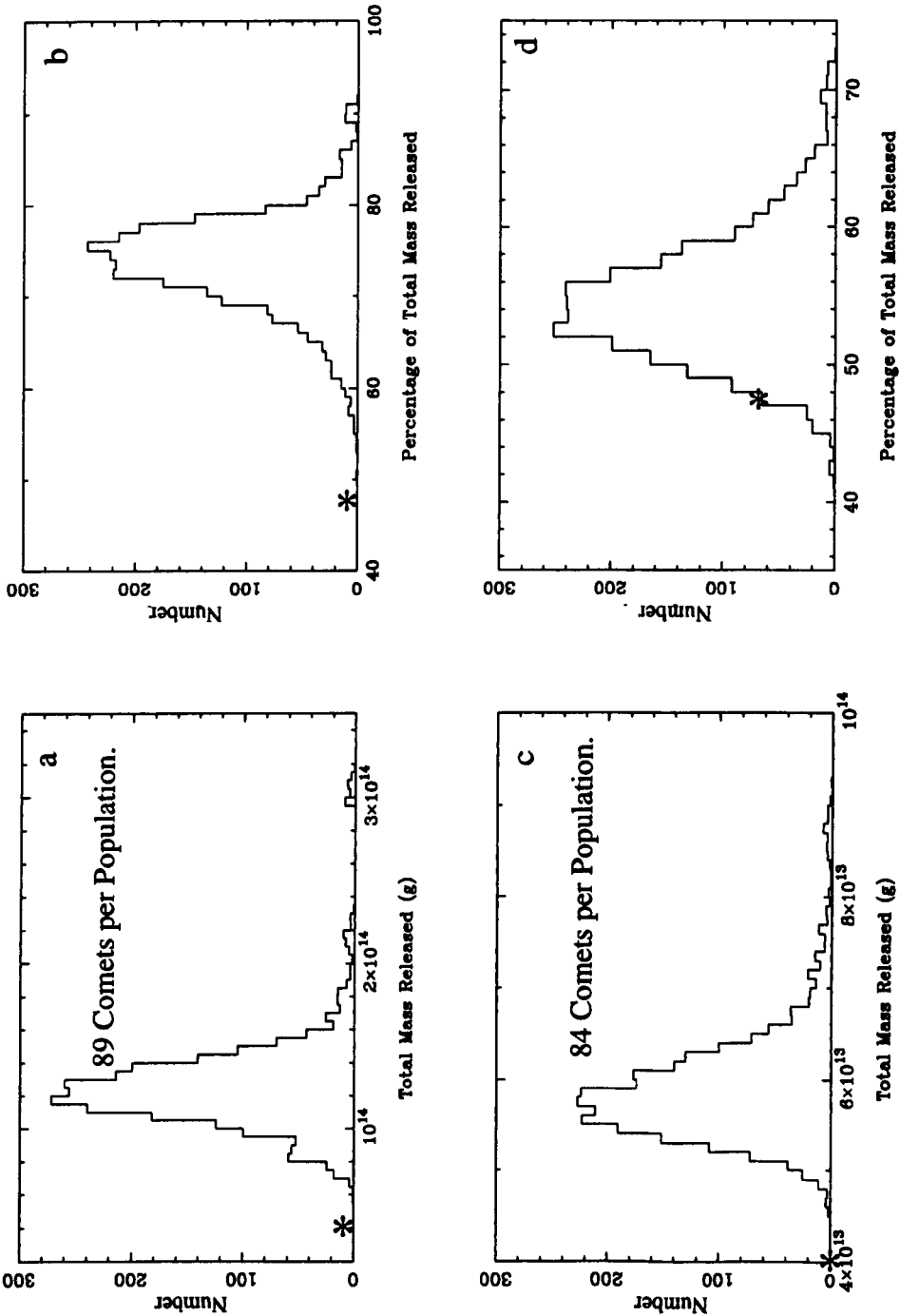


Figure 6.1: The distributions of  $M_{pop}$  and the percentage of  $M_{pop}$  released by the top 10 dust releasing comets in each population. Plots (a) and (b) are the  $M_{pop}$  and percentage of  $M_{pop}$  (released by the top ten comets) distributions for the 89 comet population. Plots (c) and (d) are the corresponding distributions for the 84 comet population. Notice in plot (b) the asymmetry is in the opposite sense to all the other distributions. This is because the 5,  $q > 2.8$  AU comets, if allowed onto small perihelia will dominate the contribution to  $M_{pop}$ .

The asterisks refer to the value of  $M_{pop}$ , or the percentage of  $M_{pop}$ , for the known population of comets. Notice that these values are so low that they do not appear on the distributions.

The bin width of (a) is  $0.5 \times 10^{13}$  g, (b) is 1%, (c) is  $1.0 \times 10^{12}$  g and (d) is 1%.

### 6.4.2 The Population of 84 Comets ( $q < 2.8$ AU)

Figure (6.1c) shows the distributions for the populations of 84 comets with  $q < 2.8$  AU. The distribution is confined to a much smaller range, between  $0.5 \times 10^{14}$  g and  $1.0 \times 10^{14}$  g. This is a consequence of excluding the unusually big comets with  $q > 2.8$  AU shown table (6.2). When these low  $\bar{H}_{10}$ , large radius, comets are associated with perihelia less than 2.8 AU they dominate the total amount of dust released by the population.

The distribution is still asymmetric, therefore the asymmetry cannot be a result of including the comets of table (6.2). The most likely value for  $M_{pop}$  is  $(0.58 \pm 0.03) \times 10^{14}$  g. Notice that the known population value for  $M_{pop}$  is still  $0.4 \times 10^{14}$  g. This is the same as in the 89 comet population since, by definition, the five comets with  $q > 2.8$  AU in the 89 comet population do not release any dust.

Figure (6.1d) shows the percentage of  $M_{pop}$  contributed by the top ten dust releasing comets in each population. Here, the most likely value has reduced to  $(52 \pm 2)\%$ . The known population value of 47% now falls on the lower part of the distribution. Notice that the asymmetry in figure (6.1d) is in the same sense as in figure (6.1c). This means the mismatch in the sense of the asymmetry in figure (6.1a) and figure (6.1c) is due to the five,  $q > 2.8$  AU, comets dominating the mass of dust released by the population and shifting the peak of the distribution to the right.

## 6.5 Why is $M_{pop}$ so Small for the Current Population?

It was expected that the different model populations would release widely varying amounts of dust. What is not so obvious is why the value of  $M_{pop}$  for the known population should be so low that it does not appear on the distributions in figure (6.1a) and figure (6.1c).

That the known population has a very low value of  $M_{pop}$  compared to the new model populations indicates that either:

1.  $\bar{H}_{10}$  is not related to the size of the nucleus by equation (6.2) but is the result of a physical effect that is dependent on the perihelion distance, e.g. the fraction of the nucleus surface that is active,  $f$ , may be a function of perihelion distance.
2. The mean absolute magnitude,  $\bar{H}_{10}$ , of the cometary nucleus is a function of perihelion distance because the data set is incomplete, i.e. fainter comets can be detected at smaller perihelion distances but are missed as perihelion distance is increased.
3.  $\bar{H}_{10}$  is a function of the perihelion distance because the time elapsed since the comets became members of the short period population is sufficient for cometary decay to be important.

### (1) Active Areas

Rickman et al. (1991) suggested that short period comets have less dust covering the surface of the nucleus at greater perihelion distances and/or have smaller mean

radii at larger perihelion distances<sup>1</sup>. If the active fraction of the surface area of the cometary nucleus,  $f$ , is a function of perihelion distance then the approximation of a constant value of  $f$  made in equation (6.2) cannot be applied to all short period comets. This would not, however, affect the validity of equation (6.3) since this equation only relates the rate at which the mass of dust is released to  $\bar{H}_{10}$ . Although it is assumed in this chapter that the absolute magnitude is related to the equivalent radius of the comet it is not essential for equation (6.3) to be valid. Unfortunately, an investigation into possibility (1) is beyond the scope of this thesis.

## (2) Incomplete Data Set

The sample of short period comets that make up the known population is incomplete because many faint comets will have been missed. It is likely that as perihelion distance increases the absolute magnitude that a comet must have to be detected will decrease. Therefore, it is expected that possibility (2) will play a part producing an apparent relationship between  $\bar{H}_{10}$  and the perihelion distance.

## (3) Cometary Decay

It is expected that, for the known population of short period comets possibility (3) is likely to be true. Hughes (1982) stated that “comets seen from Earth which have periods less than 200 years are, in the majority of cases, well on their way to death and can be regarded as ‘middle aged’ ”. Regardless of the validity of possibility (1), if Hughes’ statement is correct then it would be reasonable to expect a correlation

---

<sup>1</sup>Note that this relationship between the size of cometary radii and perihelion distance would imply, if equation (6.2) is used, that the average value of  $\bar{H}_{10}$  should *increase* with increasing perihelion distance, *i.e.* the faintest comets should have the largest perihelia. This is contrary to the plot of  $\bar{H}_{10}$  against  $q$  shown in figure (6.2).

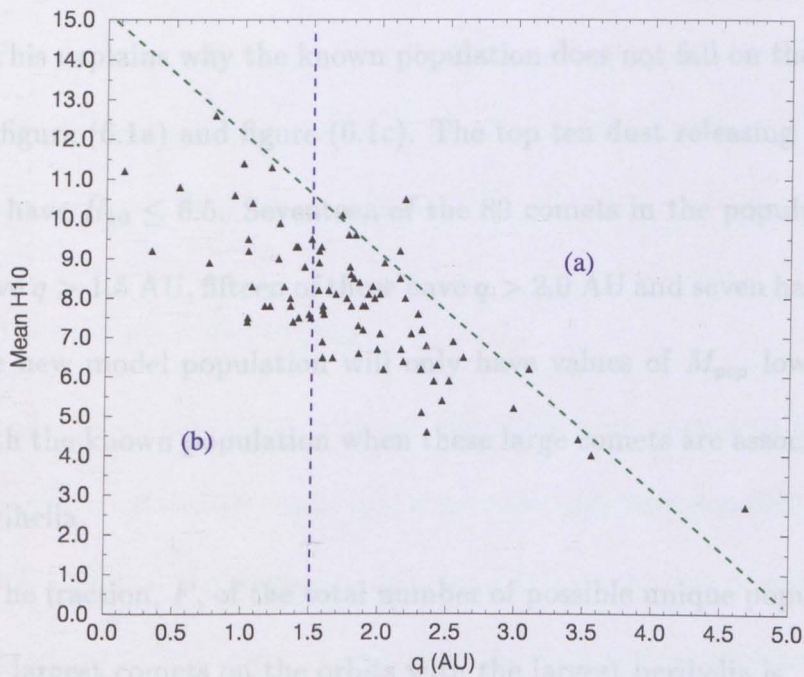


Figure 6.2: The decreasing trend in  $\bar{H}_{10}$  with perihelion distance could be due to (1) a physical connection between the fraction of the surface area of the nucleus that is active and perihelion distance, or (2) observational selection, or (3) a well decayed population.

The population of comets considered in this chapter is only a fraction of the actual number of short period comets that exist. Comets are missing from region (a) because of the difficulty in detecting faint comets. What is not expected from an observational bias, however, is the lack of bright comets in region (b) *i.e.*,  $q < 1.5$  AU (see section (5.3)).

The line fitted to the upper border is the one produced by Fernández et al. (1992) (see equation (6.6)) using all 120 short period comets from the Kresák and Kresáková catalogues (1989, 1994).

between absolute magnitude and perihelion distance that was, at least in part, due to cometary decay.

### 6.5.1 $\bar{H}_{10}$ as a Function of Perihelion Distance

Figure (6.2) shows perihelion distance against  $\bar{H}_{10}$  for the known population of short period comets. There is a clear decreasing trend in the mean absolute magnitude as perihelion distance increases. Using equation (6.2), this means that cometary nuclei

detected at larger perihelion distances are on average bigger than those detected at smaller perihelion distances.

This explains why the known population does not fall on the distributions shown in figure (6.1a) and figure (6.1c). The top ten dust releasing comets in table (6.1) all have  $\bar{H}_{10} \leq 6.5$ . Seventeen of the 89 comets in the population with  $\bar{H}_{10} \leq 6.5$  have  $q > 1.5$  AU, fifteen of these have  $q > 2.0$  AU and seven have  $q > 2.5$  AU. Thus, the new model population will only have values of  $M_{pop}$  low enough to compare with the known population when these large comets are associated with such large perihelia.

The fraction,  $F$ , of the total number of possible unique populations that have all the largest comets on the orbits with the largest perihelia is,

$$F = \frac{n!(N-n)!}{N!}, \quad (6.5)$$

where  $N$  is the number of comets in the population and  $n$  is the number of large comets.

This number will be very small for a population of 89 comets. For example, the fraction of the total number of new populations that have all of the fifteen,  $\bar{H}_{10} \leq 6.5$ , comets on orbits with  $q > 2.0$  AU is only  $2.6 \times 10^{-17}$ . Therefore, it is not surprising that the known population does not fall on the distributions in figure (6.1a) and figure (6.1c).

The approach taken from this point will be to assume that the relationship between  $\bar{H}_{10}$  and  $q$  is due entirely to cometary decay. A simple approach will be taken by only considering linear relationships between  $\bar{H}_{10}$  and perihelion distance.

The first step is to determine which is the best line to fit to the data set. There are three possibilities considered in this section: (1) fit a line to the upper border of the data, *i.e.* the largest value of  $\bar{H}_{10}$  at each perihelion distance, (2) fit a line to the lower border of the data, *i.e.* the smallest value of  $\bar{H}_{10}$  at each perihelion distance or (3) fit a linear regression to all the data.

### (1) The Upper Boundary

Fernández et al. (1992) took all 120 short period comets from the Kresák and Kresáková catalogues (including those with only one recorded apparition) and plotted  $\bar{H}_{10}$  against the perihelion distance (AU) for the first observed apparition. They suggested that the upper boundary of the data points represents the detection limit for short period comets.

They found that the detection magnitude,  $H_d$ , is related to the perihelion distance,  $q$ , by,

$$H_d = 15.2 - 3.0q \quad (6.6)$$

This is shown as the green line in figure (6.2). Unfortunately, only one high magnitude (*i.e.* faint) comet need be recorded at each value of  $q$  to define the upper boundary. Therefore, it is unlikely that all short period comets have been seen with mean absolute magnitudes below this line.

Unfortunately, accounting fully for observational bias would be a project in itself and so no attempt was made to add ‘missing’ comets to the model population. The possible effect that observational selection has on the results will be discussed in

section (6.7).

## (2) The Lower Boundary

Observational bias tends towards missing the faintest comets. In figure (6.2) there is a lack of bright comets in region (b) ( $\bar{H}_{10} < 7$ ,  $q < 1.5$  AU) in comparison to the bright comets in the  $1.5 \text{ AU} \leq q < 2.8 \text{ AU}$  region. Since this lower boundary of the data in figure (6.2) is defined by the lowest values of  $\bar{H}_{10}$  at each value of  $q$  (i.e. the brighter, larger comets) the effect of observational selection should be negligible. Therefore, it is expected that this boundary is due to the process of cometary decay.

## (3) A Linear Regression

A linear regression is biased by the incompleteness of the data set. Although the linear regression can be used to remove most of the dependency of  $\bar{H}_{10}$  on  $q$  it is affected by both the physical relationship between  $\bar{H}_{10}$  and  $q$  and the missing data. This technique may therefore be considered as a way of finding the maximum dependency of  $\bar{H}_{10}$  on the perihelion distance.

### 6.5.2 'Correcting' for Cometary Decay

The approach, taken from this point, will be to assume that  $H_{10}$  is a function of perihelion distance because of cometary decay. If the slope in figure (6.2) is due to a well decayed population then compensating for the slope should indicate the absolute magnitude distribution of the comets before they started to decay.

Figure (6.3a) and figure (6.3b) show the  $\bar{H}_{10}$  against  $q$  plots for the 89 and 84 comet populations respectively. The blue lines are simple linear regressions applied

Pop. Size	Linear Regression (Blue line)	Fit to Lower Boundary (Red line)
89	$\bar{H}_{10} = -(1.92 \pm 0.17)q + (11.32 \pm 0.33)$ [5.96]	$\bar{H}_{10} = (-1.4 \pm 0.2)q + (9.0 \pm 0.8)$ [5.08]
84	$\bar{H}_{10} = -(1.92 \pm 0.24)q + (11.34 \pm 0.42)$ [5.95]	$\bar{H}_{10} = (-2.0 \pm 0.4)q + (10.0 \pm 0.2)$ [4.40]

Table 6.3: For both the 89 and the 84 comet populations linear regressions were applied and lines fitted to the lower border of the data shown in figure (6.3). The linear regressions are expected to be biased by the incompleteness of the data set. The main consequence is that the gradients found from the linear regressions in figure (6.3) should be overestimates, *i.e.* too steep. The lower borders represent the smallest mean absolute magnitude at each perihelion distance. This is expected to be less affected by observational selection. The numbers in the square parentheses are the values of  $\bar{H}_{10}$  where the lines cross  $q = 2.8$  AU.

to the data and are expected to be heavily influenced by the incompleteness of the data sets. The red lines are fits to the lower boundary of the data points.

The equations of the lines are shown in table (6.3), and indicate that for every 1 AU increase in perihelion distance, the average absolute magnitude of a short period comet decreases by 1.2 to 2.4 magnitudes.

### 6.5.3 The Expected Decay Rate

It is worth comparing the fits in figure (6.3a) and figure (6.3b) with the expected decay rate for short period comets. In chapter (4) the average depth of the layer lost from the cometary nucleus,  $\Delta R$ , at each perihelion passage was,

$$\Delta R \propto q^{-\frac{1}{2}}, \quad (6.7)$$

where  $q$  is the perihelion distance in AU of the comet.

Equation (6.7) can then be combined with equation (6.2) to find the expected

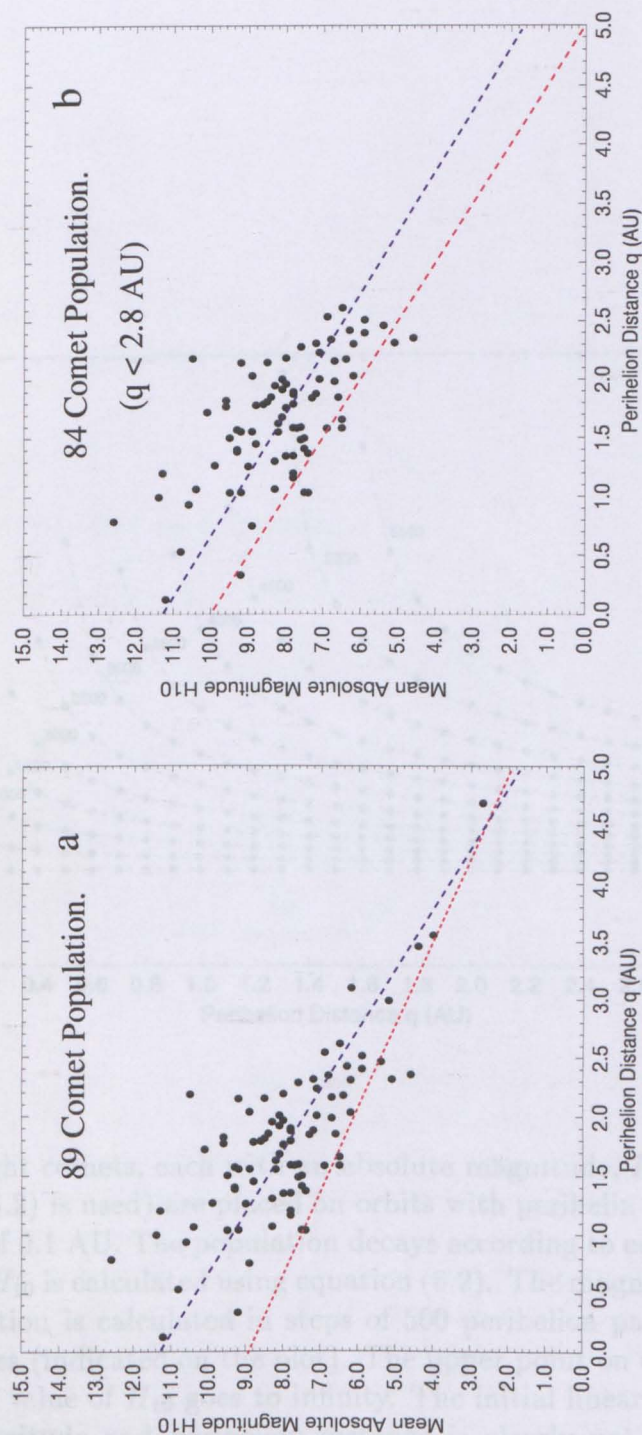


Figure 6.3: Plots of  $\bar{H}_{10}$  against perihelion distance,  $q$ , for the 89 comet population (a) and the 84 comet ( $q < 2.8$  AU) population (b). The blue lines are linear regressions applied to the complete data sets and are expected to be biased towards an unrealistically steep gradient by the incompleteness of the data, *i.e.* high magnitude comets missed at large  $q$  distances give the impression of a steep gradient. The red lines are fits to the lower border of the plots. Since these represent the comets with the lowest absolute magnitude (*i.e.* the brightest comets) at each perihelion distance, the red lines are considered to be closer to a description of cometary decay than the blue lines.

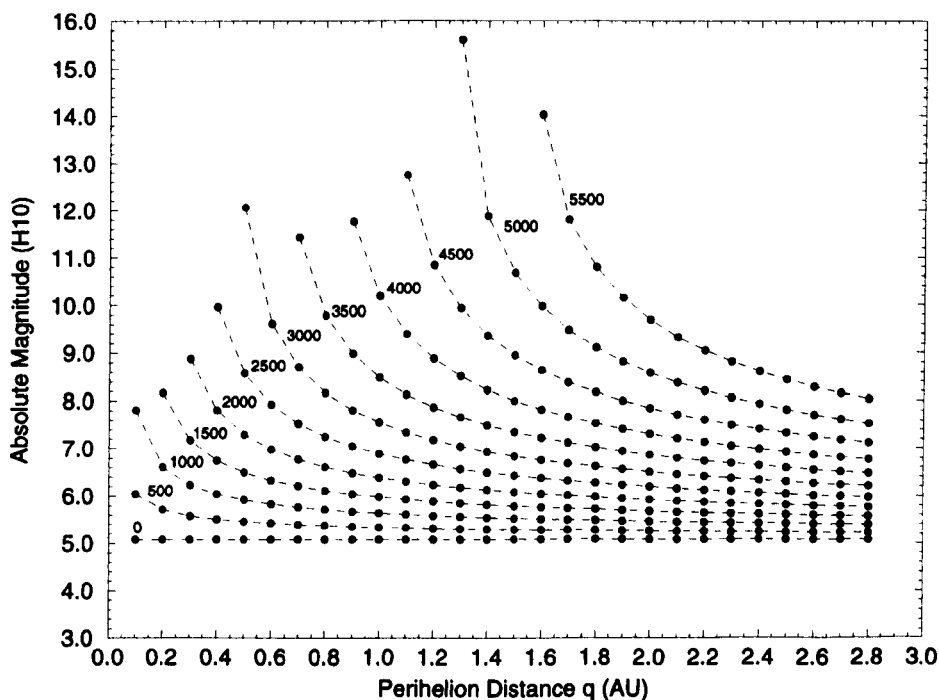


Figure 6.4: Twenty eight comets, each with an absolute magnitude,  $H_{10}$ , of 5.08 (6.79 km if equation (6.2) is used) are placed on orbits with perihelia from 0.1 AU up to 2.8 AU in steps of 0.1 AU. The population decays according to equation (6.7) and each new value of  $H_{10}$  is calculated using equation (6.2). The magnitude of each member of the population is calculated in steps of 500 perihelion passages up to 5500 perihelion passages (indicated on the plot). The upper point on each curve is the last one before the value of  $H_{10}$  goes to infinity. The initial linear relationship between absolute magnitude and perihelion distance is clearly not preserved if comets decay according to equation (6.7).

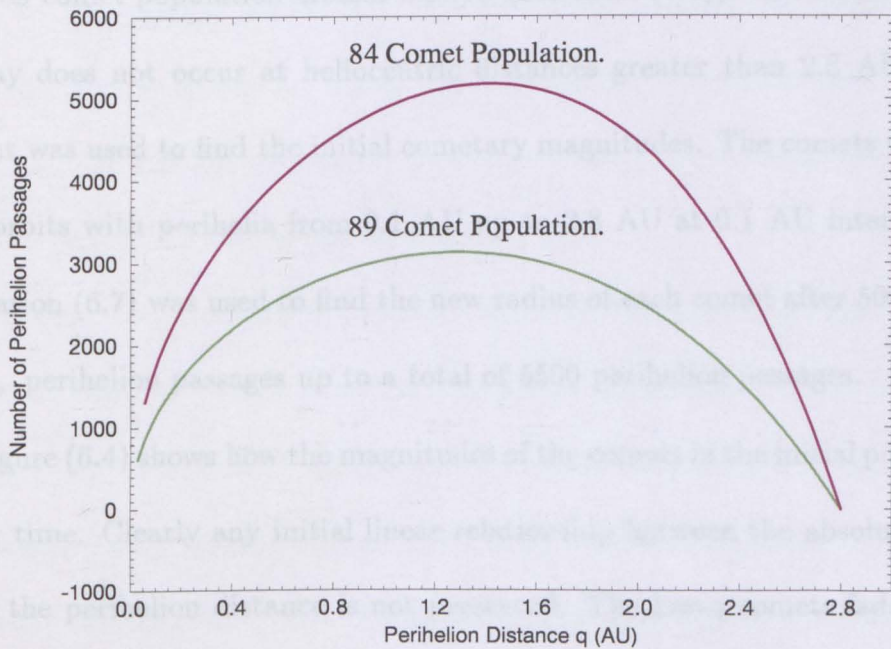


Figure 6.5: The number of perihelion passages that a comet takes to decay such that the absolute magnitude,  $H_{10}$ , agrees with the either of the red lines in figure (6.3). The comets begin with a magnitude calculated from the point where the red lines cross 2.8 AU. The brown line corresponds to comets of initial magnitude  $H_{10} = 4.4$  decaying until their absolute magnitude agrees with the 84 comet red line equation in table (6.3) at each perihelion distance. The green line corresponds to a comet of initial magnitude  $H_{10} = 5.08$  decaying until the absolute magnitude agrees with the 89 comet red line equation in table (6.3) for each perihelion distance. Neither of these lines are horizontal (*i.e.* at each perihelion distance the comets take the same time to fade to the red line position) and this illustrates the incompatibility between equation (6.7) and the red lines as descriptions of cometary decay.

curve corresponds to comets with initial absolute magnitudes of 4.4 (the point where the red line crosses 2.8 AU for the 84 comet population) fading until they reach the absolute magnitude that agrees with the red line for the 84 comet population in figure (6.3).

change in  $H_{10}$  over a number of perihelion passages.

### A Model $H_{10}$ against $q$ Curve

In this model each comet initially has an absolute magnitude of  $H_{10} = 5.08$ , ( $R = 6.79$  km using equation (6.2)). This corresponds to the point where the red line for the 89 comet population crosses 2.8 AU (see table (6.3)). In this model cometary decay does not occur at heliocentric distances greater than 2.8 AU and so this point was used to find the initial cometary magnitudes. The comets were then put on orbits with perihelia from 0.1 AU up to 2.8 AU at 0.1 AU intervals. Finally, equation (6.7) was used to find the new radius of each comet after 500, 1000, 1500, etc., perihelion passages up to a total of 5500 perihelion passages.

Figure (6.4) shows how the magnitudes of the comets in the initial population fade over time. Clearly any initial linear relationship between the absolute magnitude and the perihelion distance is not preserved. The low- $q$  comets fade quickly and the result is the curved shape seen in the plot.

### The Number of Perihelion Passages Required to Produce the Red Lines

A different approach is taken in figure (6.5). The green curve represents the number of perihelion passages required by comets with an initial magnitude of  $H_{10} = 5.08$ , at different perihelion distances, to fade until they have an absolute magnitude that agrees with the red line for the 89 comet population (see figure (6.3a)). The brown curve corresponds to comets with initial absolute magnitudes of 4.4 (the point where the red line crosses 2.8 AU for the 84 comet population) fading until they reach the absolute magnitude that agrees with the red line for the 84 comet population in figure (6.3b).

The fact that neither line is horizontal indicates that there is an incompatibility between the red lines in figure (6.3) as a description of a single decaying population and the rate of decay expected using equation (6.7) and equation (6.2).

Clearly, the assumption that the comets all have the same initial absolute magnitude and begin to decay at the same time is far too simplistic. The red lines may be the result of an influx of new comets, of varying  $H_{10}$  values, to the short period comets population. Thus, the incompatibility between the expected decay rate and the red lines is not conclusive evidence against the gradients of the red lines in figure (6.3) being due to cometary decay.

Unfortunately, calculating the influx of new short period comets is not easy. Short period comets may come from the long period population or from the Edgeworth-Kuiper belt. The rate at which comets transfer to short period orbits is low. For example, Bailey (1990) concluded that Van Woerkom's dynamical analysis of the transfer of long period comets onto short period orbits, via close encounters with Jupiter, indicated a net increase in new short period comets of 0.15 per century.

Reproducing figure (6.2) from a model population that is supplemented by new short period comets is left as a future project.

### Compensating for the Gradients

The mean absolute magnitude,  $\bar{H}_{10}$ , is a function of the perihelion distance for the data set used here. Irrespective of the reason for this a 'correction' was applied to compensate for the gradients shown in figure (6.3). If all the comets were captured on to short period orbits at the same time this correction would 'reset' the comets back to their initial absolute magnitudes.

The technique used was as follows:

1. Either a linear regression (blue line) is applied to the  $\bar{H}_{10}$ - $q$  data or a line is fitted to the lower boundary of the data set (red line) shown in figure (6.3).
2. The residuals in  $\bar{H}_{10}$ , about this line, are calculated.
3. Using the equation of the fitted line the value of  $\bar{H}_{10}$  at  $q = 2.8$  AU is calculated.
4. New corrected values of  $\bar{H}_{10}$  are found by summing the value found in step (3) with the residuals found in step (2). In this way the dependance of  $\bar{H}_{10}$  on  $q$  is removed. When these new  $\bar{H}_{10}$  values are associated with the correct values of  $q$  and  $e$  they will be referred to as the 'known (corrected) population'.

The value found in step (3) is arbitrary but a standard point was required to fit to the residuals in  $\bar{H}_{10}$ . Since, in this model, comets do not decay if they are at a heliocentric distances greater than 2.8 AU this was considered a reasonable value to choose.

## 6.6 The New (Corrected) Populations

The method for creating the frequency distributions in figure (6.1) was used to produce frequency distributions based on the new known (corrected) populations. For both the 89 and the 84 comet populations the distributions that were created were either based on the red line (fit to the lower boundary of the data) or blue line (linear regression) known (corrected) populations.

Table (6.4) summarises the main features of the distributions shown in figure (6.1), figure (6.6) and figure (6.7).

### 6.6.1 The 89 Comet Population

#### Red line correction

Figure (6.6a) shows the  $M_{pop}$  distribution after the red line correction is applied. The distribution peaks at  $(1.8 \pm 0.1) \times 10^{14}$  g. Since most of the values of  $\bar{H}_{10}$  decrease after the correction, this peak occurs at a value of  $M_{pop}$  greater than the uncorrected distribution peak,  $(1.2 \pm 0.1) \times 10^{14}$  g, shown in figure (6.1a).

The known orbits matched to the known (corrected) absolute magnitudes produce a population that releases  $1.6 \times 10^{14}$  g. This is on the low edge of the distribution. This means that the mass of dust released by the known population *was not* a likely value in this model. The red line in figure (6.3) is unduly weighted towards those comets with  $q > 2.8$  AU and this will distort the correction technique used here.

Figure (6.6b) shows the maximum percentage of  $M_{pop}$  that can be released by ten comets. The distribution peaks at  $(40 \pm 2)\%$ . The known (corrected) population

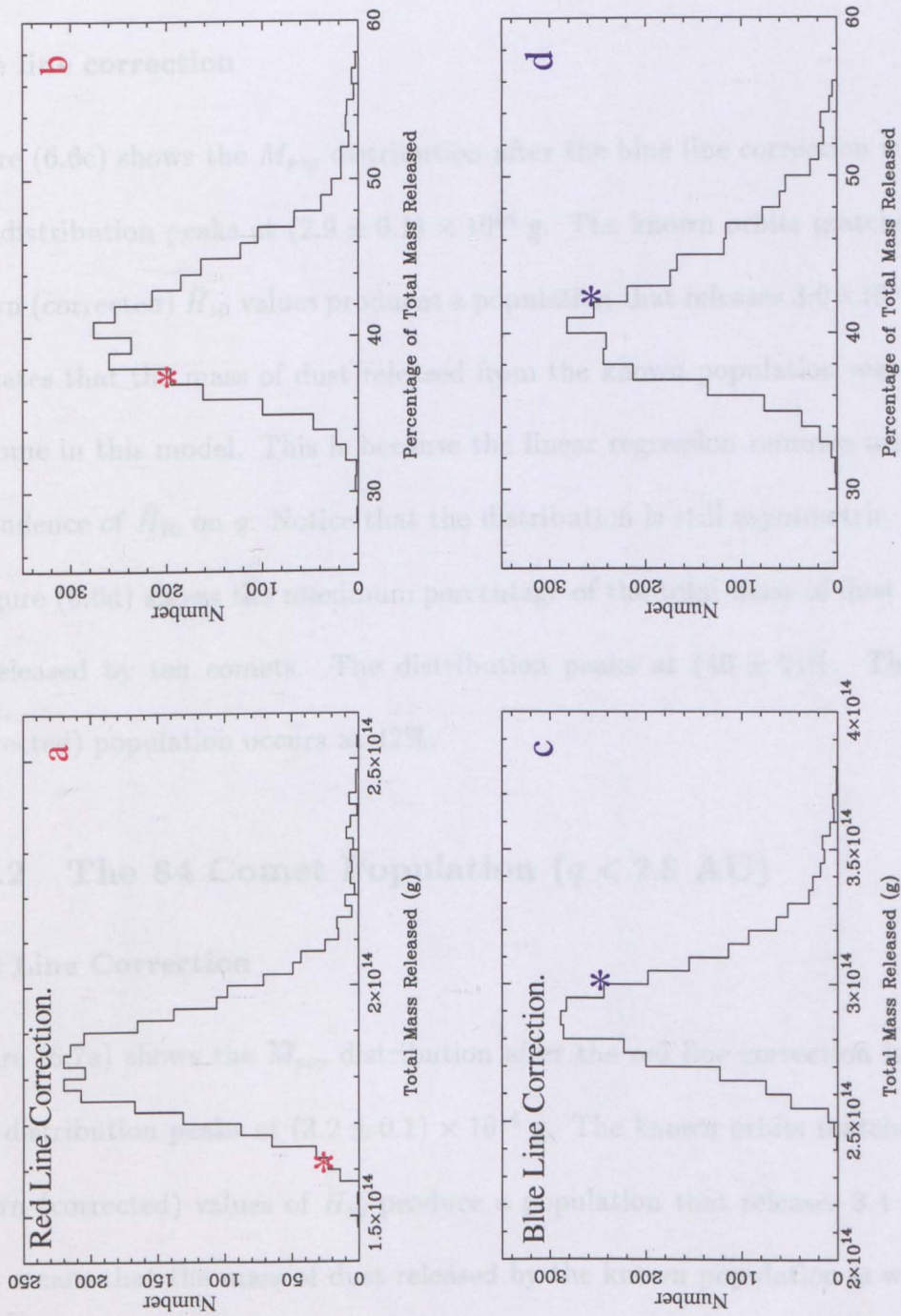


Figure 6.6: **The 89 comet population corrected distributions.** Plot (a) shows the  $M_{pop}$  distribution after the red line correction is applied. Plot (c) shows the  $M_{pop}$  distribution after the blue line correction is applied. Plot (b) shows the distribution of the percentage of  $M_{pop}$  that is contributed by the top ten dust releasing comets after the red-line correction is applied. Plot (d) shows the corresponding blue line corrected distribution.

The asterisks are used to denote where the known (corrected) populations values are on the plots. Plots (b) and (d) indicate that the most probable outcome is for ten comets to contribute  $(40 \pm 2)\%$  of the total mass of dust that is released by the population. The bin size of (a) is  $0.5 \times 10^{13}$  g, (b) is 1%, (c) is  $0.5 \times 10^{13}$  g and (d) is 1%.

value occurs at 37%

### Blue line correction

Figure (6.6c) shows the  $M_{pop}$  distribution after the blue line correction is applied. The distribution peaks at  $(2.9 \pm 0.1) \times 10^{14}$  g. The known orbits matched to the known (corrected)  $\bar{H}_{10}$  values produces a population that releases  $3.0 \times 10^{14}$  g. This indicates that the mass of dust released from the known population *was* a likely outcome in this model. This is because the linear regression removes most of the dependence of  $\bar{H}_{10}$  on  $q$ . Notice that the distribution is still asymmetric.

Figure (6.6d) shows the maximum percentage of the total mass of dust that can be released by ten comets. The distribution peaks at  $(40 \pm 2)\%$ . The known (corrected) population occurs at 42%.

## 6.6.2 The 84 Comet Population ( $q < 2.8$ AU)

### Red Line Correction

Figure (6.7a) shows the  $M_{pop}$  distribution after the red line correction is applied. The distribution peaks at  $(3.2 \pm 0.1) \times 10^{14}$  g. The known orbits matched to the known (corrected) values of  $\bar{H}_{10}$  produce a population that releases  $3.4 \times 10^{14}$  g. This means that the mass of dust released by the known population is within  $2 \sigma$  of the uncertainty in the location of the peak.

Figure (6.7b) shows the maximum percentage of  $M_{pop}$  that can be released by ten comets. The distribution peaks at  $(40 \pm 2)\%$ . The known (corrected) population value is 44%

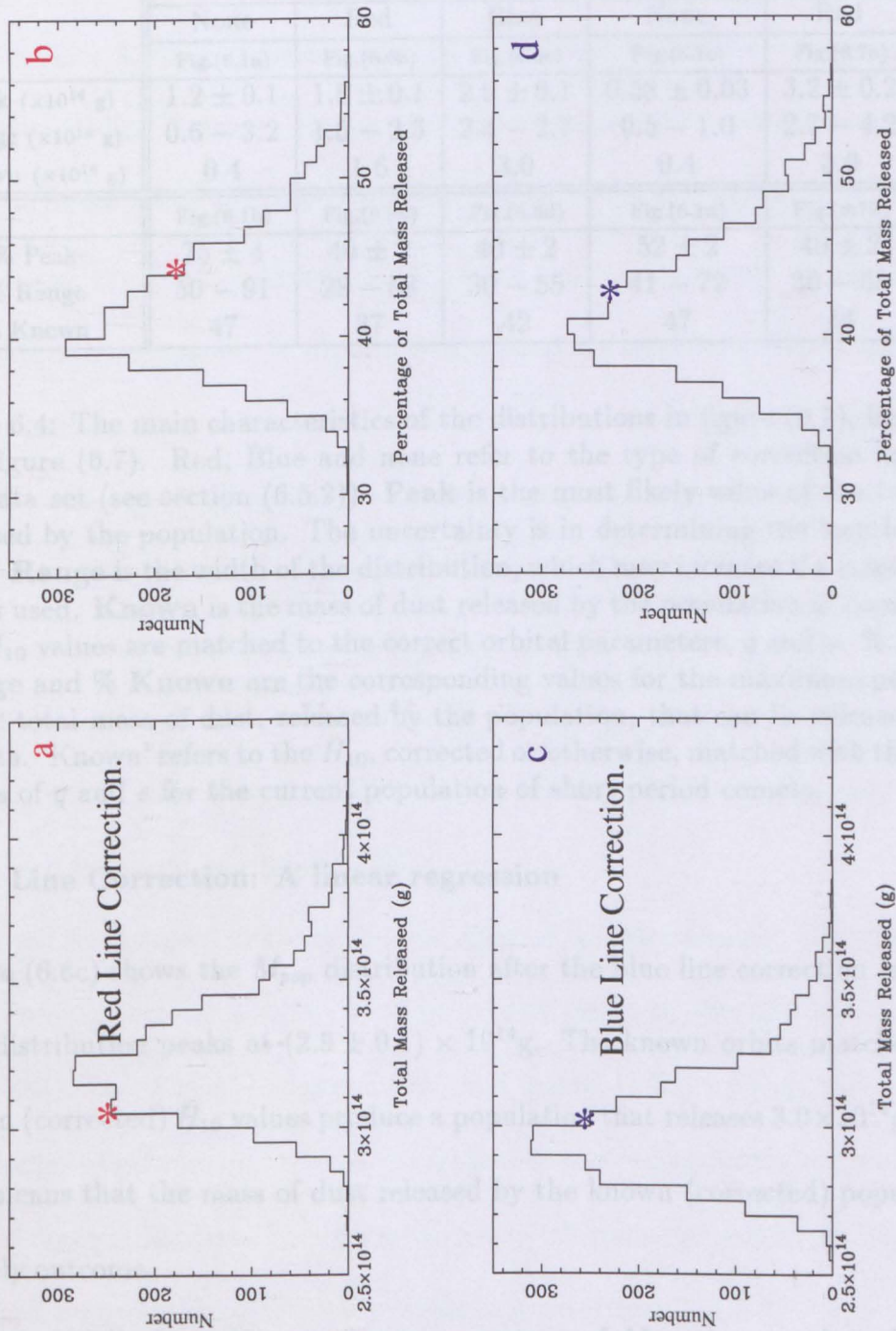


Figure 6.7: **The 84 comet population corrected distributions.** Plot (a) shows the  $M_{pop}$  distribution after the red line correction is applied. Plot (c) shows the  $M_{pop}$  distribution after the blue line correction is applied. Plot (b) shows the distribution of the percentage of  $M_{pop}$  that is contributed by the top ten dust releasing comets after the red-line correction is applied. Plot (d) shows the corresponding blue line corrected distribution.

The asterisks are used to denote where the known (corrected) populations values are on the plots. Plots (b) and (d) indicate that the most probable outcome is for ten comets to contribute  $(40 \pm 2)\%$  of the total mass of dust that is released by the population. The bin size of (a) is  $0.25 \times 10^{13}$  g, (b) is 1%, (c) is  $0.5 \times 10^{13}$  g and (d) is 1%.

	89 Comets			84 Comets		
	None	Red	Blue	None	Red	Blue
	Fig.(6.1a)	Fig.(6.6a)	Fig.(6.6c)	Fig.(6.1c)	Fig.(6.7a)	Fig (6.7c)
Peak ( $\times 10^{14}$ g)	$1.2 \pm 0.1$	$1.8 \pm 0.1$	$2.9 \pm 0.1$	$0.58 \pm 0.03$	$3.2 \pm 0.2$	$2.9 \pm 0.1$
Range ( $\times 10^{14}$ g)	0.6 – 3.2	1.5 – 2.5	2.4 – 2.7	0.5 – 1.0	2.7 – 4.2	2.6 – 3.9
Known ( $\times 10^{14}$ g)	0.4	1.6	3.0	0.4	3.0	3.0
	Fig.(6.1b)	Fig.(6.6b)	Fig.(6.6d)	Fig.(6.1d)	Fig.(6.7b)	Fig (6.7d)
% Peak	$75 \pm 4$	$40 \pm 2$	$40 \pm 2$	$52 \pm 2$	$40 \pm 2$	$40 \pm 2$
% Range	50 – 91	28 – 58	30 – 55	41 – 72	30 – 55	30 – 56
% Known	47	37	42	47	44	42

Table 6.4: The main characteristics of the distributions in figure (6.1), figure (6.6) and figure (6.7). Red, Blue and none refer to the type of correction applied to the data set (see section (6.5.2)). **Peak** is the most likely value of the total mass released by the population. The uncertainty is in determining the location of the peak. **Range** is the width of the distribution, which may increase if a larger sample size is used. **Known** is the mass of dust released by the population of comets when the  $\bar{H}_{10}$  values are matched to the correct orbital parameters,  $q$  and  $e$ . **% Peak**, **% Range** and **% Known** are the corresponding values for the maximum percentage of the total mass of dust, released by the population, that can be released by ten comets. ‘Known’ refers to the  $\bar{H}_{10}$ , corrected or otherwise, matched with the correct values of  $q$  and  $e$  for the current population of short period comets.

### Blue Line Correction: A linear regression

Figure (6.6c) shows the  $M_{pop}$  distribution after the blue line correction is applied. The distribution peaks at  $(2.9 \pm 0.1) \times 10^{14}$ g. The known orbits matched to the known (corrected)  $\bar{H}_{10}$  values produce a population that releases  $3.0 \times 10^{14}$ g. Again, this means that the mass of dust released by the known (corrected) population is a likely outcome.

Figure (6.7d) shows the maximum percentage of  $M_{pop}$  that can be released by ten comets. The peak occurs at  $(40 \pm 2)\%$ . The value for the known (corrected) population occurs at 42%.

## 6.7 Discussion

The blue line, linear regression, correction removes most of the dependency of  $\bar{H}_{10}$  on the perihelion distance. Hence, the known (corrected) population values agree with the peaks in the  $M_{pop}$  distributions in figure (6.6c) and figure (6.7c). For these populations the mass of dust released by the known (corrected) population was a probable outcome given the distribution of absolute magnitudes and perihelia.

The corresponding values for the maximum mass of dust released by ten comets in the population falls within  $2\sigma$  of the uncertainty of the peak position for the percentage distributions in figure (6.6d) and figure (6.7d). This also indicates that in this model the known (corrected) population was a likely outcome. The differences between the model for the 89 comet population and the 84 comet population are very small, only the range that the distributions span are different, the peak values are the same (see table (6.7)).

The red line correction should be less affected by observational bias. The known (corrected) values do not fall as close to the peaks of the distributions in figure (6.6a), figure (6.6b), figure (6.7a) and figure (6.7b). Using this correction technique the differences between the 89 and 84 comet population are more noticeable. This is because the red line fit to the 89 comet population in figure (6.3) is biased towards the comets with perihelia greater than 2.8 AU.

The  $M_{pop}$  distribution for the 84 comet population covers a larger range  $(2.7 - 4.2) \times 10^{14}$  g than the  $(1.5 - 2.5) \times 10^{14}$  g range for the 89 comet population. This is because the red line crosses 2.8 AU at  $\bar{H}_{10} = 4.40$  for the 84 comet population as opposed to  $\bar{H}_{10} = 5.08$  for the 89 comet population. This means that the average comet in the model 84 comet corrected population is more active than in the model

89 comet corrected population.

Unfortunately, straight line fits such as these are likely to be an over simplification. The analysis in section (6.5.3) indicates that the relationship between  $\bar{H}_{10}$  and  $q$  should not be linear. The incompatibility between the expected decay rate in section (6.5.3) and the red line fits indicates that either  $\bar{H}_{10}$  is a function of perihelion distance because of a physical effect other than cometary decay (e.g. a change in the size of the active area with perihelion distance) or that equation (6.7) is too simplistic a description of cometary decay.

All of the  $M_{pop}$  distributions are asymmetric. This may be due to the incompleteness of the data set. This is indicated by figure (6.1b). Here, the plot showing the maximum percentage of dust mass released by ten comets has a peak shifted strongly to the right at  $(75 \pm 4)\%$ . This was attributed to the dominance of the five,  $q > 2.8$  AU comets. A supply of smaller (or less active) comets would tend to reduce the influence that the largest (or most active) comets have on the total mass of dust released by the population.

For all the correction techniques and for both the 89 and 84 comet populations the most likely outcome is for ten comets to contribute  $(40 \pm 2)\%$  of the total mass of dust released by the population. This indicates that the mass of dust released by the population is likely to change significantly if the number of large comets in the population changes.

Hughes (1996b) calculated the average mass of dust released by a comet per year using,

$$\dot{m} = 8 \times 10^4 R^2 q^{-0.5} P^{-1} \text{ gs}^{-1} \quad (6.8)$$

Here,  $R(\text{km})$  is the equivalent radius,  $q(\text{AU})$  is the perihelion distance and  $P(\text{years})$  is the orbital period. Using equation (6.8) Hughes calculated that 80% of the influx of dust to the Solar System dust cloud is provided by only 6 comets. This lead him to conclude that the “influx might vary considerably from epoch to epoch”, specifically that the number of dominant comets would vary randomly, with a standard deviation of  $\sqrt{6}$ .

Although Hughes found the average rate of dust released for each comet in his model, whereas here it is the total mass lost per orbit ( $M_{ap}$ ) the conclusion is similar, *i.e.* the mass of dust released by the population is likely to be very susceptible to a small change in the number of the largest (or most active) comets.

### Hale-Bopp

For comparison with the model populations, the  $M_{ap}$  program was used to calculate the mass of dust released by Hale-Bopp during its 1997 perihelion passage. A value of  $H_{10} = -2$  was interpolated from a light curve produced by Morris (1997), while the orbital eccentricity ( $e = 0.995075$ ) and perihelion distance ( $q = 0.913959$ ) were taken from the *Catalogue of Cometary Orbits* (Marsden & Williams 1996). The calculated value of  $M_{ap} = 4.23 \times 10^{15} \text{ g}$  implies that the mass of dust contributed by a single long period comet may be a factor of 10, or more, greater than the mass of dust released by the population of short period comets as a whole.

However, since the orbit of a long period comet is more parabolic than for a short

period comet it is more likely that dust from a long period comet will be ejected onto hyperbolic orbits. Also, since CO outgassing is significant for Hale-Bopp, the  $M_{ap}$  program may not be directly applicable to this comet.

## 6.8 Summary

The assumption that the absolute magnitude of a comet is independent of its perihelion distance is not true for the current known population of short period comets. As suggested by Rickman (1991) this could be due to the cometary radius being a function of perihelion distance and/or the amount of dust on the surface of the cometary nucleus also being a function of perihelion distance.

A study of how active areas on a cometary nucleus vary in size with perihelion distance was beyond the scope of this chapter. Only the possibility of cometary radii being a function of perihelion distance was examined. A simple model where the average depth of the layer lost from a cometary nucleus at each perihelion passage,  $\Delta R$ , is proportional to  $q^{-0.5}$  was combined with equation (6.2) to produce a model relationship between the mean magnitude of a comet and its perihelion distance. This simple model was unable to explain the apparent linear trend for a decreasing mean magnitude with increasing perihelion distance.

Irrespective of the reason for the relationship between  $\bar{H}_{10}$  and perihelion distance, a correction technique was applied to try to reset the population back to the time when each comet had just started to decay (or when the build up of dust was just about to begin).

The main result of this chapter is that a small number of comets (in this case ten) has a large influence on the total mass of dust released by the population.

The most likely percentage contributed by the top ten comets only gets as low as  $(40 \pm 2)\%$  in this model. This suggests that the amount of dust released by the population is very susceptible to a few large (or very active) comets that are in the population.

# Chapter 7

## Discussion and Possible Future Work

### 7.1 Discussion

- **Chapter (4):** Linear regressions, applied to  $H_{10}$  data, should be used with caution as they can lead to unrealistic secular fading (or brightening) rates. There is probably more information in plots of  $H_{10}$  against time than can be found from using linear regression analysis.

Because 2P/Encke has the highest number of recorded apparitions, (*i.e.* 55), it is the best comet for a study of the variation in  $H_{10}$  over several apparitions. Unfortunately, the asymmetry in the light curve of this comet has been very significant for past apparitions of the comet and this can give the false impression of structure in plots such as in figure (4.6a). Even so, there is tentative evidence that the  $H_{10}$  data forms the shape of a band.

The  $H_{10}$  data for comet 4P/Faye provides the best evidence for a progressive

variation in the activity of a comet over several apparitions. Converting the  $H_{10}$  magnitudes of this comet to the percentage of the nucleus surface that is active, using equation (4.1) indicates that the active region of 4P/Faye has varied between  $\sim 2\%$  and  $54\%$  of the total surface area of the cometary nucleus.

**Possible Future Work:** If the value of  $H_{10}$  could be found for *both sides* of the light curve for every apparition of 2P/Encke then the apparent band structure in the  $H_{10}$  data could be constrained or eliminated.

The  $M_{ap}$  program is based on the assumption that outgassing from a comet is symmetrical around perihelion. A more sophisticated version of the program, that takes account of asymmetrical outgassing would be desirable.

- **Chapter (5):** A model population of short period comets was created and the individual comets were allowed to decay. The model was based on the mass distribution index of the known population of short period comets. The known population is dominated by the brightest comets, *i.e.* the largest nuclei using equation (4.2). This does not limit the model too severely as the smallest comets do not last long and the mass distribution of the population will eventually be dominated by the remaining large comets.

It was found that the mass distribution index of the large comet region decreases, non-linearly, as the comets decay. It would be unwise to presume that the value of the index applies to the whole population of comets, as the percentage of the population of comets used to calculate the index may be very small.

**Possible Future Work:** The cometary decay model was simplistic. In chap-

ter (4) it was shown that the active fraction of the nucleus surface of short period comets is likely to vary from apparition to apparition. Thus, the assumption of a 1 m layer loss from the cometary nucleus at each apparition could be varied for each comet. The  $M_{ap}$  program, discussed in section (4.5), could be used, in combination with an estimate of the masses of several cometary nuclei, to calculate the depth of the layer lost at each apparition. This could be done for several apparitions of different comets and a range of  $\Delta R$  values could then be produced. Individual comets in the population could then decay at different rates.

- **Chapter (6):** The program used to calculate the mass released by a comet per apparition,  $M_{ap}$ , was taken a step further and used to calculate the mass of dust released by an entire population of comets,  $M_{pop}$ . Comets within the population were randomly mixed up and re-assigned back to a fixed list of orbital parameters. Thus, a frequency distribution of  $M_{pop}$  was produced. It was found that the current known population produces a very low value of  $M_{pop}$  and this was attributed to the average  $\bar{H}_{10}$  value decreasing with increasing perihelion distance, i.e. the brightest comets had the largest perihelia. It was suggested that  $\bar{H}_{10}$  may be a function of perihelion distance because of cometary decay, i.e. comets with low values of  $q$  have decayed more and so are fainter. An attempt was made to correct for the relationship between  $\bar{H}_{10}$  and  $q$  and so 'reset' the comets back to their original  $\bar{H}_{10}$  values.

**Possible Future Work:** The value of  $M_{pop}$  was calculated by allowing each comet in the population one perihelion passage and then summing the individual

values of  $M_{ap}$ . Another approach would be to sum the values of  $\frac{M_{ae}}{P}$ , where  $P$  is the orbital period. This would produce the rate at which the population of comets is releasing dust.

# Bibliography

- A'Hearn, M. F., H. Campins, D. G. Schleicher, & R. L. Millis (1989, December).  
*ApJ* 347, 1155–1166.
- Ahearn, M. F., D. G. Schleicher, R. L. Millis, P. D. Feldman, & D. T. Thompson  
(1984, April). *AJ* 89, 579–591.
- Allen, C. (1973). *Astrophysical quantities* (3 ed.). Athlone Press.
- Bailey, M. E., S. V. M. Clube, & W. M. Napier (1990). *The origin of comets*.  
Pergamon Press.
- Beech, M. (1998, February). *MNRAS* 294, 259–264.
- Belyaev, N. A., L. Kresak, E. M. Pittich, & A. N. Pushkarev (1986). *Catalogue  
of Short Period Comets*. Slovak Academy of Sciences, Astronomical Institute.
- Biver, N., H. Rauer, D. Despois, R. Moreno, G. Paubert, D. Bockelee-Morvan,  
P. Colom, J. Crovisier, E. Gerard, & L. Jorda (1996). *Nature* 380, 137–139.
- Brandt, J. C. & R. D. Chapman (1981). *Introduction to Comets*. Cambridge  
University Press.
- Carusi, A., G. B. Valsecchi, L. Kresak, & M. Kresakova (1991, December).  
*A&A* 252, 377–384.
- Chatfield, C. (1970). *Statistics for technology*. Penguin Books Ltd.

- Cochran, A. (1989). In *Asteroids, Comets, Meteors 3*, pp. 281–284. Astronomical Observatory of Uppsala.
- Daniels, P. A. & D. W. Hughes (1981, April). *MNRAS* *195*, 205–212.
- Donnison, J. R. (1990, August). *MNRAS* *245*, 658–664.
- Feldman, P. D., M. C. Festou, M. F. Ahearn, C. Arpigny, P. S. Butterworth, C. B. Cosmovici, A. C. Danks, R. Gilmozzi, W. M. Jackson, & L. A. McFadden (1986, December). *ESA Proceedings of the 20th ESLAB Symposium on the Exploration of Halley's Comet. Volume 1: Plasma and Gas 1*, 325–328.
- Fernández, J. A. & H. Rickman (1992). Periodic comets. In *Periodic Comets, [Montevideo, Uruguay] : Universidad de la Republica, Facultad de Ciencias*.
- Gil-Hutton, R. & J. Licandro (1994, April). *Revista Mexicana de Astronomia y Astrofisica* *28*, 3–6.
- Green, S. F., J. A. M. McDonnell, C. H. Perry, S. Nappo, & J. C. Zarnecki (1987, September). In *Diversity and Similarity of Comets*, pp. 379–384.
- Greenberg, J. M. (1998, February). *A&A* *330*, 375–380.
- Hartmann, W. K., D. J. Tholen, & D. P. Cruikshank (1987, January). *Icarus* *69*, 33–50.
- Hughes, D. W. (1983a, July). *MNRAS* *204*, 23–32.
- Hughes, D. W. (1983b, September). *MNRAS* *204*, 1291–1295.
- Hughes, D. W. (1985, March). *MNRAS* *213*, 103–109.
- Hughes, D. W. (1987, September). In *Proceedings of the International Symposium on the Diversity and Similarity of Comets, ESA*, pp. 43–48.

- Hughes, D. W. (1988a, January). *Icarus* 73, 149–162.
- Hughes, D. W. (1988b, September). *MNRAS* 234, 173–176.
- Hughes, D. W. (1989a). In *Asteroids, Comets, Meteors III, Uppsala*.
- Hughes, D. W. (1989b, August). *A&A* 220, 301–305.
- Hughes, D. W. (1990, March). *Q. Jl R. astr. Soc* 31, 69–94.
- Hughes, D. W. (1991, July). *MNRAS* 251, 26P–29P.
- Hughes, D. W. (1996a, July). *Plan. Space. Sci.* 44, 705–710.
- Hughes, D. W. (1996b). *Q. Jl. R. astr. Soc* 37, 593–604.
- Hughes, D. W. & P. A. Daniels (1980, May). *MNRAS* 191, 511–520.
- Hughes, D. W. & P. A. Daniels (1982, February). *MNRAS* 198, 573–582.
- Hughes, D. W. & P. A. Daniels (1983, March). *Icarus* 53, 444–452.
- Hughes, D. W. & N. McBride (1989, September). *MNRAS* 240, 73–79.
- Kamel, L. (1991, October). *Icarus* 93, 226–245.
- Karttunen, H., P. Kröger, H. Oja, M. Poutanen, & K. J. Donner (1987). *Fundamental astronomy*. Springer-Verlag, Berlin Heidelberg.
- Keller, H. U., W. A. Delamere, H. J. Reitsema, W. F. Huebner, & H. U. Schmidt (1987, November). *A&A* 187, 807–823.
- Kresák, L. (1987, November). *A&A* 187, 906–908.
- Kresak, L. & M. Kresakova (1987, September). In *Diversity and Similarity of Comets*, pp. 37–42.
- Kresák, L. & M. Kresáková (1989, September). *Bulletin of the Astronomical Institutes of Czechoslovakia* 40, 269–284.

- Kresák, L. & M. Kresáková (1994, February). *Plan. Space. Sci.* 42, 199–204.
- Kresák, L. (1974). *Bull. Astron. Inst. Czech.* 25, 87–112.
- Kresáková, M. (1987, November). *A&A* 187, 935–936.
- Lamy, P. & I. Toth (1995, January). *A&A* 293, L43–L45.
- Marsden, B. G. & G. Williams (1996). *Catalogue of Cometary Orbits 1996*. Central Bureau for Astronomical Telegrams, Minor Planet Center, IAU.
- Meech, K. J., M. J. S. Belton, B. E. A. Mueller, M. W. Dickson, & H. R. Li (1993, September). *AJ* 106, 1222–1236.
- Morris, C. S. (1997, 9 May). [http://encke.jpl.nasa.gov/hale\\_bopp/hb\\_light.html](http://encke.jpl.nasa.gov/hale_bopp/hb_light.html).
- Richter, K., W. Curdt, & H. U. Keller (1991, October). *A&A* 250, 548–555.
- Rickman, H., L. Kamel, M. C. Festou, & C. Froeschle (1987, September). In *Diversity and Similarity of Comets*, pp. 471–481.
- Rickman, H., L. Kamel, C. Froeschle, & M. C. Festou (1991, October). *AJ* 102, 1446–1463.
- Russell, H. N. (1916). *ApJ* 43, 173–196.
- Sekanina, Z. (1982, January). *AJ* 87, 161–169.
- Sekanina, Z. (1989, December). *AJ* 98, 2322–2345.
- Steel, D. I. & D. J. Asher (1996, August). *MNRAS* 281, 937–944.
- Štohl, J. (1987, November). *A&A* 187, 933–934.
- Svoreň, J. (1991). *Contributions of the Astronomical Observatory Skalnaté Pleso* 21, 15–49.

Vsekhsvyatskii, S. (1964). *Physical characteristics of comets*. Israel Program for Scientific Translations.

Whipple, F. L. (1950). *AJ* 111, 375-394.

Wyckoff, S. (1982). Overview of comet observations. In *Comets, University of Arizona Press*, pp. 3-55.

### Acknowledgements

I wish to thank the Astronomy group for their help and support during the years leading up to the completion of this thesis. I especially wish to thank Clive Broadley and Bob Dickson for many interesting and useful discussions that helped enormously, and Paul Kerry for being very patient with my endless computer 'mishaps'.

The biggest thanks go to my parents. Their uncompromising support enabled me to get this far in my education. Therefore, this thesis is dedicated to them.